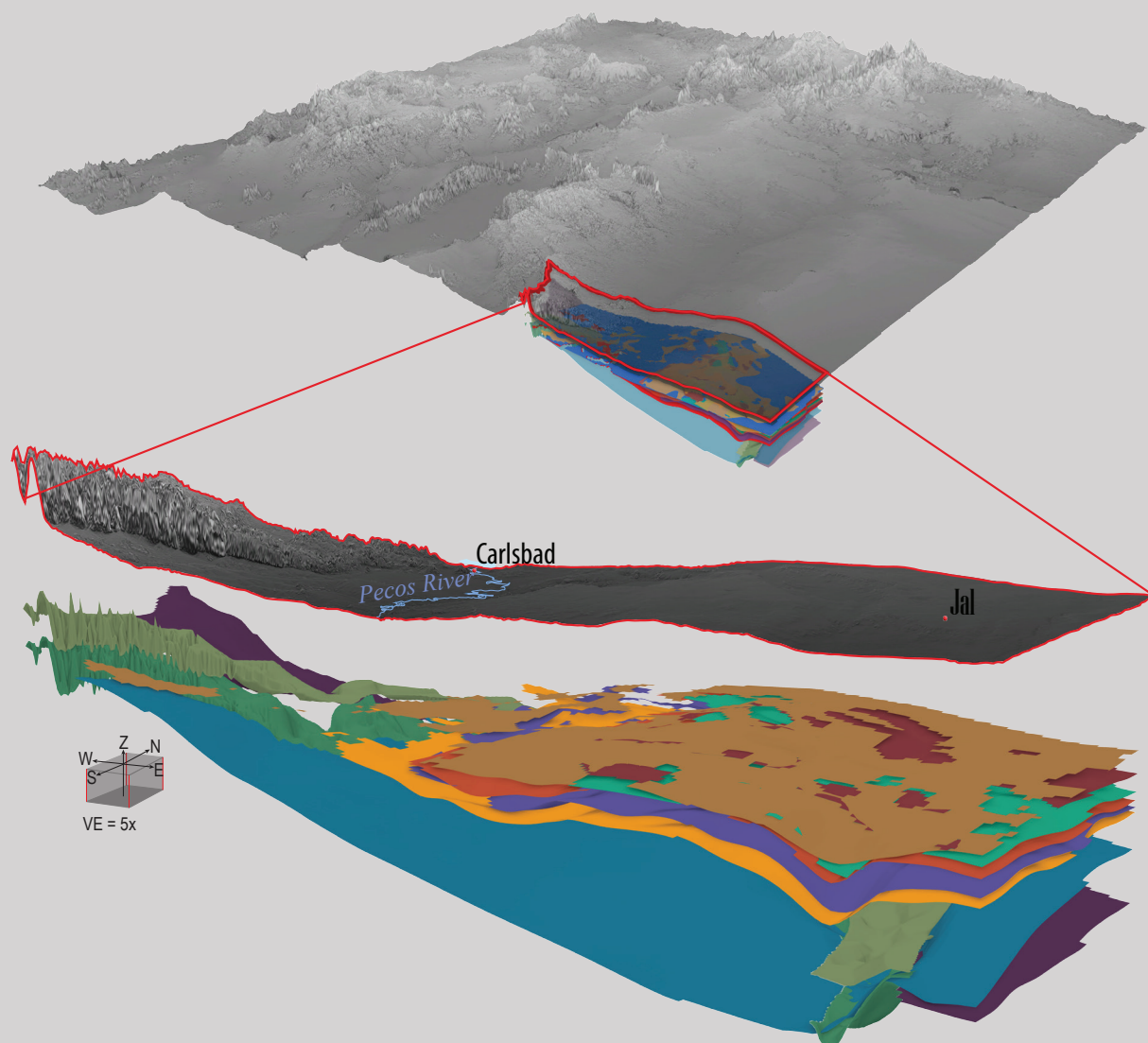# Three-Dimensional Hydrogeologic Framework of Aquifer Units in the Delaware Basin, Southeastern New Mexico

Marissa M. Fichera, B. Talon Newton, Cristopher Morton, Laila Sturgis, Alyssa Baca, and Amanda Doherty

OPEN-FILE REPORT

Open-File Report 623—Three-Dimensional Hydrogeologic Framework of Aquifer Units in the Delaware Basin, Southeastern New Mexico

Marissa M. Fichera, B. Talon Newton, Cristopher Morton, Laila Sturgis, Alyssa Baca, and Amanda Doherty

Graphics Support: Amanda Doherty

Copyediting: Frank Sholedice

Layout: Lauri Logan

Publications Program Manager: Barbara J. Horowitz

Cover Artwork: Three-dimensional view of the Delaware basin model, looking northeast from the southern corner of the state. The vertical scale has been exaggerated five times to show detail.

ACKNOWLEDGMENTS

CONTENTS

Figures

Tables

EXECUTIVE SUMMARY

Three-dimensional, geographic information system (GIS)-based subsurface geologic models are becoming increasingly common tools for visualizing, evaluating, and managing subsurface resources. The New Mexico Bureau of Geology and Mineral Resources Aquifer Mapping Program is developing 3D hydrogeologic-framework models of groundwater basins in New Mexico. These models include a suite of geologic raster surfaces, geologic control points, aquifer boundaries, and groundwater level, water depth, and water quality data compiled in a readily available GIS map package. The result is a repository of pertinent shallow subsurface data for a given groundwater basin.

The project described here is for the Delaware basin of southeastern New Mexico, where shallow groundwater aquifers overlie some of the world's most prolific oil and gas reservoirs. The New Mexico Energy, Minerals and Natural Resources Department Oil Conservation Division funded this project to better protect and manage water resources in this part of the state, facilitate the well drilling permit process, and make spill response quicker and more informed. The study area encompasses roughly 4,200 mi^2 and 6,000 ft of depth in New Mexico's Eddy and Lea Counties. The western boundary of the study area coincides with the western side of the Guadalupe Mountains. The northern boundary coincides with the southern boundary of the previously completed Pecos Slope/Southern High Plains 3D hydrogeologic model. The eastern and southern boundaries extend to the New Mexico-Texas state line. The main population centers include Carlsbad, Hobbs, Lovington, and Jal, together with the smaller communities of Loving and Malaga located along the Pecos River. The Guadalupe Mountains are a significant recharge area for groundwater resources in the Carlsbad area and the southernmost reach of the Pecos River in New Mexico. Oil and gas production and associated saltwater injection activities are strikingly conspicuous throughout the project area, and underground mines southeast of Carlsbad are an essential source of the nation's potash supply. Additionally, the Waste Isolation Pilot Plant's radioactive waste repository is located in the north-central portion of the study area. The amount and variety of subsurface activity highlight the need for digital 3D hydrogeologic data suitable for efforts to manage subsurface resources in this region.

We developed digital elevation models (geologic-structure maps) for the basal contacts of the following lithologic units (formations or groups, in ascending order): the Permian-age Capitan Formation, Artesia Group, Castile Formation, Rustler Formation, and Dewey Lake Formation; the Triassic Dockum Group; and undivided Cenozoic deposits, which include primarily Quaternary alluvial and piedmont deposits and some Ogallala Formation. Aquifer systems are delineated using lithologic boundaries and inferred hydrologic connectivity between lithologic units, resulting in two distinct aquifer systems referred to as the Delaware Basin Aquifer System (DBAS) and the Capitan Reef Aquifer System (CRAS). The DBAS comprises the Rustler Formation at its base and overlying Permian- through Triassic-age formations and extends from the Pecos River south and east to the New Mexico-Texas state line. The CRAS includes the Capitan Formation and Artesia Group strata and surrounds the Delaware structural basin. We developed digital maps of aquifer extent and base elevation, potentiometric surface, depth to water, maximum saturated thickness, and water quality for the DBAS and CRAS.

Spatial variability in permeability within formations created challenging conditions for mapping aquifers in this region. Due to the frequently confined conditions of aquifer units, aquifer volumes are not estimated here. Caution should also be used in interpreting saturated thickness values, which represent a maximum depth over which several different aquifer zones may be found. In general, groundwater with total dissolved solids (TDS) concentrations less than 10,000 mg/L occurs within 1,000 ft of the surface; however, while groundwater with TDS concentrations greater than 10,000 mg/L occurs at depths greater than 1,000 ft below the surface, these high-TDS waters are also observed within 1,000 ft of the surface.

INTRODUCTION

The Delaware basin is one of three major structural subbasins (Delaware, Midland, and Val Verde) in the greater Permian basin, which covers more than 75,000 mi² in southeastern New Mexico and western Texas (Fig. 1). This region has been the focus of geological investigations for over 100 years, and interest intensified when oil was discovered in the 1920s (Keller et al., 1983). The Permian basin is one of the largest hydrocarbon-producing basins in the world (Energy Information Administration, 2022). As a result, Permian and older geologic units have been intensively studied and characterized for their hydrocarbon-bearing and saltwater-disposal potential.

The pear-shaped Delaware basin encompasses roughly 13,000 mi² in Lea and Eddy Counties in southeastern New Mexico, and Loving, Winkler, Ward, Reeves, Culberson, Jeff-Davis, and Pecos Counties in western Texas (Figs. 1 and 2). The structural basin is surrounded by Permian marine shelf-margin carbonate rocks of the Capitan Formation, colloquially referred to as the "Capitan Reef." This study focuses on relatively shallow geologic units that underlie the New Mexico portion of the Delaware basin and the surrounding marine shelf. Shallow lithostratigraphic units emphasized in this study include (in ascending order) the Permian-age Capitan Formation, Artesia Group, Castile Formation, Salado Formation, Rustler Formation, and Dewey Lake Formation; overlying Triassic Dockum Group strata; and Cenozoic deposits, including the Ogallala Formation and Quaternary alluvial and piedmont deposits (Figs. 3 and 4). These sedimentary units include Permian evaporites (gypsum, salt), low-permeability to cavernous carbonates (dolomite/limestone), and siliciclastic deposits ranging in grain size from mudstone to conglomerate. Importantly, these near-surface geologic units host the region's groundwater resources, economically significant potash deposits, the federally administered Waste Isolation Pilot Plant (WIPP) radioactive waste repository, and tourist attractions, including Carlsbad Caverns National Park (Fig. 2).

Groundwater is present in each of the geologic units mentioned above and can be grouped into two major aquifer systems. The Delaware Basin Aquifer System (DBAS) is largely east of the Pecos River and formed by the Rustler, Dewey Lake, Dockum, and Cenozoic deposits, including those east of the Guadalupe Mountains escarpment in the Black River valley. Distinction between these formations was difficult at this modeling scale, with geophysical logging rare or difficult to resolve at these shallow depths, and water well logs that show completion over multiple zones in some regions. The Capitan Reef Aquifer System (CRAS) is formed by the Capitan Reef formation and parts of the Artesia Group along the Capitan Reef trend in the western and northern parts of the study area (Figs. 3 and 4). The aquifer systems overlap beneath the city of Carlsbad (pop. 31,888; U.S. Census Bureau, 2021), where groundwater from the Capitan Reef formation is the principal source of fresh water for municipal use.

Groundwater withdrawals in Eddy and Lea Counties are primarily used for agricultural irrigation of approximately 25,000 acres between Avalon Dam and the mouth of the Black River near Malaga (Bogener, 1993). Groundwater use for this practice is estimated at approximately 70 to 80% of total withdrawals for Eddy and Lea Counties (Magnuson et al., 2019). Agriculture in the region is strongly supported by surface water from the Pecos and Black Rivers, which are managed by the Bureau of Reclamation and the Carlsbad Irrigation District.

Water use for the mining sector in this basin, including potash mining and oil and natural gas extraction, can be more difficult to tally due to a mixed use of shallow groundwater and deeper saline groundwater. A Bureau of Land Management report (BLM, 2019) estimates that, of the 95,800 acre-feet (acre-ft) of water used for mining operations in the BLM Pecos District, 99% of that water was withdrawn from a saline aquifer (note that the BLM Distict boundary roughly matches the NM portion of the Permian basin).
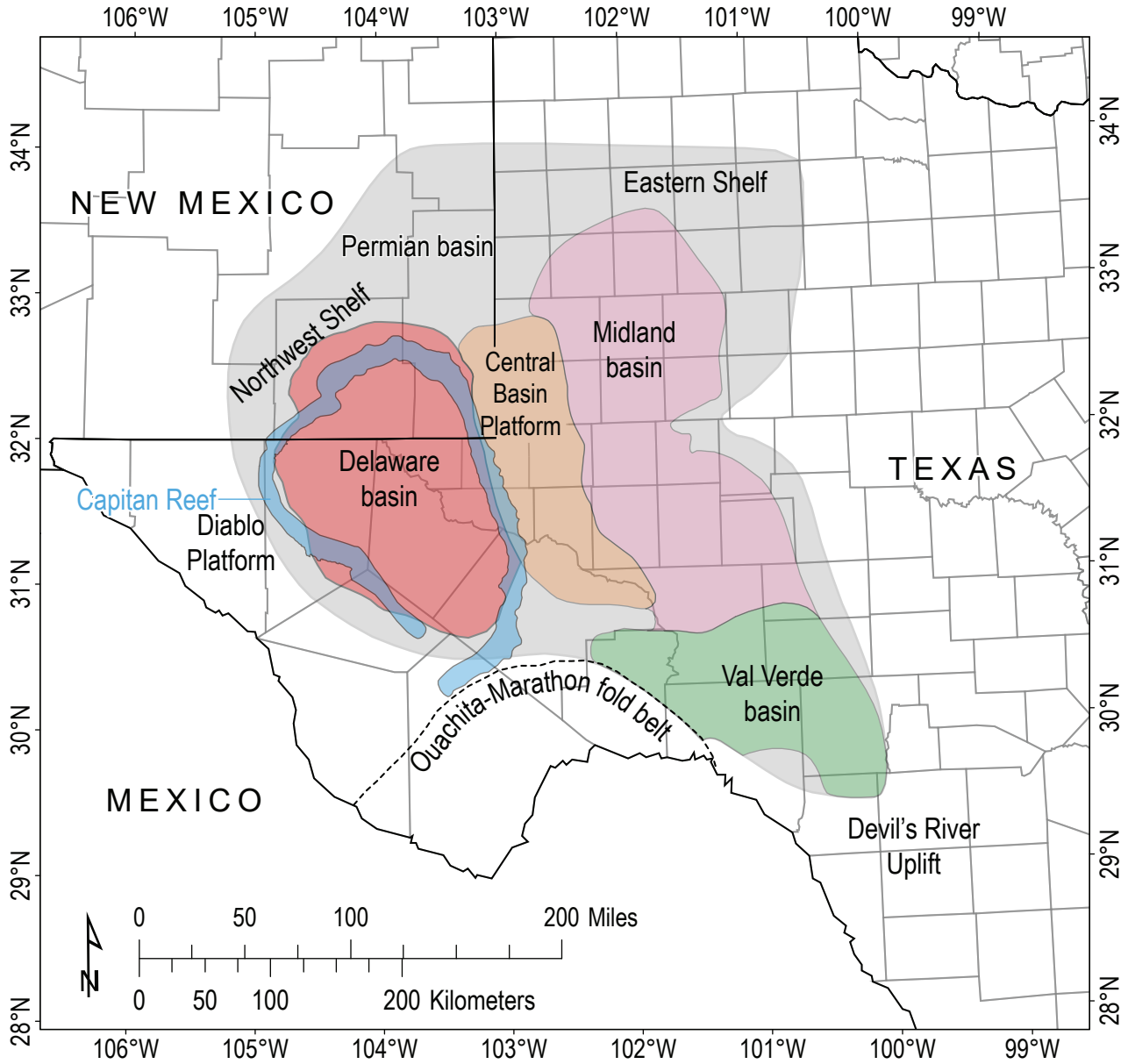
Figure 1. Extent of the Permian basin and component subbasins in southeastern New Mexico and western Texas. The New Mexico portion of the Delaware basin is the subject of this study. The Central Basin Platform, Northwest Shelf, Eastern Shelf, and Devil's River Uplift were basin-bounding highs formed during the late Paleozoic Ancestral Rocky Mountains uplift. Tectonic stress from the Ouachita-Marathon orogenic belt isolated and segmented the Permian basin. The Capitan Reef trend outlines the Delaware basin. Spatial data source: Energy Information Administration based on DrillingInfo Inc., University of Texas Bureau of Economic Geology, U.S. Geological Survey, and Texas Water Development Board.
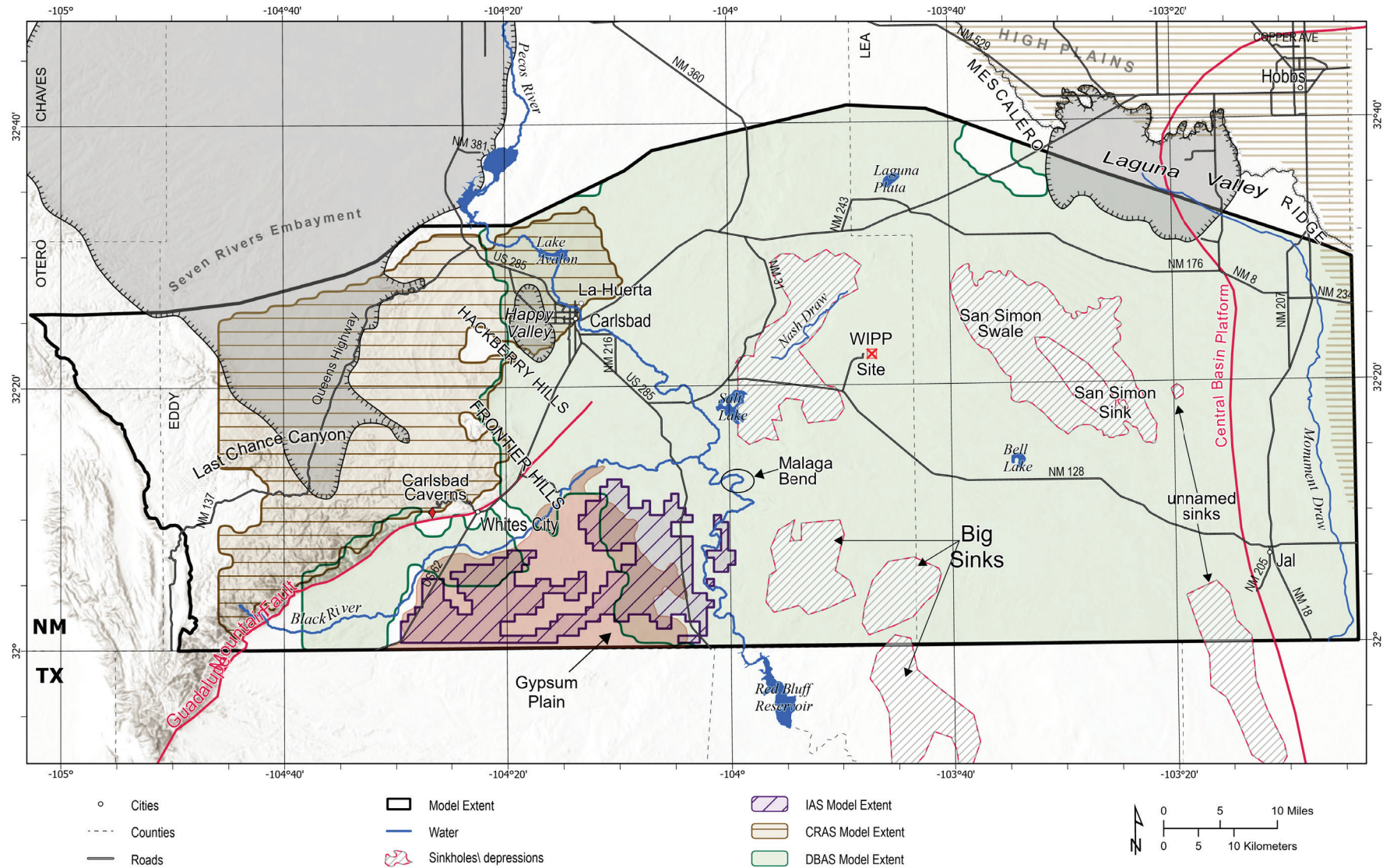
Figure 2. Key features and locations within the Delaware basin 3D mapping region in southeastern New Mexico.

Figure 3. Generalized geologic map with significant surface and subsurface geologic features noted. Dissolution features include Nash Draw east of Carlsbad, a cluster of sinks known as "Big Sinks" near the New Mexico-Texas state line, San Simon Sink and San Simon Swale, and depressions containing deep Cenozoic fill along the eastern Capitan Reef trend (Jones, 2016). Dissolution features were georeferenced from Anderson (1981).
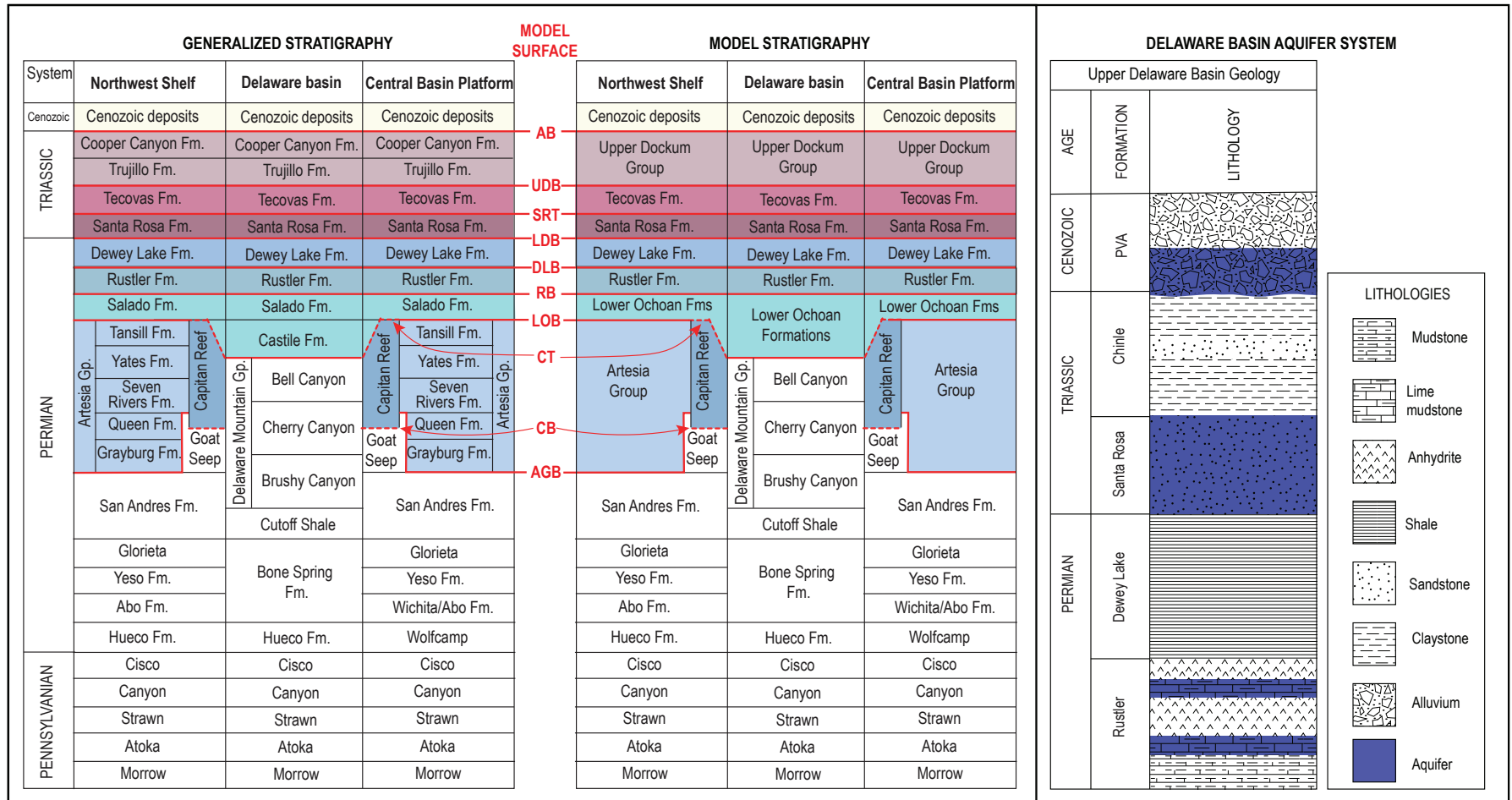
Figure 4. Generalized stratigraphic column of geologic units in the study area and corresponding model stratigraphy. Model surfaces indicate geologic contact modeled in 3D as continuous elevation surfaces (rasters) in ArcGIS. Model surfaces include AB: alluvium base (including Pecos River valley alluvium), UDB: upper Dockum Group base, SRT: Santa Rosa Fm. top, LDB: lower Dockum Group base (includes Tecovas and Santa Rosa), DLB: Dewey Lake Fm. base, RB: Rustler Fm. base, LOB: lower Ochoan fms. base, CT: Capitan Fm. top, CB: Capitan Fm. base, and AGB: Artesia Group base. A detailed view of the aquifer-bearing units of the Delaware Basin Aquifer System is shown on the right, illustrating the partially saturated nature of these units. Readers should be aware that naming conventions are not consistent for formations as they cross state lines; e.g., the Chinle Fm. is only named as such in New Mexico, and in Texas it is the Tecovas and upper Dockum Group.

The New Mexico Office of the State Engineer (NMOSE) water use by category data (Magnuson et al., 2019) do not include tracking for saline/brine water, which is pumped and then returned by injection to deep saline sources; however, NMOSE estimates that mining withdrawals account for 1% and 8% of water use in Lea and Eddy Counties, respectively. The 2019 BLM report estimates a much higher usage for mining purposes: 31% of all Lea County withdrawals. Hydraulic fracturing (fracking), used in the extraction of petroleum resources in the region, was estimated to use 5,325 acre-ft of fresh water at a rate of 3.2 acre-ft per well in Eddy County and 4.5 acre-ft per well in Lea County (Engler and Cather, 2014).

Substantial amounts of potassium salts (sylvite, potassium chloride) are concentrated in the McNutt potash zone (Fig. 3; Vine, 1963; Austin, 1978). Solution mining, the technique used to extract potash deposits, uses water to dissolve evaporite formations in the subsurface. When evaporites dissolve, overburden from overlying sediments causes dissolution collapse and creates a significant geologic hazard. Evidence of this is seen in several natural and mining-created land-subsidence features (Fig. 3) that are common across the region (Vine, 1960; Bachman, 1980, 1987; Anderson, 1981; Powers et al., 2003; Stafford, 2013). Furthermore, groundwater salinity increases as it flows through evaporitic units. The lithologic heterogeneity creates a complicated hydrogeologic system with implications for resource management and hazard mitigation.

While deeper units have been studied extensively in the form of geophysical log interpretation, seismic surveys, and log correlations, a similar comprehensive regional framework does not exist for the shallow geologic units, despite there being enough well control, geologic understanding, and societal need to do so. We compiled the region's existing geologic and hydrologic data to develop a digital, 3D hydrogeologic framework of the shallow subsurface in the Delaware basin. The resulting downloadable digital data package gives data users easy access to the extensive amount of available subsurface geologic and hydrologic data for this region, the 3D geologic surfaces developed for this project, updated aquifer mapping, potentiometric surfaces, and depth-to-water maps. This 3D framework and accompanying data can lead to a more in-depth understanding of the shallow subsurface in the Delaware basin.

GEOLOGIC SETTING

The geologic history of the Permian basin has been discussed in many reports (e.g., King, 1942; Keller et al., 1983; Hills, 1984; Kues and Giles, 2004), and no attempt is made here to provide a complete account. Basin development occurred during the Mississippian through the Permian collision of Laurentia with Gondwana (Muehlberger, 1965; Sales, 1968; Kluth and Coney, 1981; Goetz and Dickerson, 1985; Pindell, 1985; Ross and Ross, 1985; Budnik, 1986; Algeo et al., 1991; Dickerson, 2003; Dickinson and Lawton, 2003). Prior to the collision, the southern continental margin of Laurentia contained the Tobosa basin (Walper, 1982; Keller et al., 1983; Arbenz, 1989; Li et al., 2008), a region characterized by subsidence and relatively continuous accumulation of sediment during the early Paleozoic time (Galley, 1958; Hills, 1984; Horak, 1985). Northward-directed thrusting of lithospheric crust formed the Ouachita-Marathon orogenic belt and caused the development of a segmented foreland basin to the north, creating several uplifts and adjacent basins (Fig. 1; Kues and Giles, 2004). Tectonic stress and preexisting zones of weakness in Proterozoic basement rocks segmented the Permian basin along the Central Basin Platform (Ross, 1986; Yang and Dorobek, 1995; Ewing, 2016; Soto-Kerans et al., 2020), with the deep Delaware basin lying to the west (Fig. 1; Ewing, 1993).

As Kues and Giles (2004) summarized, tectonism, sea level changes, and climatic variations all played important roles in determining the character of the late Paleozoic stratigraphic record. During Pennsylvanian time, the Ancestral Rocky Mountains (ARM) to the north provided siliciclastic sediment to the Delaware basin, and a succession of mixed carbonate and siliciclastic sediment was deposited (Fig. 4). Subsidence of the Delaware basin and continued deposition of carbonate and siliciclastic sediment of the Wolfcamp and Bone Spring Formations continued in early Permian (Cisuralian) time, and by middle Permian (Guadalupian) time the ARM highlands were eroded away, leaving the Delaware basin surrounded by a relatively shallow marine shelf. The Artesia Group, Capitan Formation, and Delaware Mountain Group record the shelf, shelf-margin, and basin deposition during this time, respectively. Thus, fine-grained siliciclastic deposits of the Delaware Mountain Group were deposited in the basin, carbonate banks (Goat Seep Dolomite/Limestone and Capitan Formations) accumulated on

the shelf margin in shallow marine conditions, and the mixed carbonate-evaporite-siliciclastic deposits of the Artesia Group accumulated on the shelf (Figs. 3 and 4).

By late Permian (Lopingian) time, the Delaware basin became nearly isolated from open marine waters and existed in a hot, arid, equatorial environment (Kues and Giles, 2004). The Castile, Salado, Rustler, and Dewey Lake Formations were deposited during this time interval (Fig. 4). As discussed in some detail by Hill (1996), the Castile Formation consists mainly of calcium sulfate (gypsum/anhydrite); the Salado Formation contains thick sequences of salt (halite, with economically important amounts of potash minerals); the Rustler Formation consists of a mixed succession of siliciclastic, evaporite (sulfate), and carbonate deposits; and the Dewey Lake Formation records the deposition of red bed silt, mud, and sand. According to some researchers, the region was subjected to erosion and tilted eastward during early and middle Triassic times, producing an angular unconformity between the Dewey Lake Formation and overlying Triassic strata (Kues and Giles, 2004).

Terrestrial clastic depositional environments dominated during the late Triassic time. Triassic stratigraphic nomenclature varies in southeastern New Mexico. Lucas and Anderson (1993) and Lucas (2004) refer to Triassic rocks as the Chinle Group, whereas Lehman (1994) assigns these strata to the Dockum Group, consisting of (in ascending order) the Santa Rosa and Tecovas Formations of the lower Dockum Group, and the Trujillo, Cooper Canyon, and Redonda Formations of the upper

Dockum Group (Fig. 4). While in some literature the formations above the Santa Rosa are labeled simply as the Chinle, the Dockum Group terminology is used here for consistency with surrounding 3D models (Ewing et al., 2012; Deeds et al., 2015; Cikoski et al., 2020). Both sequences are dominantly fluvial, with local lacustrine deposits that may be associated with paleodepressions caused by subsurface salt dissolution (Lehman and Chatterjee, 2005).

Shallow marine conditions returned to the area during Cretaceous time; however, subsequent erosion has, for the most part, removed these rocks from the study area (Fallin, 1988, 1989). Since the Cretaceous, subaerial conditions have persisted across the study area. The Ogallala Formation and overlying Quaternary piedmont-alluvial deposits reflect dominantly alluvial and eolian depositional processes during the Cenozoic (Cikoski et al., 2020).

REGIONAL HYDROGEOLOGY

We define the multiple recognized aquifer units of the Delaware basin as (1) the Capitan Reef Aquifer System (CRAS), which contains the Artesia Group and Capitan Formation (Table 1), including the Capitan Reef escarpment; (2) the Delaware Basin Aquifer System (DBAS) that covers most of the basin and contains geologic units overlying the Salado and Castile Formations; and (3) an intermittent alluvial aquifer discontinuously present across the study area, extending eastward from the Pecos River where generally non-fresh-water-bearing units (Salado, Castile Formations) contain isolated zones of alluvium and valley fill with acceptable water quality for stock or domestic uses.

Table 1. Summary of aquifer characteristics for primary water-bearing formations.

Aquifer system	Formation	Specific capacity (gpm/ft)	Hydraulic conductivity (ft/d)	Transmissivity (ft^2/d)
DBAS	Alluvium	12–1,200	13–281	170–38,765
DBAS	Rustler	1.7–8.6*	0.001–307	0.0003–8,172
DBAS	Santa Rosa	11.2*	9.4–10.8*	350–3,200*
CRAS	Capitan Reef	40–275	1–25	500–53,469

* In Texas

Sources: Hale, 1945; Hendrickson and Jones, 1952; Bjorklund and Motts, 1959; Mercer, 1983; Richey et al., 1985; Barroll et al., 2004; Berry, 2011.

Note: Coefficients of transmissibility in (gal/d)/ft and permeability in (gal/d)/ft^2 from literature were converted to transmissivity (ft^2/d) and hydraulic conductivity (ft/d), respectively, by dividing the latter by 7.48, as per Hood (1977). DBAS: Delaware Basin Aquifer System, CRAS: Capitan Reef Aquifer System.

The aquifer systems described here range from zones of confining conditions to highly permeable conditions, often within the formations/groups themselves. Several examples include mudstones overlying sandstones in the upper Dockum Group and fine-grained limestones/evaporates overlying karstic/highly permeable limestones in the Rustler Formation. The DBAS in particular is best described as a series of perched aquifer systems with zones of high and low mixing and saturation. The limited resolution of water level and well completion/ formation data resulted in the combined mapping of the semi-confined units in this region.

Precipitation in the Guadalupe Mountains is the primary source of groundwater recharge for the Eddy County portion of the study area, where diffuse percolation and focused recharge contribute to both the CRAS and DBAS (Richey et al., 1985). Literature indicates that there is extensive mixing between the DBAS and CRAS in the area around and north of Carlsbad, where the Pecos River provides a potentiometric low and groundwater from the surrounding area is discharged (Hale, 1945; Hiss, 1980; Richey et al., 1985). Mixing between the two systems is facilitated by the historical erosion and deposition of alluvium by the Pecos River, which effectively creates a conduit of relatively high hydraulic conductivity for water to discharge to, while effectively recharging the alluvial aquifer of the DBAS (Richey et al., 1985). Most of the groundwater of the CRAS and the DBAS west of the Pecos River that is not evapotranspired or intercepted by shallow wells is discharged to the Pecos River (Hale, 1945; Hiss, 1980). Irrigation withdrawals for agriculture are a source of groundwater discharge from both the CRAS and DBAS, while irrigation return flows also contribute to recharging the alluvial aquifer, though only to a minor extent (Bjorklund and Motts, 1959).

Groundwater in southeastern Lea County is recharged in areas near Bell Lake and in the High Plains north of the study area, where water percolates from temporary lakes formed after precipitation events; groundwater in southwestern Lea County is recharged by precipitation on and around outcroppings of the Santa Rosa Sandstone and Cenozoic deposits, where it creates a sort of groundwater "mound" from which water flows outward (Nicholson and Clebsch, 1961; Hiss, 1980; NMOSE, 2016a, 2016b). Nicholson and Clebsch

(1961) cite Theis (1937) for a suggested recharge rate of 0.25–0.5 in. per year for southern Lea County. Some of the groundwater in western Lea County of the study area flows west and discharges to the Pecos River, while some moves east and south into Texas (Nicholson and Clebsch, 1961; Hiss, 1980). Groundwater is thought to flow vertically from the Santa Rosa Formation to underlying Permian-age formations, especially in areas of collapse structure such as the San Simon Swale, or otherwise continue flowing to the southeast following the regional dip of Triassic rocks (Nicholson and Clebsch, 1961). The dominant uses of groundwater throughout the study area are irrigation, mining (including oil/gas), and public supply (Magnuson et al., 2019). In 2015, irrigation withdrew 256,093 acre-ft, mining withdrew 94,129 acre-ft, and public supply withdrew 26,500 acre-ft of groundwater in Eddy and Lea Counties combined, though 98% of mining withdrawals were of saline water (Magnuson et al., 2019). These figures represent groundwater withdrawals throughout the entire counties, not just the portions within the study area.

Myriad sinkholes, depressions, springs, and caves from the dissolution of salts and carbonates can be found throughout the study area due to the abundance of soluble evaporite and carbonate deposits in the region. These features are created by surface (epigene) and subsurface (hypogene) hydrologic processes that incise from above and erode from below, though epigene karst formations are more limited in size and extent than hypogene formations (Stafford et al., 2008). Hypogene karst formations form in evaporites by pressure and density differentials that cause groundwater unsaturated in minerals to upwell from deeper geologic units, while the denser saturated groundwater descends, driving convection and further dissolution (Stafford et al., 2008; Stafford, 2013). Extensive dissolution can lead to larger collapse structures that are visible from the surface and topographic depressions, such as Nash Draw and San Simon Swale (Fig. 2). These depressions can contain playas and salt lakes where groundwater discharges into playas, and may assist groundwater recharge after precipitation events (Bjorklund and Motts, 1959; Nicholson and Clebsch, 1961; Land, 2005). Karst features also play a role in the mixing of groundwater between geologic units in the area around Carlsbad, especially from the Capitan Reef to the Pecos River alluvium (Bjorklund and Motts, 1959; Richey et al., 1985).

WATER QUALITY

Surface water in this region has been described since at least 1582, when Spanish explorers noted salt springs along the Pecos River (Kunkler, 1980). The Pecos River generally increases in salinity as it moves downstream; however, the hydrologic groundwater flow paths within the study area are particularly complex. In the stretch of the Pecos River from Brantley Dam to Malaga, there is an observed 40% reduction in flow rate and a 4% reduction in total dissolved solids (TDS), indicating a strong recharge to groundwater (Yuan and Miyamoto, 2005). At Malaga Bend, an upward-leaking brine from the base of the Rustler Formation results in discharge of about 0.5 ft^3/s of saturated brine, which contributes approximately 200 to 400 tons of sodium to the river per day (Havens and Wilkins, 1979; Kunkler, 1980). Between Malaga Bend and the state line (Red Bluff gage), the flow rate and TDS in the river remain relatively unchanged, suggesting that the river is not gaining or losing much water in this reach (Yuan and Miyamoto, 2005).

There has been much hydrochemical research in the Delaware basin and other surrounding subbasins of the Permian basin (Nicholson and Clebsch, 1961; Geohydrology Associates Inc., 1978; Richey et al., 1985; Dutton and Simpkins, 1986; Lambert and Harvey, 1987; Siegel et al., 1991; Davidson, 2003; Reyes, 2014). Most of this research has focused on the shallow phreatic aquifer system, which produces water for agriculture, industry, and municipalities and overlies Ochoan formations, which form an evaporite capstone to the deep basin aquifer (Rosenau-Davidson, 2003). For the DBAS, we analyzed hydrochemical data for wells that are mostly producing water from the shallow phreatic aquifer, which includes (from oldest to youngest) the Rustler Formation, the Dewey Lake Formation, the upper and lower Dockum Group, the Ogallala Formation, and Cenozoic alluvium. In general, water quality in this shallow system is fair to good, with TDS concentrations less than 3,500 mg/L. However, Na-Cl brines are observed to significantly impact water quality throughout this system in localized areas of the DBAS. This system is primarily recharged in outcrops in the Guadalupe Mountains, local outcrops of other aquifer lithologies, and dune deposits in Lea County.

The following assessment of groundwater chemistry for the DBAS and CRAS uses Piper diagrams (Fig. 5) to graphically categorize water types based on relative concentrations of major cations [calcium (Ca^{2+}), magnesium (Mg^{2+}), sodium (Na$^+$), potassium (K$^+$)] and anions [chloride (Cl$^-$), sulfate (SO$_4^{2-}$), bicarbonate (HCO$_3^-$)]. The relative ion concentration for a specific cation or anion is plotted as the proportion of the total cations (left ternary plot) or anions (right ternary plot). Identification of the dominant cation(s) and anion(s) is used to determine the water type for the water sample. Data points are projected from each ternary diagram onto the diamond portion of the Piper diagram. Figure 5 shows where the different water types plot on the diamond section.

The CRAS includes the Artesia Group and the Capitan Limestone, which is highly permeable due to interconnected fractures and solution channels. This system collects water from different recharge sources, including floods in canyons and arroyos in the Guadalupe Mountains and inflow of groundwater from adjacent shelf formations (Artesia Group). Relatively fresh water (TDS <700 mg/L) occurs from the southern part of Carlsbad southwestward for over 20 mi (Bjorklund and Motts, 1959). These waters are Ca-HCO$_3$ water type due to the dissolution of limestone and dolomite. Underlying the western and northern parts of Carlsbad is water with TDS concentrations ranging from 700 to 1,700 mg/L. This increase in TDS is due to the mixing of fresh water moving northeastward through the CRAS with moderately saline water flowing southward. Going farther to the north toward Lake Avalon, water quality declines, with TDS concentrations above 1,700 mg/L. These higher salinities to the north are likely due to higher evaporite (primarily gypsum) content in the Artesia Group. Water quality in this area also tends to decline with depth.

The Pecos River valley alluvial aquifer to the west of the Pecos River yields water of varying quality, with TDS concentrations ranging from 500 to over 4,000 mg/L. This aquifer is largely composed of limestone, dolomite, gypsum, sand, and silt (Bjorklund and Motts, 1959). Therefore, groundwater types can range from Ca-HCO$_3$ to Ca-SO$_4$, where the Ca-SO$_4$ waters are generally higher in TDS and not potable. The best water in this aquifer occurs to the west of Carlsbad. In general, for groundwater in the alluvium, TDS concentrations increase as the distance to the river decreases.

Siegel et al. (1991) analyzed water samples from the Rustler/Salado contact zone that were determined to be Na-Cl brines. Rosenau-Davidson (2003) characterized brines in the deep aquifer below the Rustler Formation by analyzing chemistry data for produced waters associated with oil and gas production for aquifers ranging from Permian to pre-Cambrian rocks, and all brines appear to be affected by the dissolution of halite, resulting in Na-Cl-type water. As will be seen below, as TDS in groundwater increases above 3,000 mg/L, Na and Cl concentrations increase significantly, indicating that the mixing of fresher water in the shallow aquifer with these brines strongly affects water quality in the study area. Therefore, high-TDS (>3,000 mg/L), Na-Cl-type water is likely due to upward movement of these deep brines into the shallow system.

The Rustler Formation contains two water-bearing units, the Culebra and the Magenta units, that are composed of dolomite with fractured and dissolution zones. The western edge of the Rustler Formation crops out in the study area along the eastern portion of Eddy County and dips toward the east (Lowry et al., 2018). In general, hydraulic conductivities are higher to the west and lower to the east, correlating to fresher water in the west and brackish water to the east. Water produced from the Rustler Formation is primarily used for watering livestock.

Siegel et al. (1991) identified four hydrochemical facies in the Culebra Member of the Rustler Formation: (A) saline Na-Cl brine with Mg:Ca molar ratio between 1.2 and 2, low transmissivity; (B) dilute $CaSO_4$ water type, high transmissivity; (C) waters of variable composition, Mg:Ca molar ratio ranges from 0.5 to 1.2, variable permeability; and (D) brine with high K:Na weight ratios (0.22). Data used by Siegel et al. (1991) identify these different hydrochemical facies, which are shown on a Piper diagram in Figure 6. The data for the Rustler Formation (Culebra and Magenta units) appear to plot along a mixing line, representing the mixing of a high-TDS, Na-Cl-type water with a low-TDS, Ca-SO$_4$-type water. Although there are only two water samples, groundwater from the Dewey Lake Formation may exhibit a different chemical composition, with a higher relative HCO_3 concentration than the Culebra Member samples.

The Triassic lower Dockum Group is composed of the Santa Rosa and Tecovas Formations, and the upper Dockum Group consists of the Trujillo, Cooper Canyon, and Redonda Formations (Fig. 4). The Dockum Group is present in Lea County and eastern Eddy County, overlying Permian confining mudstones and evaporites and lying beneath Cenozoic alluvium. The Dockum aquifer is extensive, occurring throughout eastern New Mexico and western Texas and the western part of the Texas Panhandle. While water is produced from many sandstone and conglomerate units in the Dockum group, much of this water is produced from a lower sandstone unit (Bradley and Kalaswad, 2003), which is likely the Santa Rosa Sandstone of the lower Dockum Group. Dutton and Simkins (1986) analyzed water chemistry data for groundwater in the lower Dockum Group aquifer in the Texas Panhandle and eastern New Mexico and determined that the water chemistry is mostly controlled by water/mineral interactions, including silicate weathering, equilibration with calcite and dolomite, and ion exchange. Figure 7 shows a Piper diagram for water chemistry data for lower Dockum Group groundwater in Eddy and Lea Counties presented by Dutton and Simkins (1986). Groundwater produced from the Dockum Group in Lea County is characterized by Ca^{2+} being the dominant cation, while dominant anions include HCO_3^-, mixed anions, and SO_4^{2-}. Groundwater from the Dockum Group in Eddy County exhibits Ca^{2+} and mixed cations to be the dominant cations, while dominant anions are primarily SO_4^{2-}. These groundwaters show TDS concentrations ranging from less than 400 to over 7,000 mg/L. However, most groundwater in the Dockum aquifer in the study area has TDS concentrations less than 5,000 mg/L (Bradley and Kalaswad, 2003).

The Ogallala Formation is part of the High Plains aquifer and occurs in small volumes of the eastern portion of the study area. Figure 8 shows water chemistry data for the Ogallala and alluvial aquifers (east of the Pecos River) plotted on a Piper diagram (Geohydrology Associates Inc., 1978). Groundwater from the Ogallala Formation is generally of good quality, with TDS concentrations less than 1,000 mg/L; dominant cations are Ca, mixed cations, and Na, and dominant anions are mixed anions and SO$_4$. TDS concentrations for water in the alluvial aquifer range from less than 500 to 3,000 mg/L; dominant cations are Ca, mixed cations, and Na, and dominant anions are HCO$_3$, mixed anions, and SO$_4$.
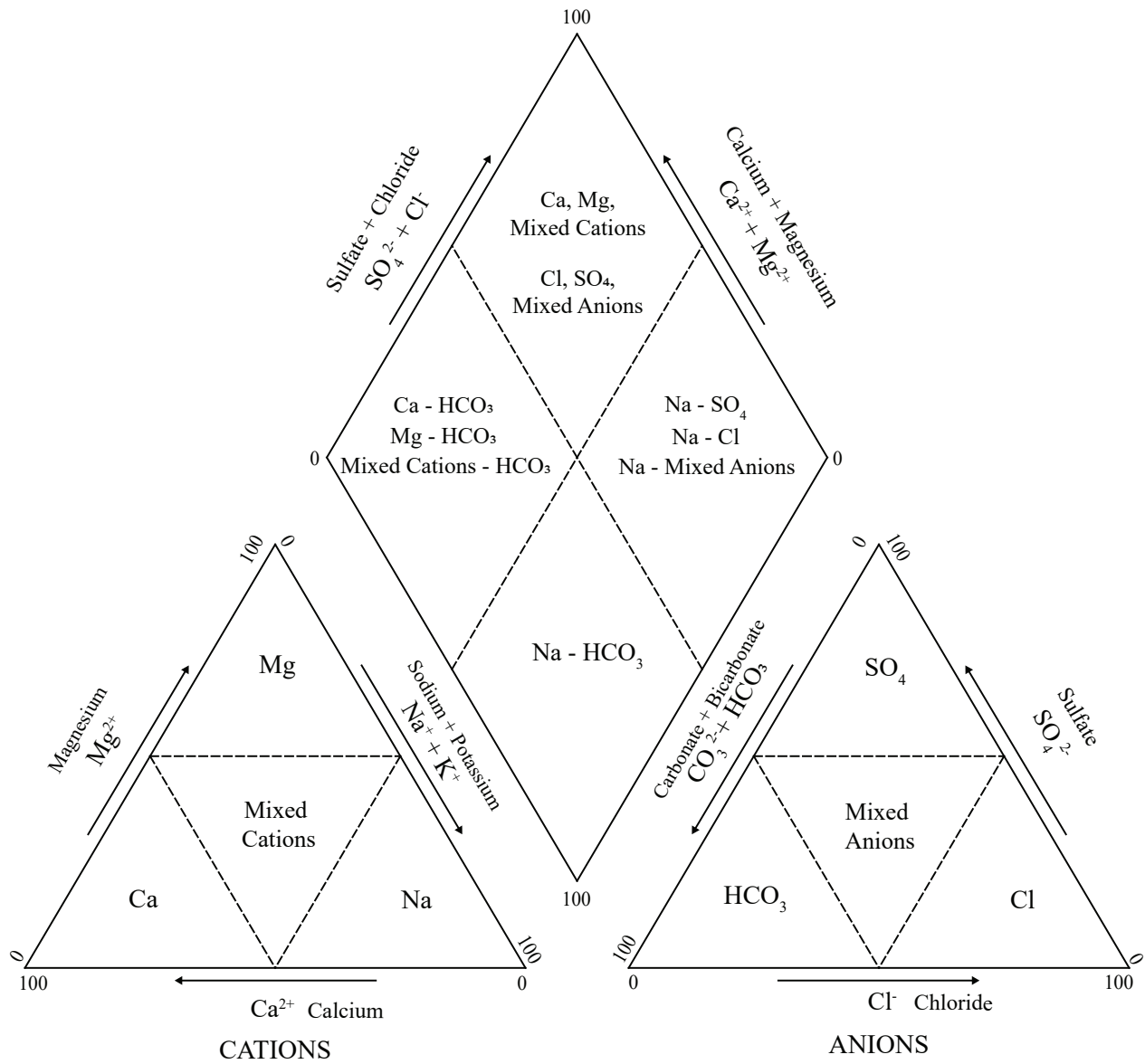
Figure 5. Example Piper diagram that shows where different water types plot.

Rustler Formation and Dewey Red Beds Groundwater
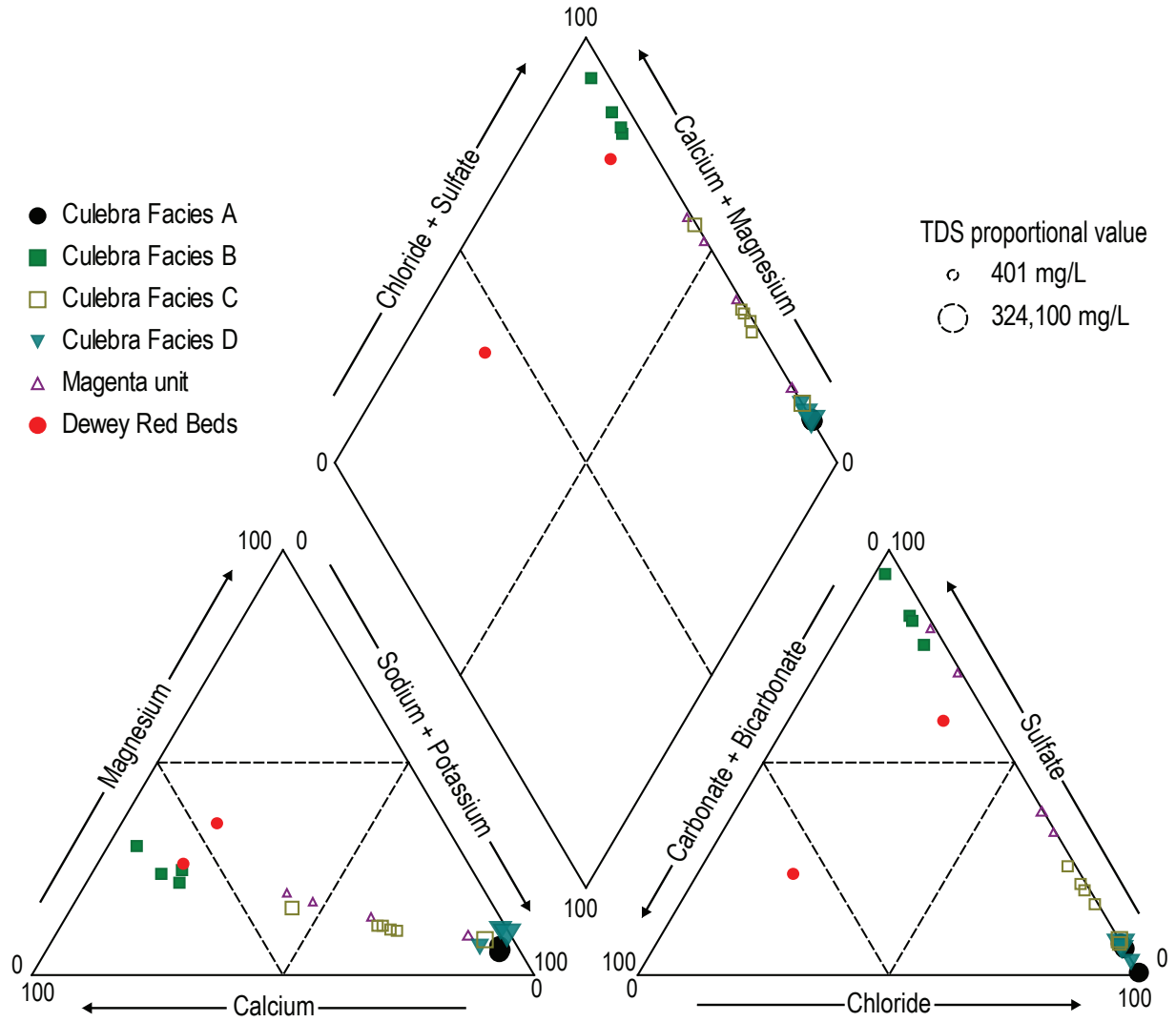
Figure 6. Piper diagram showing water chemistry data for groundwater from the Rustler and Dewey Lake Formations (data from Siegel et al. [1991]). The size of the data point is proportional to TDS concentrations; however, many of the data points fall within a similar range of concentrations.

Dockum Group Groundwater
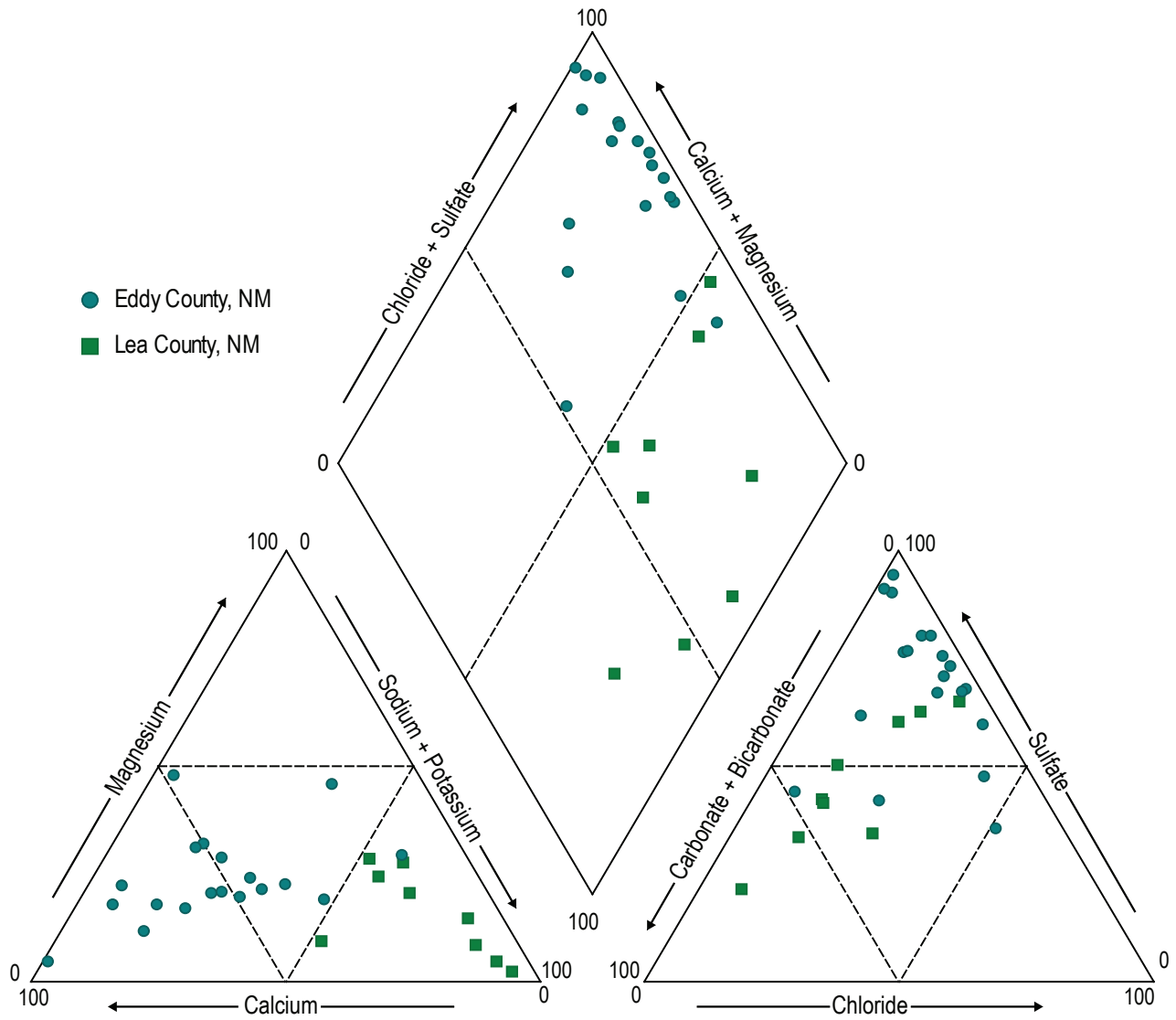
Figure 7. Piper diagram showing water chemistry for groundwater produced from the Dockum Group aquifer in Eddy and Lea Counties (data from Dutton and Simpkins [1986]).

Ogallala and Alluvial Aquifers
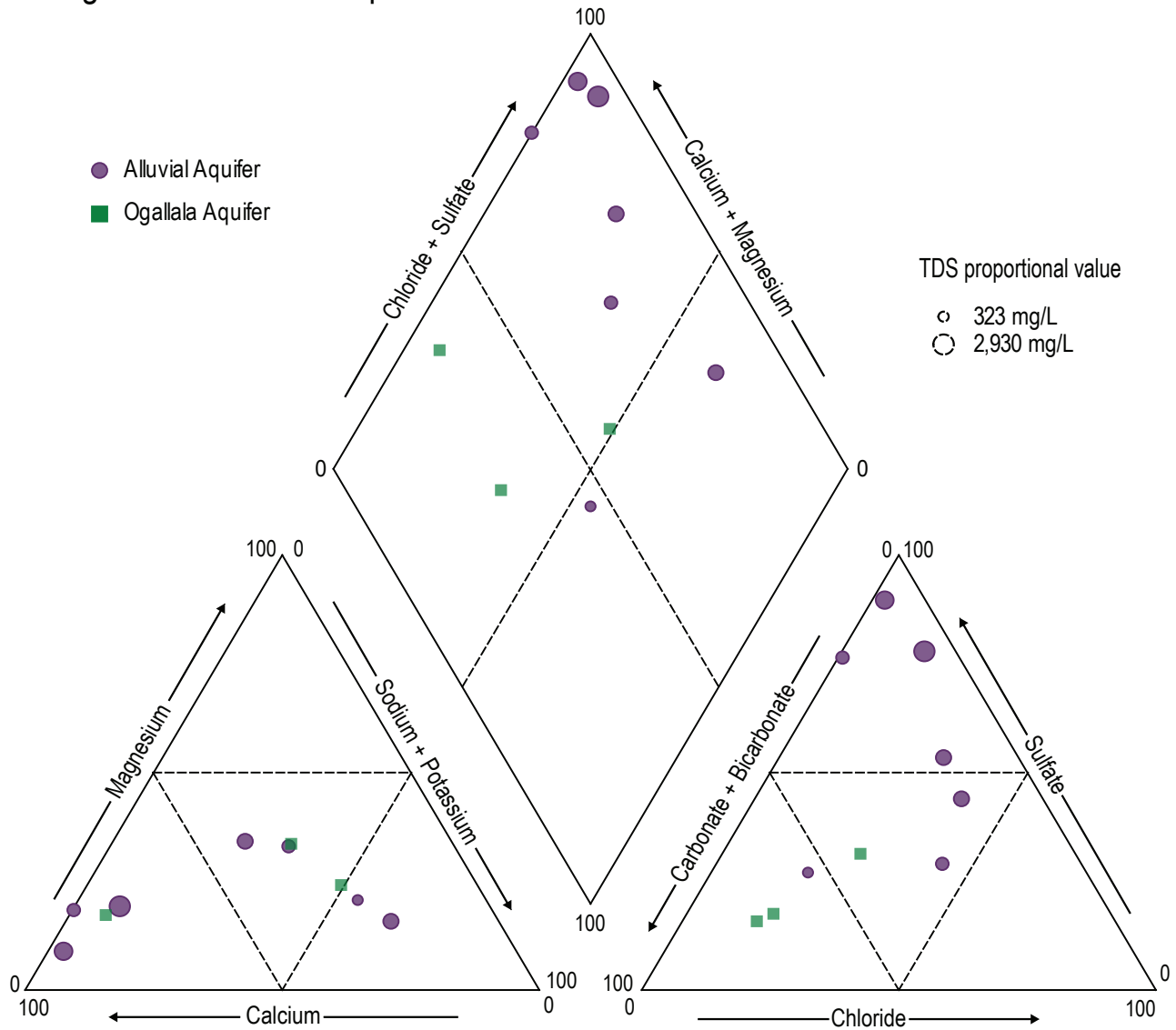
Figure 8. Piper diagram showing water chemistry data for groundwater produced from the Ogallala Formation and Cenozoic alluvium (data from Geohydrology Associates Inc. [1978]).

METHODS

3D GEOLOGIC MODEL METHODS

We developed a repeatable, robust, data-driven 3D mapping method to provide a digital package of shallow subsurface data for the Delaware basin region of southeastern New Mexico. The resulting 3D hydrogeologic model is presented as an Esri map package and contains digital geologic and hydrologic datasets representing roughly 4,000 mi^2 and over 6,000 vertical feet of subsurface geology and hydrology in southeastern New Mexico. We modeled subsurface elevations corresponding to eight geologic contacts, including (from youngest to oldest) base of Cenozoic deposits, upper Dockum Group base, Santa Rosa Formation top, lower Dockum Group base, Dewey Lake Formation base, Rustler Formation base, Salado/Castile Formations base, and Artesia Group base (Figs. 4 and 9, Table 2). The Capitan Reef formation is included from the Texas Water Development Board (TWDB) Capitan Reef Complex aquifer groundwater availability model (GAM), with

no additional processing performed (Jones, 2016). We then mapped three distinct aquifer systems within the 3D geologic framework: (1) the Delaware Basin Aquifer System (DBAS), (2) the Capitan Reef Aquifer System (CRAS), and (3) a spatially intermittent alluvial aquifer.

We performed the following processing steps to build the 3D hydrogeologic model (modified from Cikoski et al., 2020; Table 3):

1. Compile/synchronize data
2. Identify and remove outliers
3. Generate surfaces
4. Build geologic model
5. Assess uncertainty
6. Map aquifer systems using geologic framework
7. Combine geologic and hydrologic model data, rasters, and contour maps into hydrogeologic model

Table 2. Descriptions of geologic model stratigraphy.

Model stratigraphy		Model surface	General description	Base elevation ranges (ft)	Thickness (ft)
Upper Dockum Gp.		UDB	Includes Cooper Canyon and Trujillo Fms. (McGowen et al., 1977; Ewing et al., 2008; Deeds et al., 2015). Dominantly sandstones and mudstones, generally fining upward.	2,600–3,700	1–640
Lower Dockum Gp.	Tecovas Fm.	SRT	Mainly shale and sandy shale.	1,600–3,450	23–949
	Santa Rosa Fm.	LDB	Fine- to coarse-grained sandstone, minor shale layers (Nicholson and Clebsch, 1961). Generally fining upward.		13–651
Dewey Lake Fm.		DLB	Upper Ochoan series (uppermost Permian) strata. "Red beds"; terrestrial, fine-grained, clastic, thin-bedded siltstone (Cooper and Glanzman, 1971).	998–3,268	45–873
Rustler Fm.		UOB	Upper Ochoan series (uppermost Permian) strata. Clastic sedimentary rocks, evaporites, and local carbonates.	650–3,257 ft	15–894
Lower Ochoan fms.		LOB	Lower Ochoan series (uppermost Permian) strata. Salado and Castile Fms. Principally evaporites.	2,350–4,150	133–4,115
Artesia Gp.		AGB	Artesia Group shelf and/or backreef strata. Includes (in ascending order) Grayburg Fm., Queen Fm., Seven Rivers Fm., Yates Fm., and Tansill Fm.	-1,559–6,143 ft	24–1,641
Capitan Fm.*		CT	Fossil limestone reef; forms Delaware basin boundary. Massive, fossiliferous limestone in Guadalupe Mountains.	-2,505–5,770	250–2,250
		CB			

* Capitan Fm. top and base were unmodified from Standen et al. (2009) and the TWDB Capitan Reef Complex Groundwater Availability Model.
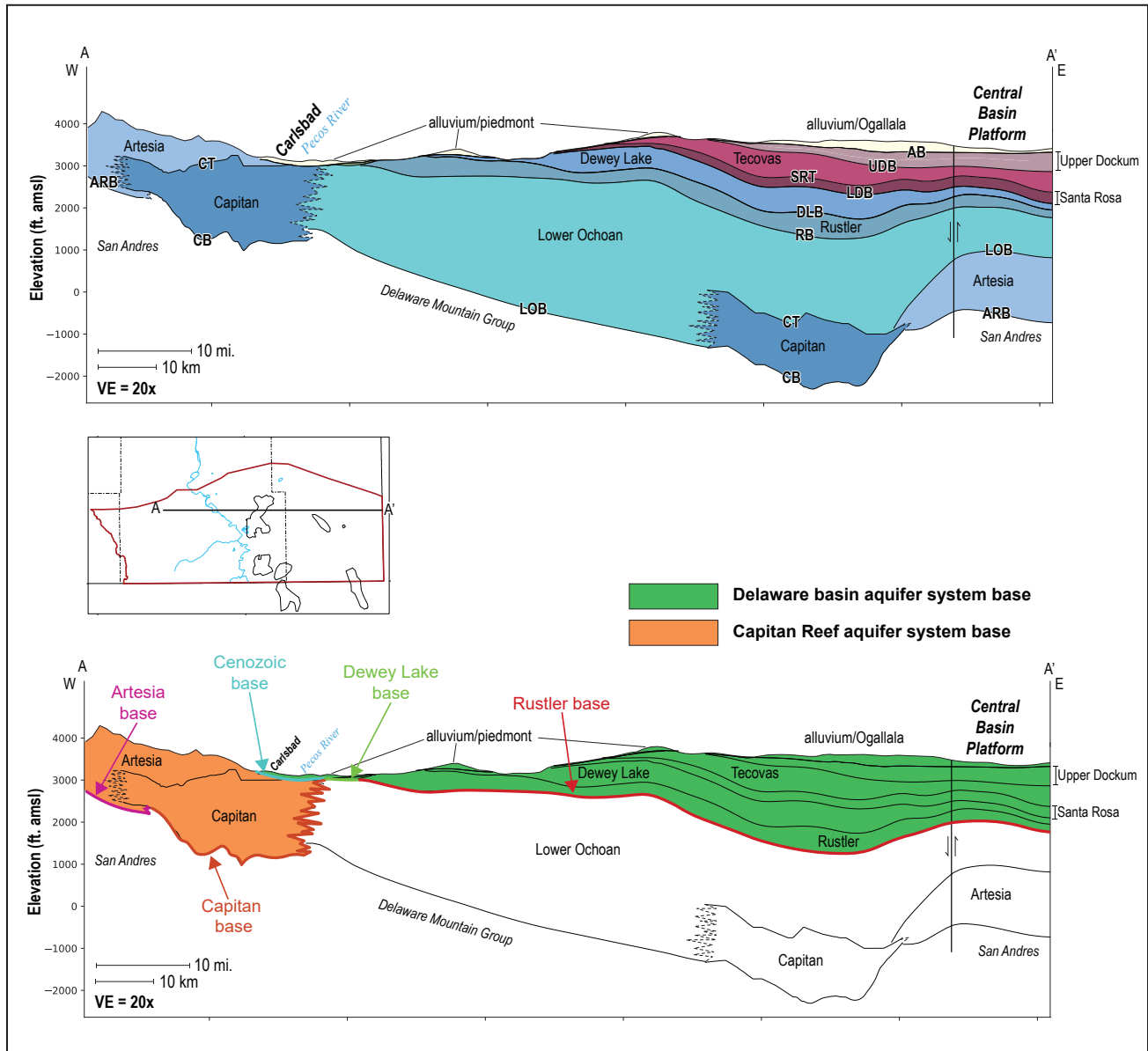
Figure 9. Geologic cross section through northern half of study area. Location shown on map. VE: vertical exaggeration.

Table 3. Data processing steps to build the 3D hydrogeologic model.

Stage	Step	Summary
(Parameters)	Processing extent	Data were collected for and processing was conducted on the study area, plus a 5-km buffer around the study area. Results were subsequently clipped to the actual extent of the study area.
	Snap raster	A 1,000-m cell size snap raster was used to ensure that rasters generated during processing had collocated and equal-sized raster cells.
	Existing rasters	Rasters for the top, base, and thickness of the Capitan Fm. are included from Standen et al. (2009).
	New rasters	Rasters generated in this project include Cenozoic deposits base, upper Dockum base, Santa Rosa top, lower Dockum base, Dewey Lake base, Rustler base, lower Ochoan series base, and Artesia Group base.
Data collection	Data management	Geologic control points are stored as point-type feature classes with easting, northing, unique ID, elevation, and data source attributes. Methodological control points that were used to develop the geologic model are not included in the final geodatabase.
	Data sources	Data were harvested from published and unpublished compilations of formation tops in well data, published structure contours, surface geologic mapping, and data collected from the NMBGMR Subsurface Library and NM OCD website.
Data synchronization	Format synchronization– line data	Line data (surface-mapped geologic contacts, structure contours) were converted to points using the ArcGIS Generate Points Along Lines tool. Points were placed every 1,000 m.
	Format synchronization– cross sections	No cross sections were digitized for this model.
	Input geologic units to model units	Data were collected on geologic units, then aggregated to model units.
Data assessment	Outlier identification and removal	Model unit control data were evaluated for outliers by fitting a Topo to Raster unit top/base elevation model to the data. Data with "error" magnitudes of >100 ft were removed. This process was repeated three times for each model unit dataset.
Data densification	Offset control estimates	Offset control estimates were generated by using published unit thickness estimates to determine the bottom and top elevations of adjacent model units at locations with control data for only some model units. Offset control estimates were used to (1) densify data-poor datasets, (2) project contacts above the land surface where a unit has been eroded, and (3) provide controls to project a contact toward where a unit pinches out or transitions to another unit in the subsurface.
Model surface generation	"Build-down" of the geologic model	A "sealed" geologic model was developed by progressively comparing each contact surface raster to the overlying contact surface raster, keeping the lower value of the two at each raster cell location. This method constructs a series of "continuous" contact surfaces that are defined at every raster cell location in the study area. Where a unit is absent, either due to erosion or a subsurface pinch out, the continuous contact surface will lie at the same elevation as the continuous contact surface of the overlying unit, and thus the model unit thickness will be 0. Discrete contact surfaces are generated by clipping each continuous contact surface to the extent across which the model unit thickness is greater than 0.
Uncertainty assessment	Data density uncertainty	Uncertainty associated with data gaps was not quantified. However, the distribution of control data is shown on all maps for assessment.
	Dataset uncertainty maps	Uncertainties in the dataset were assessed using an LXO n-fold cross-validation method (n = 500, X = 25% for each model surface). Five-hundred prediction surfaces were generated for each unit, leaving out a random selection of 25% of the data, and the standard deviation between surfaces was calculated. We then mapped the standard deviation at each grid cell to create the uncertainty map.

We compiled the following existing geologic control data: the 1:500,000 statewide geologic map of New Mexico (Scholle, 2003), well data (Bjorklund and Motts, 1959; Ewing et al., 2012; Deeds et al., 2015; Broadhead and Ulmer-Scholle, unpublished data), and structure contours (Kelley, 1971; Hiss, 1976; Ewing et al., 2012; Deeds et al., 2015; Meyer, 2020; Appendix A). We compiled data located within the study area boundary as well as within a 5-km buffer around the study area to minimize edge effects during processing. Additionally, we leveraged 1,908 newly interpreted gamma-ray logs as geologic control data for the Santa Rosa, Dewey Lake, and Rustler Formations (Appendix B).

We identified and removed outliers in each control dataset by fitting a surface to elevation data using the ArcGIS Topo to Raster interpolation tool and assessing the difference between the known elevation (i.e., the control point elevation) and the predicted elevation (i.e., the elevation predicted by the Topo to Raster interpolation at the control point's location). If this difference was equal to or greater than 100 ft, the control point was removed (Table 3). We repeated the process four times for each model unit dataset. We used the final result to create model unit datasets containing point features with easting (x), northing (y), and elevation (z) attributes.

Control data abundance varies between units. If datasets do not extend across the model extent for each unit, inaccuracies in contact extent and unit geometry tend to arise in the model-building process. We addressed this challenge by estimating control data based on average unit thickness in regions where necessary. This process is described in detail in Cikoski et al. (2020) under *Offset Control Estimates*. We then fit a final surface to each unit dataset, and the resulting raster for each model unit was input into the next model-build processing step.

The model-building process required combining individual model surfaces to create the geologic model. We implemented the iterative procedure described as the "build-down" method in Cikoski et al. (2020). This method combines surfaces in a way that accounts for erosional effects and preserves stratigraphic principles (Table 3).

We then developed uncertainty maps for each model surface using Monte Carlo methods (Table 3).

These maps represent uncertainty in the fitted surface for each model unit and **do not incorporate or represent uncertainty in the geologic control data.** For each model unit, we extracted a random sample of 75% of the geologic control data used to create the model surface that was input into the model-building process. We then ran the Topo to Raster interpolation tool on the data subset using identical parameters. We repeated this process 500 times, using a different random 75% sample subset each time. This resulted in 500 elevation rasters. We calculated and mapped the ensemble standard deviation at each grid cell to create the final uncertainty map for each unit. Uncertainty is generally high in regions of (a) sparse data coverage and (b) high topographic gradients. The latter indicates influential data points, the removal of which causes large changes in the fitted surface. We emphasize that high-uncertainty regions do not necessarily indicate unreliable control data just as low-uncertainty regions do not necessarily indicate reliable control data. We recommend that map users evaluate control data in detail for all site-specific studies, especially those located within high-uncertainty regions.

Final digital geologic datasets include (per geologic model unit) base elevation of geologic unit (raster and contour), subsurface extent (polygon), estimated uncertainty (raster and contour), and model input control data (point).

3D AQUIFER MAPPING METHODS

We mapped two aquifer systems and an area of spatially intermittent groundwater availability using the geologic framework; legacy water data, including depth-to-water measurements, water chemistry, and well depth; and new water data collected as part of this study. We compiled water well locations, water levels, well depths, and water quality data from the following sources: the New Mexico Bureau of Geology and Mineral Resources' (NMBGMR) internal database; the New Mexico Office of the State Engineer (NMOSE); the U.S. Environmental Protection Agency (EPA); the U.S. Geological Survey (USGS); the New Mexico Energy, Minerals and Natural Resources Department (NM EMNRD); and the Texas Water Development Board (TWDB). The TWDB completed several studies that characterized interstate New Mexico-Texas aquifers along the

eastern and southern borders of New Mexico as a part of their groundwater availability modeling and brackish water resources programs. These water data are publicly available in the form of GIS files and in the Brackish Resources Aquifer Characterization System Database (Fallin, 1989; Standen et al., 2009; Ewing et al., 2012; Meyer et al., 2012; Deeds et al., 2015; Jones, 2016; Meyer, 2020).

We mapped the water level surfaces for each aquifer system using water level measurements collected within the past 10 years (with the exception of two older data points included in very data-sparse areas of the model) and the 3D geologic framework as a 3D spatial constraint (Fig. 10). Control points representing the Pecos River elevation were included in the potentiometric surface calculation; however, including spring elevations typically increased model errors in those vicinities. We calculated water level elevations by subtracting the reported depth to water from the land surface elevation (extracted from a high-resolution [4.5 m] digital elevation model [DEM]). We then interpolated a water level surface with the Esri Topo to Raster tool. We created a depth-to-water surface by subtracting the water level surface from the DEM.

We considered the 3D extent of aquifer units, well depths, recharge/discharge zones, and water quality to define the aquifer systems (Fig. 11). The extent of each aquifer system is defined by the area in which the water level surface elevation is higher than the aquifer base. The aquifer base is defined by the base of the deepest aquifer unit that contains usable groundwater as determined by water quality and well depth data: the base of the Capitan Reef and Artesia Group for the Capitan Reef Aquifer System (CRAS), and the contact between lower Ochoan strata and overlying formations for the Delaware Basin Aquifer System (DBAS; Fig. 9).

The maximum potential saturated thickness of the aquifer was calculated by subtracting the bottom elevation surface from the top elevation surface. Aquifer properties vary horizontally and vertically within geologic units in the region, and therefore saturated thickness maps represent the maximum potential saturated thickness of the aquifer system at a given location.

WATER QUALITY

Regional characterization of water quality focused on total dissolved solids (TDS), major cations (Ca^{2+}, Mg^{2+}, Na^+, K^+), and major anions (SO_4^{2-}, HCO_3^-, Cl^-) since these are the most commonly measured and reported water quality parameters. The goal of the water quality analysis is to identify zones within the region of usable versus brackish waters. The EPA defines "Underground Sources of Drinking Water" as aquifers with waters containing 10,000 mg/L or less of TDS, and these aquifers are critical to protect in this quick-moving industrial region of the state. The available water quality data (Fig. 8) were split into two categories depending on the amount of TDS in the water: (1) treatable, with TDS concentrations less than 10,000 mg/L, and (2) untreatable, with TDS concentrations greater than 10,000 mg/L.

The water chemistry dataset includes 3,629 samples that were analyzed for at least one hydrochemical constituent of many different analytes, including major cations and anions, trace metals, environmental tracers, and others. Data sources includes the EPA, TWDB, NM EMNRD Oil Conservation Division (OCD) spill monitoring reports (Appendix C), USGS, and others (Fig. 12). The NMBGMR collected new water samples for this study at 22 locations in 2021. These samples were analyzed for major cations and anions, trace metals, and environmental tracers, including the stable isotopes of water, tritium, and carbon-14 (^{14}C). After removing all duplicate sampling locations and keeping the most-recent samples, the number of samples was reduced to 870 records. From this dataset with unique sample locations, there were 147 samples with complete cation and anion chemistry data for evaluation of water sources. Water chemistry data acquired from OCD reports account for a large proportion of the total number of data points, and are associated with the monitoring of a variety of contaminant spill sites. These data usually also include multiple samples collected from many of these wells. A review of these data showed that excluding these OCD chemistry datasets did not significantly alter the apparent spatial variability. Therefore, the following analyses include most of the data from the OCD reports.
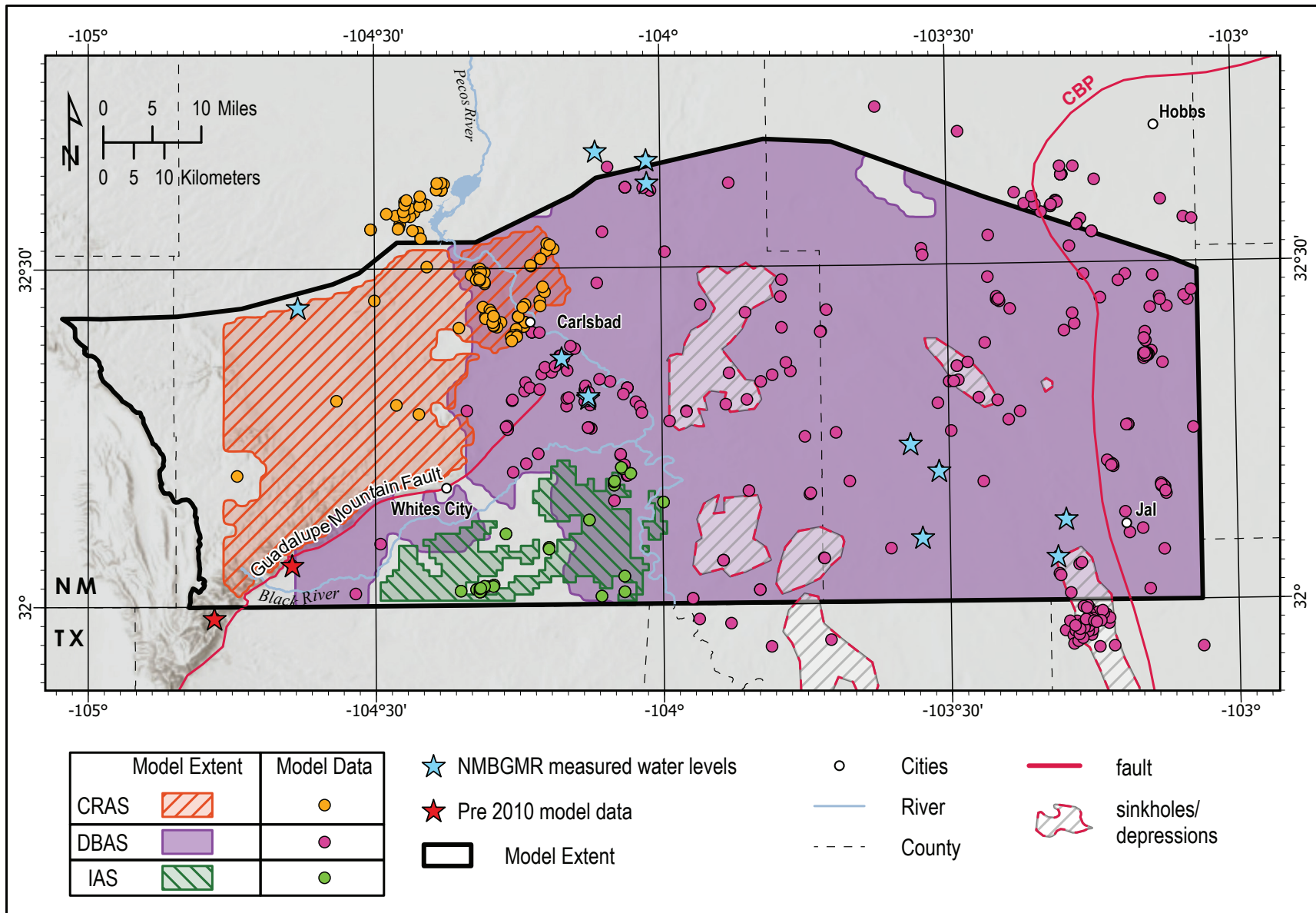
Figure 10. Locations of wells used to create the water level surface models. The depth-to-water measurements from these wells were all collected between 2010 and 2020, with a few noted exceptions in very data-poor areas. Data sources include the Texas Water Development Board, New Mexico Bureau of Geology and Mineral Resources, New Mexico Oil Conservation Division, New Mexico Office of the State Engineer, Sandia National Laboratories, and U.S. Geological Survey. CBP: Central Basin Platform.
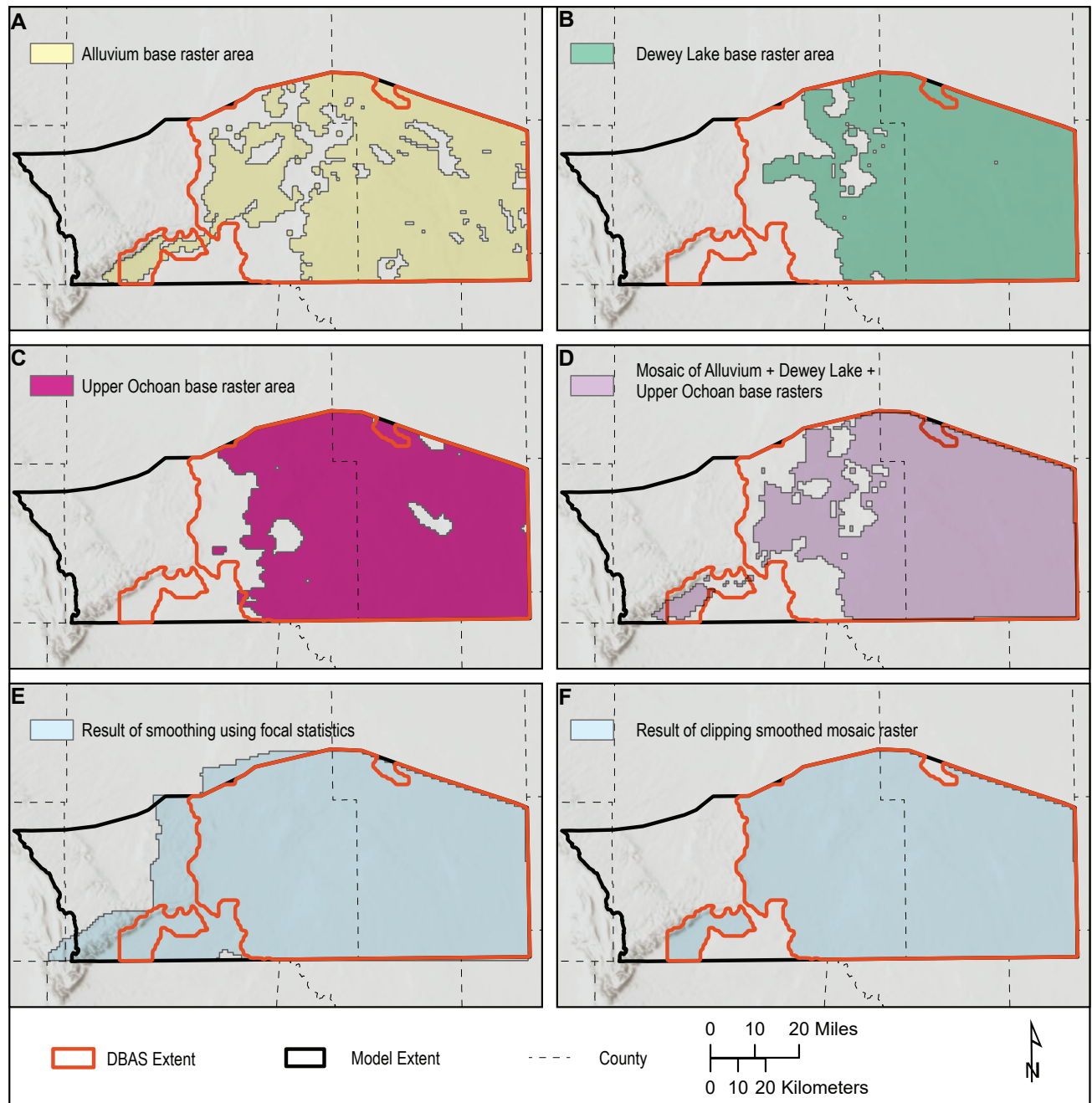
Figure 11. Aquifer base elevation surface production methods. A: Extent of upper Ochoan formation base; B: extent of Dewey Lake Formation base; C: extent of alluvium base; D: result of combing A, B, and C by mosaic to create initial aquifer base; E: result of Esri Focal Statistics smoothing of the raster, which interpolates past where there is actual data to interpolate a surface in areas where elevation is unknown; and F: final aquifer base clipped to model extent.

Water Chemistry Source
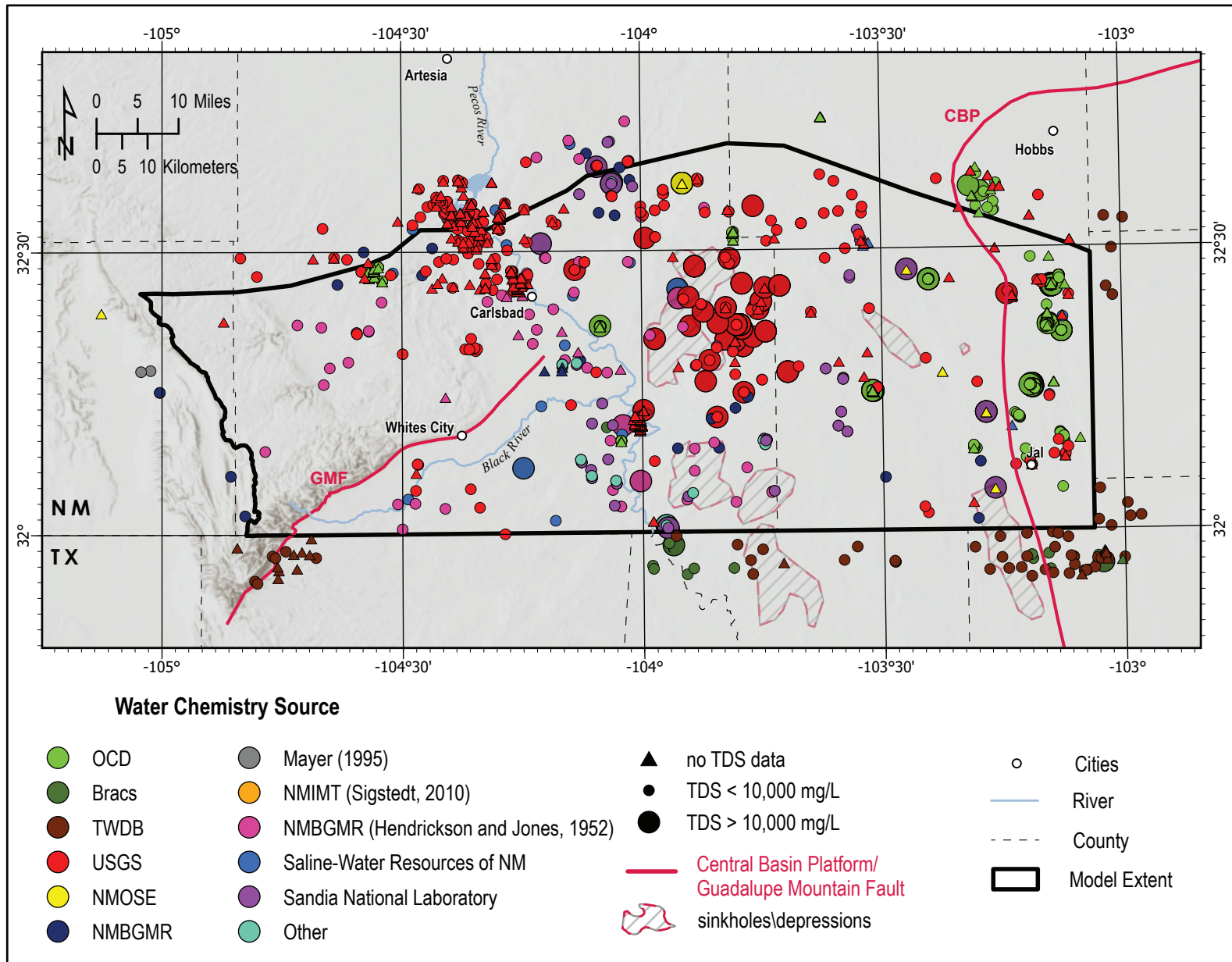
Figure 12. Locations of all wells with available water quality data, including historical data (measured earlier than 2010).

RESULTS: 3D GEOLOGIC MAP DATA

This section describes feature classes in the map package, including data type (point, raster, polygon, polyline) and geologic descriptions of lithologic units. A summary of lithologic units included in each model unit is described in Table 2 (Figs. 4 and 9). Digital data descriptions are as follows.

*<model unit>*Base: Group layer; contains model unit extent, control data, base elevation raster, and uncertainty map.

*<model unit>*BaseExtent: 2D extent of the model unit base; includes surface exposure extent and subsurface extent. Type: polygon.

*<model unit>*BaseContours_100ft: Structure contour map that represents the base elevation of the model unit in feet above mean sea level (ft amsl). Contour interval is 100 ft. Contours were developed from the base elevation raster for each unit. Type: polyline.

*<model unit>*BaseElevation_ftamsl: Raster surface that represents the base elevation of the model unit in ft amsl. Type: raster; grid size: 1,000 × 1,000 m.

*<model unit>*Thickness_50ft: Isopach contour map representing the thickness of the model unit in ft amsl. Type: polyline.

*<model unit>*ModelData: Point data used to develop geologic surfaces. Type: point.

*<model unit>*BaseUncertainty: Uncertainty map developed for model unit base surface in plus or minus (±) feet. Type: raster; grid size: 1,000 × 1,000 m.

ALLUVIUM BASE

Geologic description

Cenozoic deposits in the Delaware basin region of southeastern New Mexico consist of fine- to coarse-grained alluvium, eolian sand, and piedmont sand, silt, and gravel. Coarse-grained (gravel) deposits are commonly cemented by carbonate. Thickness is variable and greatest in areas with dissolution collapse structures (solution-subsidence depressions). Alluvium is commonly reworked into eolian dunes (Deeds et al., 2015). West of the Pecos River, discontinuous beds of gravel intercalated with silt, sand, and clay extend south of Carlsbad to the Black River, and locally provide groundwater to irrigated regions in the vicinity of Carlsbad (Hale, 1945; Henderson and Jones, 1952). East of the Pecos River, the so-called Gatuña formation consists of silt, sand, clay, and gravel. Younger alluvium forms terrace and channel deposits along the Pecos and Black Rivers.

East of the Pecos River, Cenozoic deposits include dune sands, lake and playa deposits, and the Ogallala Formation. The Ogallala Formation of late Tertiary age crops out in small, discontinuous areas in southern Lea County. Small, closed, shallow depressions contain silt and clay washed in from surrounding areas. Some of the depressions contain shallow ephemeral lakes (e.g., Salt Lake), which are actively depositing salts such as gypsum and halite. Water in these depressions is generally highly mineralized and unsuitable for domestic or municipal use. Dune sands (commonly referred to as Mescalero sands) cover most of the area east of the Pecos River. Deposits are relatively thin (about 60 ft) and variably overlie Permian and Triassic strata. Sands are above the saturation zone; however, rapid infiltration of rainwater aids in recharge to underlying formations (Nicholson and Clebsch, 1961).

The north-to-northwest-striking Monument Draw trough contains alluvial deposits nearly 800 ft thick in the study area. This trough extends north-northwest from Jal, New Mexico, along the inner margin of the Capitan Reef, and was likely formed by solution subsidence (Maley and Huffington, 1953; Richey et al., 1985).

Digital data

AlluviumBaseElevation_ftamsl,
AlluviumBaseContours_100ft

The alluvium base raster surface represents the base elevation of the contact between Cenozoic deposits and underlying geologic units. Cenozoic deposits include alluvium, colluvium, eolian sands, piedmont deposits, the Pecos River valley alluvium formation (Meyer et al., 2012), and the Ogallala Formation. Base elevation ranges from 2,116 ft amsl in the southeastern corner of the study area to 4,759 ft amsl in the southwest near the Guadalupe Mountains (Fig. 13). Topographic variation is a function of paleotopography of the underlying, slightly east-tilted sedimentary units.

AlluviumThickness_50ft

Cenozoic deposits are nearly 800 ft thick along the Monument Draw trough and between 400 and 450 ft thick along the San Simon Swale and San Simon Sink (Fig. 14).

AlluviumBaseModelData

The TWDB Brackish Resources Aquifer Characterization System (BRACS) database provided formation top elevation picks for the Dockum Group and base elevation picks for Pecos River valley alluvium. Bjorklund and Motts (1959) provided alluvium base elevations interpreted from NMOSE water well driller's logs. Additional NMOSE driller's logs were interpreted in data-poor regions west of the Pecos River as part of this study. The 1:500,000 state geologic map of New Mexico provided the surficial extent of Cenozoic deposits (Appendix A).

AlluviumBaseUncertainty

The maximum uncertainty for the alluvium base is 191 ft (Fig. 15). High-uncertainty zones are located near known, mapped sinkholes in the central and southeastern portions of the study area. These zones represent regions where the presence or absence of elevation data causes large fluctuations in the resulting interpolated surface—a phenomenon to be expected in regions with large elevation changes over short distances (such as faults or sinkholes; Appendix A). Uncertainty is generally low elsewhere.

DOCKUM GROUP

Geologic description

The Dockum Group is commonly divided into lower and upper units in hydrogeologic studies (Deeds et al., 2015). The lower Dockum Group contains the Santa Rosa Formation overlain by the Tecovas Formation (Table 2, Fig. 4). The Tecovas Formation contains mainly shale and sandy shale, whereas the Santa Rosa Formation contains mostly fine- to coarse-grained sandstone and only minor shale layers (Nicholson and Clebsch, 1961). Exposures are generally poor because of the extensive cover of drift sand (Nicholson and Clebsch, 1961); as a result, no surface exposures are mapped in the study area (Fig. 3; Scholle, 2003). The Santa Rosa is lithologically similar to sandstones of the overlying upper Dockum Group formations and is likely hydrologically connected to overlying units where the Tecovas is absent.

The upper Dockum Group contains the Trujillo, Cooper Canyon, and Redonda Formations of the greater Dockum Group (Table 2, Fig. 4). Surface exposures are limited to small, discontinuous outcrops east of the Pecos River (Fig. 3; Scholle, 2003). Lithology is principally reddish-brown mudstone with interbedded sandstone lenses (Kelley, 1971). In reference to water-bearing characteristics, Deeds et al. (2015) describe the upper Dockum aquifer as mostly confined.

We developed three model surfaces that represent geologic contacts within the Dockum Group: (1) upper Dockum Group base, (2) Santa Rosa top, and (3) lower Dockum Group base (Table 2, Fig. 4). The Santa Rosa top is equivalent to the Tecovas base. However, the control dataset for the Santa Rosa top surface contains formation top picks for the Santa Rosa Formation explicitly, rather than a combination of top and base picks as was common for other formations (Appendix A). The authors determined that the "Santa Rosa top" better represented the modeled surface than the "Tecovas base."

Digital data

UpperDockumGroupBaseElevation

The upper Dockum Group base raster surface represents the elevation of the contact between units in the upper Dockum group (Trujillo, Cooper Canyon, and Redonda Formations) and the underlying lower Dockum group units

(Santa Rosa and Tecovas Formations; Table 2, Fig. 4). Upper Dockum Group base elevation ranges from 2,634 ft amsl near Jal to 3,735 ft amsl near the northwestern edge of the mapped extent (Fig. 16). Subsurface extent is discontinuous in the Delaware basin study area, although it is generally consistent with the extent mapped in Deeds et al. (2015). Subsurface discontinuities are expected given the Triassic-Cenozoic unconformity.

UpperDockumGroupThickness

The thickness of the upper Dockum Group ranges from 640 ft in the east to pinching out to nothing along its western edge (Fig. 17).

UpperDockumGroupBaseModelData

Point data and contours associated with the Deeds et al. (2015) High Plains groundwater availability model provided the principal source of data used to generate the upper Dockum base surface (Appendix A).

UpperDockumGroupBaseUncertainty

Maximum uncertainty for the base of the upper Dockum Group is approximately 90 ft, but the majority of the unit had very low uncertainty (around 10–20 ft; see Fig. 18).

TecovasThickness

Due to the difficulty in identifying the Tecovas in gamma logs consistently throughout the study area, the Santa Rosa top elevation was selected instead. This raster surface represents the top of the sandstone-dominant portion of the Triassic Santa Rosa Formation (Fig. 4). The Santa Rosa fines upsection into a more mudstone-dominated unit typically referred to as the Tecovas Formation (Cikoski et al., 2020). The combined units constitute the lower Dockum Group (Table 2, Fig. 4). The difference between the Santa Rosa top elevation and the lower Dockum base elevation represents the Tecovas Formation thickness, shown in Figure 19.

SantaRosaTopElevation

Santa Rosa top elevation ranges from 1,802 ft amsl in the southeastern corner of the study area to 3,560 ft amsl on the western margin (Fig. 20). The surface dips slightly east. The topographic depression located southwest of Jal coincides with the collapse feature mapped in Anderson (1981) on the inner

Capitan Reef margin. Elevations increase on the Central Basin Platform (Fig. 20). The San Simon Sink and San Simon Swale roughly coincide with a surface discontinuity in the center of the mapped area (Fig. 20). A surface discontinuity located on the New Mexico-Texas state line coincides with Monument Draw trough (Fig. 2).

SantaRosaThickness

The Santa Rosa Formation ranges from 10 to 650 ft thick (Fig. 21).

SantaRosaTopModelData

Geophysical logs interpreted as part of this study provided top elevations for the Santa Rosa Formation (Appendix A).

SantaRosaTopUncertainty

The maximum uncertainty for the top of the Santa Rosa Formation is 172 ft (Fig. 22). It is highest in small, isolated zones in the northern half of the mapped area and in a larger zone near the southern boundary.

LowerDockumGroupBaseElevation

The lower Dockum Group base raster surface represents the elevation of the contact between the undivided lower Dockum Group formations (Tecovas and Santa Rosa) and the underlying Dewey Lake Formation (Fig. 4). Lower Dockum base elevation ranges from 1,642 ft amsl within the collapse feature boundary southwest of Jal to 3,467 ft amsl on the western margin near Nash Draw (Figs. 2 and 19). The lower Dockum base qualitatively exhibits more topographic irregularity than overlying model surfaces of the upper Dockum and Santa Rosa (Figs. 16 and 20). The surface displays multiple topographic depressions within the subsurface extent and a high elevation gradient coinciding with the inner Capitan Reef margin trend. Some depressions coincide with mapped sinkholes and collapse features (Big Sinks, San Simon Swale, San Simon Sink, unnamed depressions; Fig. 3); however, a handful do not correspond to any known and/or mapped collapse features. These are potentially depositional in nature as the Triassic lower Dockum Group lies unconformably over the Permian Dewey Lake Formation. Solution-collapse features are abundant in upper Permian formations (Vine, 1960; Bachman, 1980, 1987; Anderson, 1981; Stafford et al., 2008;

these are likely expressed as depressions in the lower Dockum Group base topography (Fig. 20). Discontinuities correspond to thick deposits of Cenozoic fill in Monument Draw trough (Fig. 3).

LowerDockumGroupBaseModelData

Point data and contours associated with the Ewing et al. (2012) Rustler aquifer groundwater availability model provided data used to generate the lower Dockum base surface. Geophysical logs interpreted as part of this study provided top elevations for the Dewey Lake Formation (Appendix A).

LowerDockumGroupBaseUncertainty

Maximum uncertainty for the base of the lower Dockum Group is 109 ft (Fig. 23). It is highest in topographic depression areas, such as near mapped sinkholes and along the inner Capitan Reef margin (Fig. 3), and relatively high near the western margin.

DEWEY LAKE FORMATION BASE

Geologic description

The upper Permian Dewey Lake Formation was deposited at the end of Permian time during an episode of marine regression (Austin, 1978; Hill, 1996). It consists of terrestrial, fine-grained clastic, reddish-brown, thin-bedded siltstone (Table 2; Cooper and Glanzman, 1971). The upper part of the formation is cemented with carbonate minerals and carbonate fracture fillings, and deeper exposures appear to be more completely cemented and/or filled with gypsum and anhydrite (Holt and Powers, 1990; Lowry et al., 2015). The unit contains laterally continuous channel sands up to a few meters thick (Schiel, 1988; Lowry et al., 2015). Lowry et al. (2015) indicate that the Dewey Lake Formation contains roughly 75% silt and 25% sand, and less than 7% of the stratigraphic volume is suitable aquifer material.

Digital data

DeweyLakeBaseElevation

The Dewey Lake base raster surface represents the elevation of the contact between the late-Permian Dewey Lake Formation and the underlying Rustler Formation (Figs. 4, 9, and 24). Elevation ranges from 998 ft amsl in the southeastern corner of the state to 3,268 ft amsl near the unit's western boundary (Fig. 24). Elevation generally decreases from west

to east, consistent with the regional stratigraphic dip (Fig. 9). Topographic depressions are seen southwest of Jal and north of the New Mexico-Texas state line just east of the Pecos River. A linear depression trends north-south along the Capitan Reef interior margin and Monument Draw trough, features with high solution-collapse potential (Fig. 2; Anderson, 1981). The surface contains an erosional discontinuity coincident with the location of Nash Draw, a topographic depression caused by evaporite dissolution and land subsidence (Fig. 2; Nicholson and Clebsch, 1961).

DeweyLakeThickness

The Dewey Lake Formation ranges from approximately 50 to 875 ft thick (Fig. 25). The thickest areas of this aquifer coincide with sink features.

DeweyLakeBaseModelData

Geophysical logs interpreted as part of this study, digitized structure contours (Hiss, 1976), and formation top picks from the New Mexico saline aquifer database (Broadhead and Ulmer-Scholle, unpublished data) provided geologic control data for the Dewey Lake base elevation surface (Appendix A). Hiss's (1976) Rustler Formation structure contours were digitized and converted to point elevation data as described in Cikoski et al. (2020). Geophysical logs and formation top picks from the New Mexico saline aquifer database also document the top of the Rustler Formation.

DeweyLakeBaseUncertainty

The base of the Dewey Lake Formation corresponds to the top of the Rustler Formation and is a dense dataset. As a result, uncertainty is generally low, with a mean uncertainty of ± 18.3 ft (Fig. 26). Uncertainty reaches up to 118 ft in isolated portions of the map area corresponding to sinkhole locations, as well as near unit extent and outcrop edges.

RUSTLER FORMATION BASE

Geologic description

The Permian Rustler Formation has been extensively studied for over three decades in southeastern New Mexico (Hiss, 1976; Powers et al., 1978, 2003; Hill, 1996; Powers and Holt, 2000). This is mostly the result of research conducted in support of

Project Gnome and the Department of Energy Waste Isolation Pilot Plant (WIPP; Powers et al., 1978; Holt and Powers, 1990). Ewing et al. (2012) provide a robust review of research done on the formation from southeastern New Mexico into western Texas. The Rustler Formation crops out in the south-central portion of the study area between the Pecos River and Black River (Figs. 3 and 27). Other isolated outcrops are mapped near Nash Draw and Salt Lake (Figs. 3 and 27; Scholle, 2003).

The Rustler Formation contains five thinly bedded members. In ascending order, these are the Los Medanos, Culebra Dolomite, Tamarisk, Magenta Dolomite, and Forty-niner Members (Vine, 1963). The sequence contains alternating low-permeability units and high-permeability units. The Los Medanos, Tamarisk, and Forty-niner Members generally contain clay, silt, anhydrite, and gypsum; the Culebra Dolomite and Magenta Members generally contain fractured dolomite and silty dolomite (Table 2; Vine, 2017). Beds are continuous across the study area; however, thicknesses are highly variable (Fig. 28). Thickness and facies variations are thought to result from variable gypsum content, regional differential subsidence, and fault displacement (Powers et al., 1978; Schiel, 1988; Powers and Holt, 1993, 2000). Additionally, evaporite dissolution (principally from the underlying Salado Formation) causes substantial, localized karst structures and deformation (Vine, 1960, 1963; Kelley, 1971; Bachman, 1980, 1987). In the central and southern part of Nash Draw, sinkholes range from small cavernous joints to large shallow depressions partly filled with alluvial or playa deposits (Figs. 2 and 28; Vine, 1963).

The Culebra and Magenta Dolomite Members are the principal water-bearing units of the Rustler Formation aquifer (Lowry et al., 2018). The Culebra Dolomite is a widespread, laterally continuous, fractured carbonate aquifer approximately 30 ft thick. Transmissivity decreases where halite is present in bounding formation members (Powers et al., 1978, 2003; Powers and Holt, 1993, 2000).

Digital data

RustlerBaseElevation

The Rustler base raster surface represents the elevation of the contact between the undivided Rustler Formation and the underlying lower Ochoan formations (Figs. 4, 9, and 27). Base elevation ranges from 650 ft amsl in the southeastern corner of the study area to 3,257 ft amsl near the western margin of the unit extent (Fig. 27). Regionally, the unit dips gently to the east; however, the local topography is highly variable (Figs. 9 and 27). Notable topographic variations include the linear north-to-northwest-striking depocenter coincident with the inner Capitan Reef margin and Monument Draw trough, and concentric depocenters coincident with sinkholes and collapse features (Figs. 3 and 27; Anderson, 1981).

RustlerThickness

The Rustler Formation ranges from approximately 15 to 900 ft thick (Fig. 28).

RustlerBaseModelData

The Rustler Formation base dataset contains geologic control data mostly from the TWDB BRACS database (Meyer, 2020), Ewing et al. (2012), and the New Mexico saline aquifer database (Broadhead and Ulmer-Scholle, unpublished data; Appendix A). The Salado top and Rustler base elevation points were retrieved from the BRACS database. The GIS files downloaded from the Rustler aquifer groundwater availability model (Ewing et al., 2012) contained digitized hand-drawn structure contours of the top and base of the Rustler Formation. The New Mexico saline aquifer database provided Salado top elevation control. Data-sparse regions include the northern margin of the study area and the area within the WIPP site boundary (Fig. 27).

RustlerBaseUncertainty

Uncertainty is generally low in most of the study area, with a mean uncertainty value of $\pm$ 31 ft. Maximum uncertainty of $\pm$ 190 ft occurs along the northern boundary of the study area, where data are especially sparse (Fig. 29). The eastern third of the region contains additional areas of high uncertainty. These regions are coincident with structural deformation from movement along the inner margin of the Capitan Reef, uplift of the Central Basin Platform, and dissolution collapse features (Figs. 3 and 29).

LOWER OCHOAN FORMATIONS BASE

Geologic description

The lower Ochoan series contains the salt-bearing Castile and Salado Formations (Fig. 4, Table 2). The Castile Formation is confined to the Delaware basin,

whereas the overlying Salado Formation extends northward and eastward across the northwestern shelf and the Central Basin Platform (Fig. 9; northward extent is mapped in Cikoski et al. [2020]). These salt-bearing formations are prone to dissolution from groundwater flow, resulting in numerous surficial expressions of collapse features, including Nash Draw, San Simon Swale, and Salt Lake basin (Fig. 2; Nicholson and Clebsch, 1961; Vine, 1963; Stafford, 2013).

The Castile Formation was deposited subsequent to the Capitan Reef in a deepwater, restricted marine Delaware basin at the end of the Permian (Kirkland and Anderson, 1970; Kendall and Harwood, 1989). The Castile Formation is up to 2,000 ft thick and contains laminated calcite/gypsum with interbedded halite and limestones, although most original fabrics have been diagenetically altered since deposition (Vine, 1963; Stafford, 2013). Surficial karst development where the Castile Formation crops out is substantial and extensive. Stafford et al. (2008) mapped closed depressions across the Castile outcrop in New Mexico and Texas and determined that at least 55% were collapse structures (collapse sinks) and 45% were a mix of incised arroyos and heavily modified collapse structures (solutional sinks). Upward-stopping processes, surface denudation, and meteoric processes enable these subsurface collapse features to breach the land surface (Stafford, 2013). Water resources in the Castile are scarce and generally high in TDS (primarily SO_4^{2-}). The hydrogeologic system is complex and couples shallow, gravity-driven meteoric flow with ascending fluids (Stafford, 2013).

The Salado Formation is approximately 1,500 ft thick near the WIPP site and contains mostly potassium-rich halite with lesser amounts of anhydrite (Austin, 1978; Vine, 2017). It is the first unit deposited after Capitan Reef formation, and it crosses the reef from basin to shelf (Kelley, 1971). The upper portion contains 50 to 200 ft of brecciated gypsum, siltstone, and anhydrite, and the lower portion contains massive halite, anhydrite, and soluble potash minerals (Vine, 1963). Substantial amounts of potassium salts (sylvite, potassium chloride) are concentrated in the McNutt potash zone (Fig. 3; Vine, 1963; Austin, 1978). Salt Lake basin is a closed depression on top of the Salado Formation (Fig. 3; Vine, 1963).

Digital data

LowerOchoanBaseElevation

The lower Ochoan base raster surface represents the elevation of the contact between the undivided lower Ochoan formations (Salado and Castile Formations) and underlying formations, including the Artesia Group on the Central Basin Platform, the Capitan Formation along the shelf margin, and the Delaware Mountain Group in the basin (Figs. 4, 9, and 30). Elevation ranges from 2,364 ft below mean sea level in the San Simon Swale region to 4,143 ft amsl in the southwestern portion of the study area, where the lower Ochoan formations are bounded by the Capitan Reef (Figs. 9 and 30). The Salado and Castile Formations crop out in a continuous swath between the Pecos River and the Black River, but otherwise crop out in isolated exposures in the Pecos River and Black River valleys (Figs. 3 and 30). The formations dip generally to the east (Fig. 9). Notable topographic variations include the north-south-striking San Simon Swale, a linear trough thought to be caused by dissolution of salts in the Rustler, Salado, and Castile Formations and filled by collapse of overlying sedimentary units. East of the San Simon Swale, the formation base is offset by the Central Basin Platform (Figs. 9 and 30).

LowerOchoanBaseModelData

Lower Ochoan base data include formation top elevations for the Artesia Group and Delaware Mountain Group (DMG) picked from geophysical logs. Ron Broadhead (personal communication), Broadhead and Ulmer-Scholle (unpublished data), the 1:500,000 scale New Mexico state geologic map (Scholle, 2003), and the NM EMNRD OCD online database provided surface control point data and geophysical logs and/or geologic control data (Appendix A). Artesia Group top formation picks constrained the combined Salado/Castile base elevation in the Central Basin Platform and north-central shelf regions, and DMG top formation picks constrained the Salado/Castile base elevation from the Capitan Reef to the basin center (Fig. 4). Data coverage is best near the Pecos River south of Malaga, where the Castile and Salado Formations crop out, and is generally sparse elsewhere (Fig. 30).

LowerOchoanThickness

The lower Ochoan ranges from 130 to 4,115 ft thick (Fig. 31).

LowerOchoanBaseUncertainty

Uncertainty is generally low near unit outcrops and the center of the basin, and increases to over ± 500 ft in the north-central portion of the basin and up to ± 470 ft near Jal (Fig. 32). Lack of data is the likely cause for high uncertainties, although structural features may also contribute to high uncertainty near Jal.

ARTESIA GROUP BASE

Geologic description

The Artesia Group is the back-reef equivalent to the Capitan Reef formation and contains lagoonal sandstones, anhydrites, and dolomites (Figs. 4 and 10). Formations of the Artesia Group in the study area are (in ascending order) Grayburg, Queen, Seven Rivers, Yates, and Tansill (Fig. 4, Table 2; Kelley, 1971). The carbonate facies of these units crop out in the Guadalupe Mountains and extend north and west to the study area margin (Fig. 3). The formations dip gradually east and are in the subsurface in the eastern portion of the study area (Fig. 10). Each formation principally contains dolomitic beds with lesser fine-grained siliciclastic intervals (Cikoski et al., 2020). Lithofacies within units are extremely variable and grade rapidly from massive reef complexes near the Capitan Reef to back-reef and shelf evaporitic facies to the north (Kelley, 1971; Hiss, 1975a, 1975b; Hill, 1996). The Queen Formation grades basinward into the Goat Seep Limestone, whereas the Seven Rivers, Yates, and Tansill Formations grade basinward into the Capitan Reef Limestone. The Grayburg Formation underlies the Goat Seep Limestone unconformably (Nance, 2009). The carbonate-siliciclastic facies are generally permeable and form a prolific aquifer with the San Andres Formation and Capitan Reef formation. Farther from the reef, the evaporitic facies form an impermeable confining layer and create the Roswell artesian groundwater basin north of the study area (Cikoski et al., 2020).

Digital data

ArtesiaGroupBaseElevation

The Artesia Group base raster represents the elevation of the contact between the Artesia Group and the underlying San Andres Formation (Figs. 4, 10, and 33). The Artesia Group crops out continuously in the Guadalupe Mountains (Fig. 33). The base

elevation reaches up to 6,143 ft amsl and drops to 1,559 ft below mean sea level on the Central Basin Platform (Fig. 33).

ArtesiaGroupBaseModelData

The Artesia Group ranges from 25 to 1,640 ft thick (Fig. 34).

ArtesiaGroupBaseModelData

Artesia Group base control data include San Andres top formation picks (Broadhead, personal communication) and San Andres top structure contours (Kelley, 1971; Appendix A). The geologic map of New Mexico (Scholle, 2003) provided outcrop elevation control. Data coverage is sparse.

ArtesiaGroupBaseUncertainty

Uncertainty reaches a maximum of ± 326 ft along the northeastern map margin (Fig. 35) and is generally low elsewhere. The high-uncertainty area contains no data and is a region where the Artesia Group grades basinward into the Capitan Reef.

CAPITAN FORMATION, TOP AND BASE

Geologic description

The Capitan Formation (Capitan Limestone, Capitan Reef Complex, or Capitan Reef) is a fossil limestone reef that forms the boundary for the Delaware basin throughout New Mexico and Texas (Fig. 36). It is one of the best exposed and most intensively studied reef complexes in the world (Saller et al., 1999). There are several publications that describe the Capitan Reef Complex, including detailed studies on reef development, sequence stratigraphy, and facies variations. The world-class Capitan Reef exposures are studied extensively as an outcrop analog for oil and gas reservoirs with similar depositional history and basin formation as the Delaware basin. Additionally, the formation is a significant aquifer where it is shallow. Hiss (1975a) mapped the Capitan aquifer's subsurface extent, top elevation, and thickness from the Guadalupe Mountains to the Glass Mountains (Fig. 19).

The Capitan Reef forms the shelf margin of the Delaware basin. Lithology varies along its extent, from massive and fossiliferous limestones in the Guadalupe Mountains to thin-bedded dolomite in

the Apache Mountains (Fig. 36, Table 2; Barnes et al., 1968; Wood, 1968; Hiss, 1975b). In the study area, the reef grades into back-reef facies of the Artesia Group and fore-reef sandstones, limestones, shales, and evaporites (King, 1942). The Delaware Mountain Group is the basin-facies time-equivalent unit to the Capitan Formation (Fig. 4; King, 1948). The Capitan Formation crops out along the Guadalupe Mountains' east-facing escarpment in New Mexico and is the host rock for a portion of Carlsbad Caverns (Fig. 2; Scholle, 2003; Land, 2016). This cavernous porosity is well documented along the reef's shallow subsurface extent (Henderson and Jones, 1952; Motts, 1968). As such, the Capitan Formation allows significant groundwater recharge in the Guadalupe Mountains and constitutes a prolific aquifer from Guadalupe Peak to east of Carlsbad, New Mexico (Fig. 2). The karstic aquifer is the principal source of fresh water for Carlsbad (Land, 2016). The Capitan Reef continues in the subsurface east and south through Lea County and Texas, and crops out again in the Glass Mountains of western Texas (Fig. 36; Barnes et al., 1968; Hiss, 1975b; Scholle, 2003; Standen et al., 2009).

Digital data

CapitanTopElevation, CapitanBaseElevation, and CapitanThickness

The Capitan Formation top, base, and thickness digital data included in this map package were originally developed by Standen et al. (2009; Figs. 37 and 38). Similar to the methods implemented here, Standen et al. (2009) integrated data from Hiss (1975b), Bjorklund and Motts (1959), TWDB and Texas Board of Water Engineers (TBWE) reports, geophysical logs from the Texas Bureau of Economic Geology and Texas Commission on Environmental Quality (TCEQ) Surface Casing department, TWDB's Water Information Integration and Dissemination (WIID) web service, the NMOSE database, and numerous maps and cross sections (Appendix A). The resulting digital GIS files were available in a geodatabase from the TWDB's groundwater availability model (GAM) and geodatabase downloads web page (https://www.twdb.texas.gov/groundwater/models/download.asp). No additional processing was done on these surfaces—the data, structure contours, and

surfaces are included in this map package to complete the hydrogeologic framework in New Mexico. As such, descriptions of Capitan top and base elevations and model data are directly from Standen et al. (2009) and Jones (2016).

"The top of the Capitan Reef Complex had elevations ranging from 1,500 feet below mean sea level (msl) to 8,000 feet above msl. A 250-foot contour interval was used between 1,500 feet below msl to 4,000 feet above msl (dominantly subsurface contouring) and a 500-foot contour interval for all elevations greater than 4,000 feet above msl (dominantly surface outcrop contouring)" (Standen et al., 2009, p. 36).

CapitanDataset

"A total of 643 well locations with subsurface Capitan Reef Complex tops were used to construct the surface… The *Capitan_Dataset* had a total of 575 well locations with base of the Capitan Reef Complex data that were used to determine the reef complex thickness" (Standen et al., 2009, p. 36).

CapitanBaseUncertainty

Uncertainty maps were not developed for Capitan Formation surfaces. We encourage readers to see Standen et al. (2009) for detailed descriptions of data screening, processing, and surface generation.

Cenozoic Deposits

—100— base elevation (ft. amsl) contour interval = 100 ft   subsurface   • control data   — fault   sinkholes/ depressions
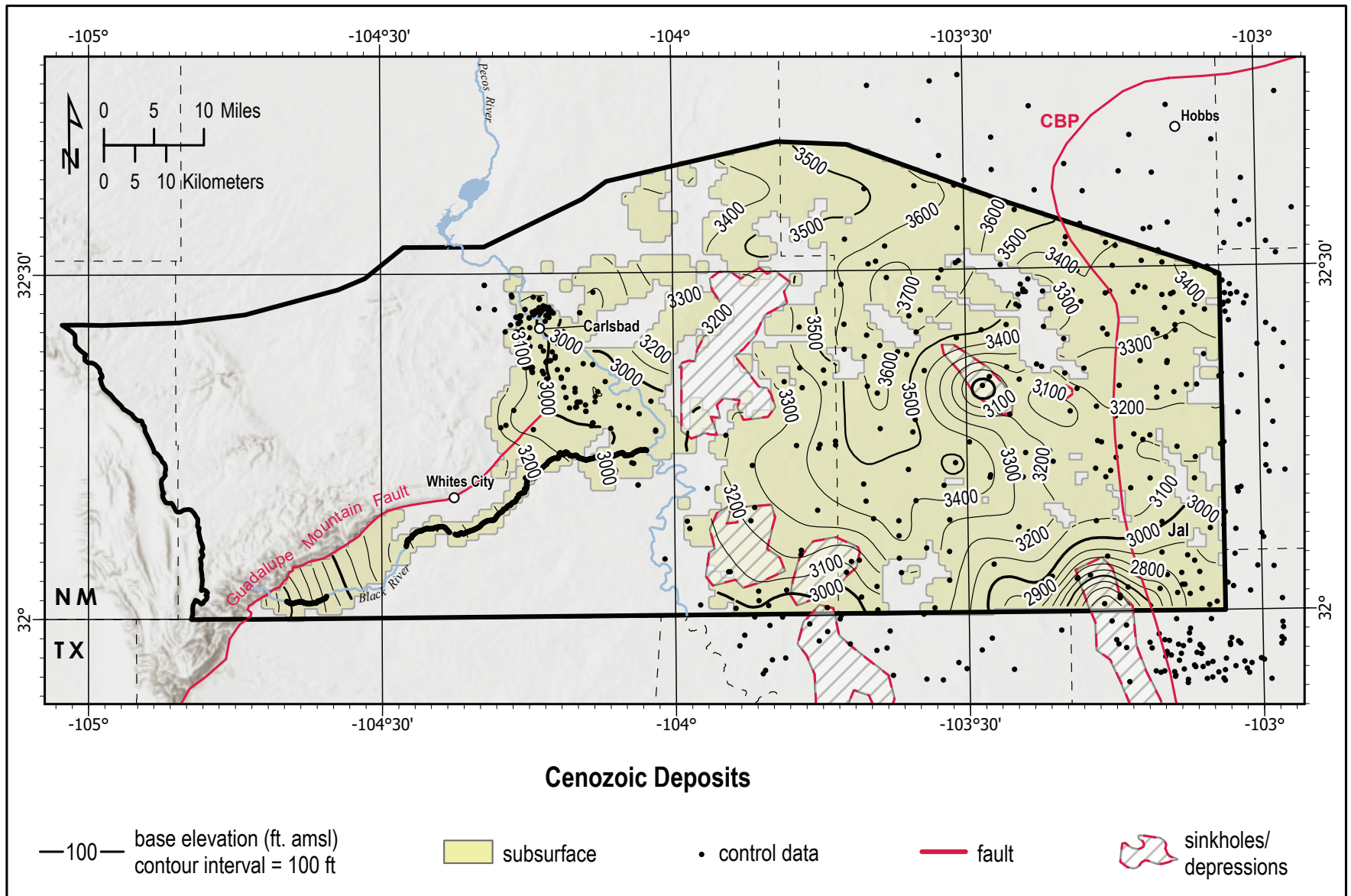
Figure 13. Structure contour map showing the base elevation of Cenozoic deposits (AB), which include the alluvium, colluvium, eolian sands, piedmont deposits, and the Pecos River valley alluvium formation. Topographic variation is a function of paleotopography of the underlying sedimentary units, sinkholes, and other depressions/collapse features. Figure 3 indicates mapped sinkhole and depression names. CBP: Central Basin Platform.

Thickness of Cenozoic Deposits (ft.)

high: 794

low: 6

contour interval = 50 ft

— 50 —

• control data

— fault

sinkholes/
depressions
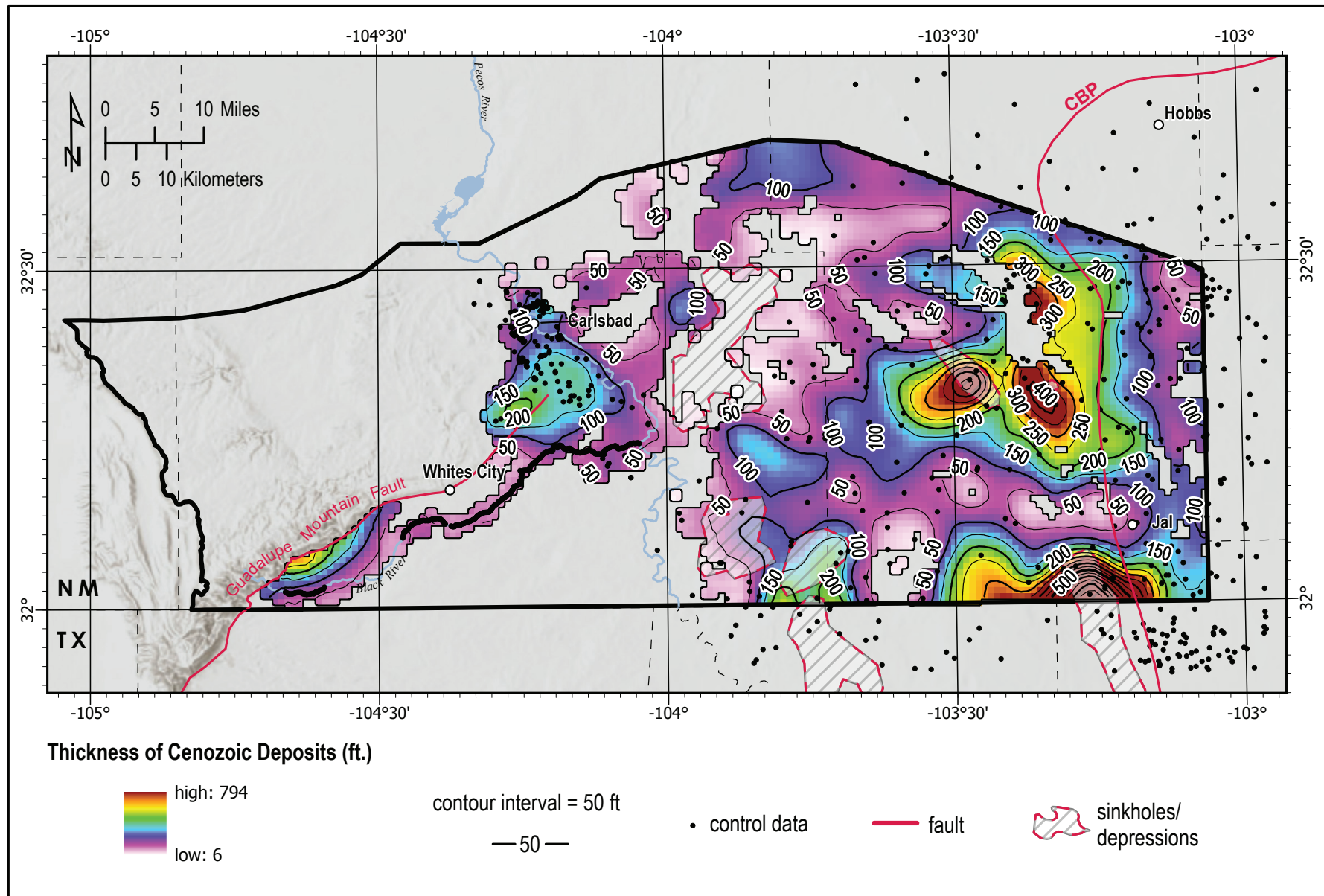
Figure 14. Isopach map showing Cenozoic alluvial, piedmont, and Pecos River valley alluvium thickness. The thickest sections of this unit are located near sink and dissolution features.
CBP: Central Basin Platform.

Model Unit: AB - Cenozoic Deposits

Uncertainty (+/- ft.)

- < 50
- 50 - 100
- 100 - 150
- 150 - 200
- > 200

contour interval = 10 ft

— 10 —

• control data

— fault

sinkholes/depressions
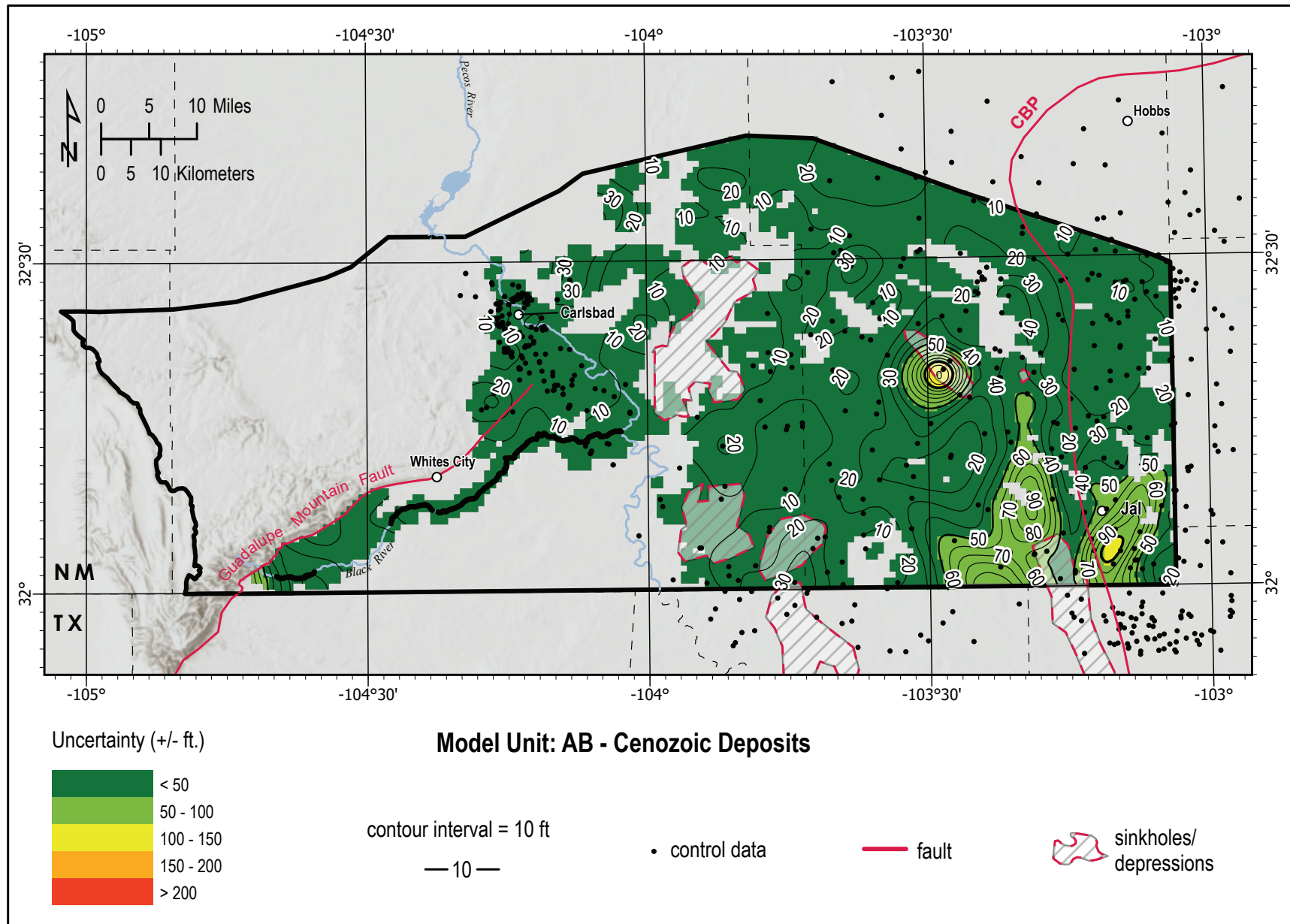
Figure 15. Calculated uncertainty in the Cenozoic surface, with a maximum uncertainty of 191 ft in the vicinity of the San Simone Swale. CBP: Central Basin Platform.
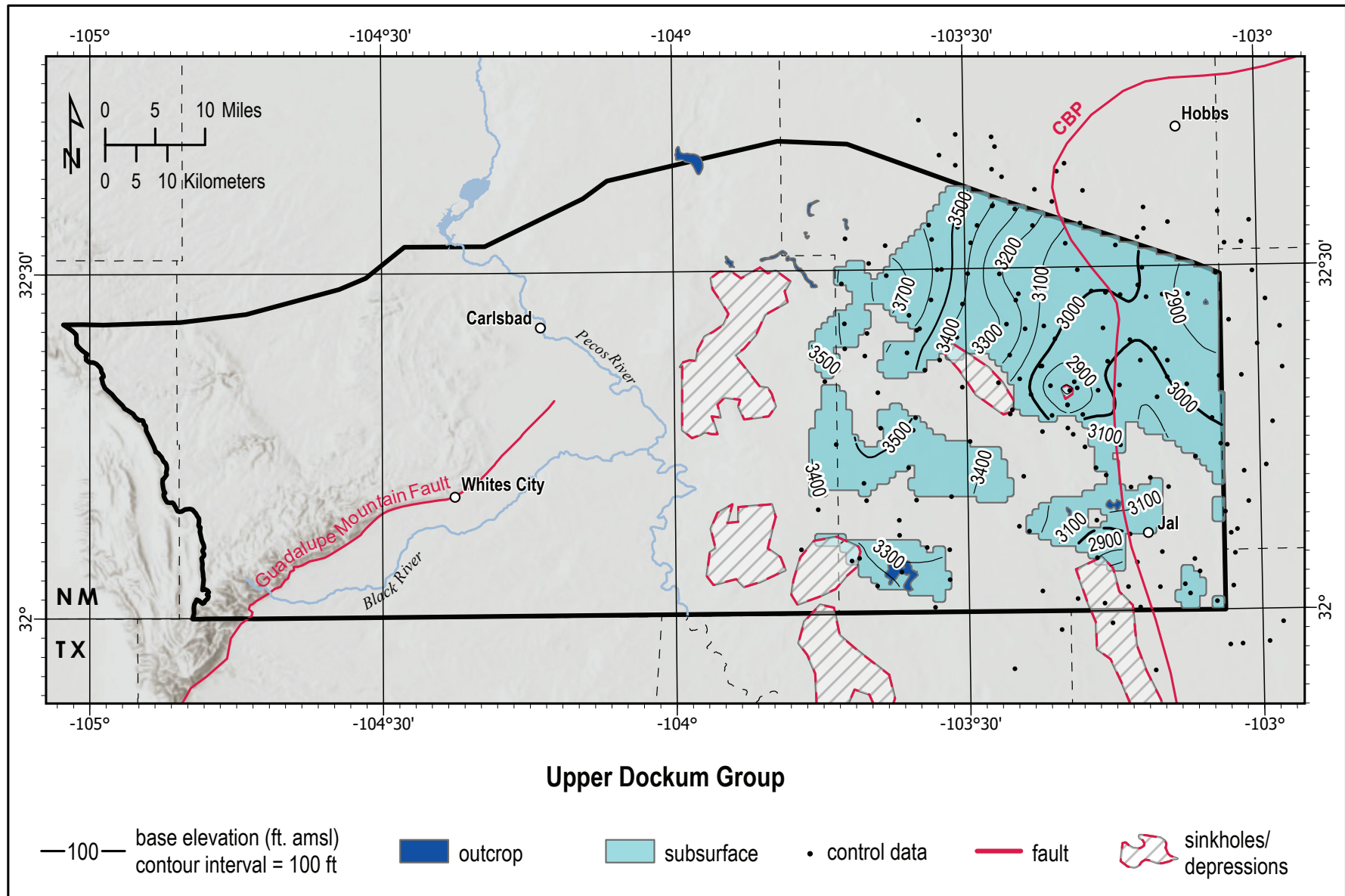
Upper Dockum Group

Figure 16. Upper Dockum Group base (UDB) elevation structure contour map. Figure 2 indicates mapped sinkhole and depression names. CBP: Central Basin Platform.
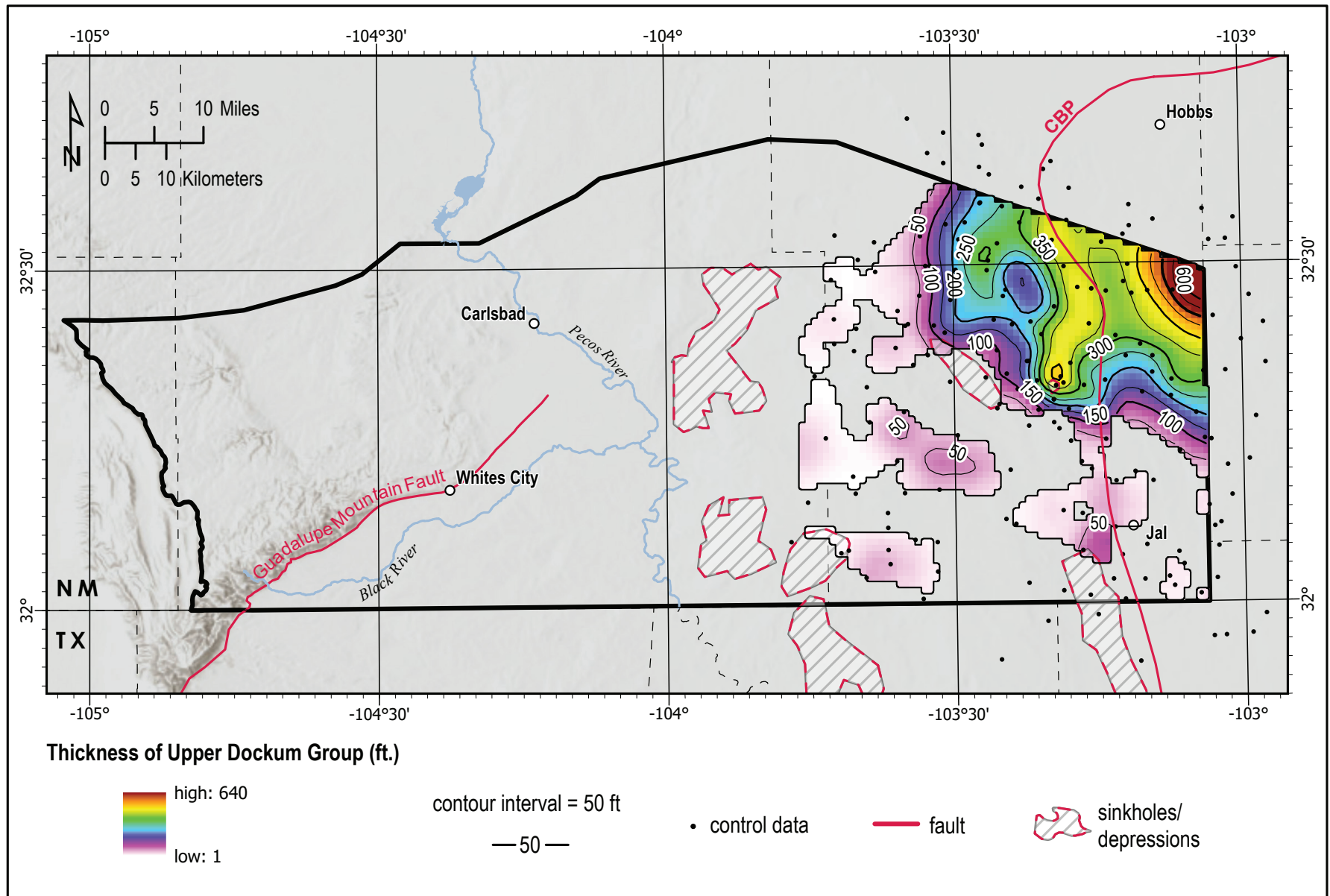
Figure 17. Isopach map showing upper Dockum Group thickness. The thickest section of this unit is 640 ft thick in the northeastern corner of the model area. CBP: Central Basin Platform.

Model Unit: UDB - Upper Dockum Group Base

Uncertainty (+/- ft.)

- < 50
- 50 - 100
- 100 - 150
- 150 - 200
- > 200

contour interval = 10 ft

—10—

• control data

— fault

sinkholes/depressions
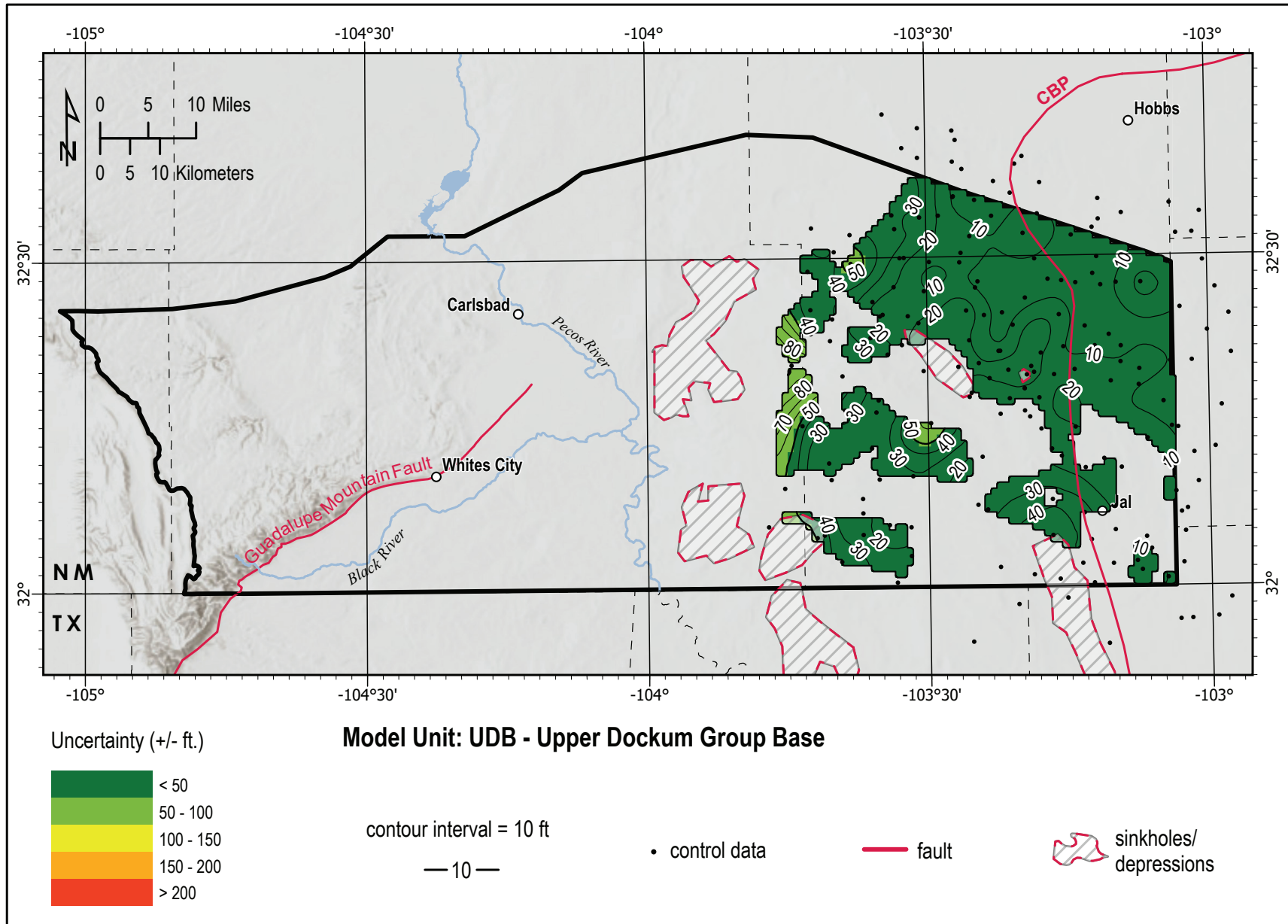
Figure 18. Uncertainty in the modeled upper Dockum Group surface is generally less than 50 ft. CBP: Central Basin Platform.

Thickness of Tecovas Formation (ft.)

high: 949
low: 23

contour interval = 50 ft

— 50 —

• control data

—— fault

sinkholes/ depressions
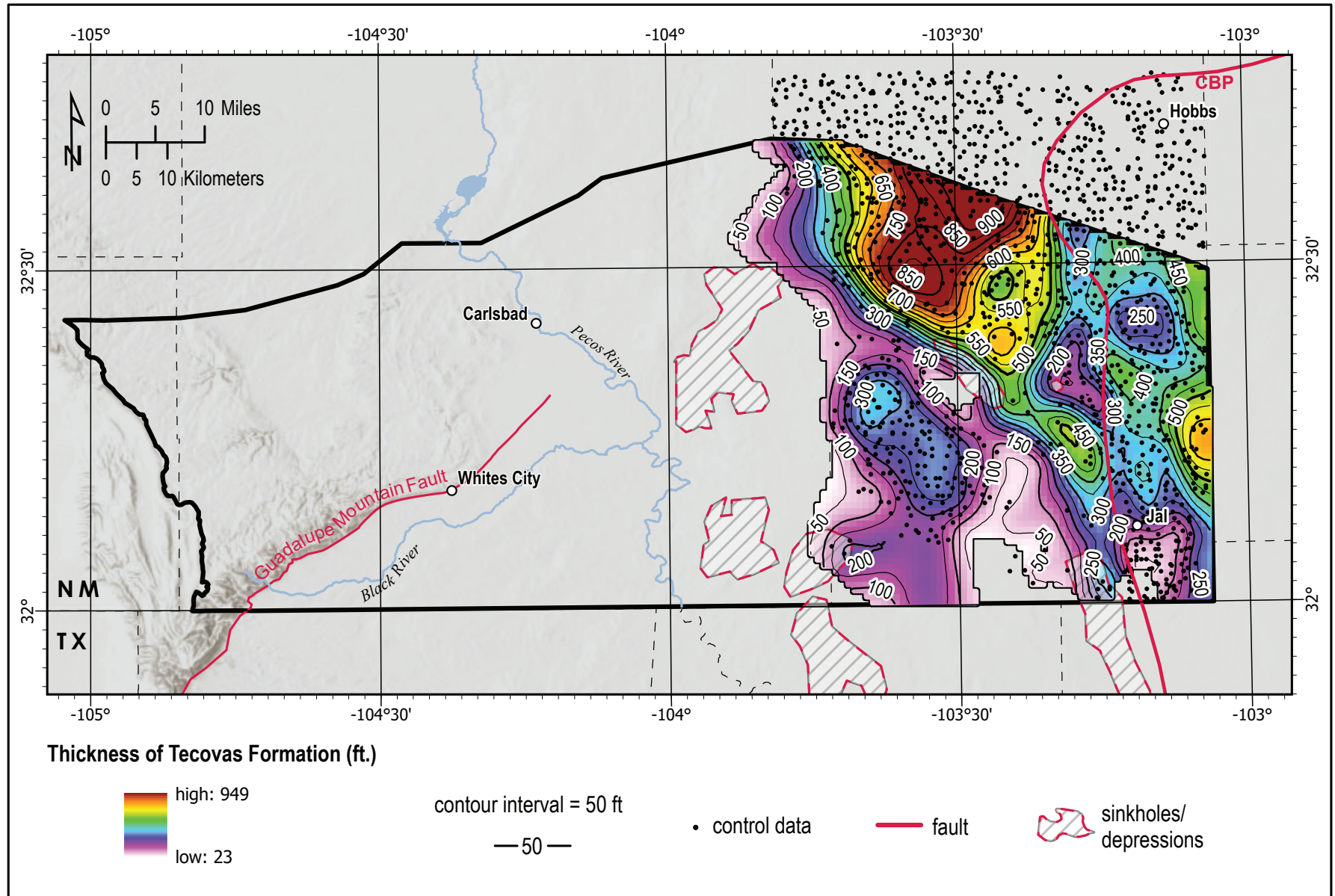
Figure 19. Isopach map showing the thickness of the Tecovas Formation. The Tecovas is not readily distinguished in geophysical logs, unlike the underlying Santa Rosa Formation. The Tecovas thickness is calculated as the difference between the top of the Santa Rosa and the base of the upper Dockum Group. Santa Rosa top elevation control points used to calculate the surface area also shown. CBP: Central Basin Platform.
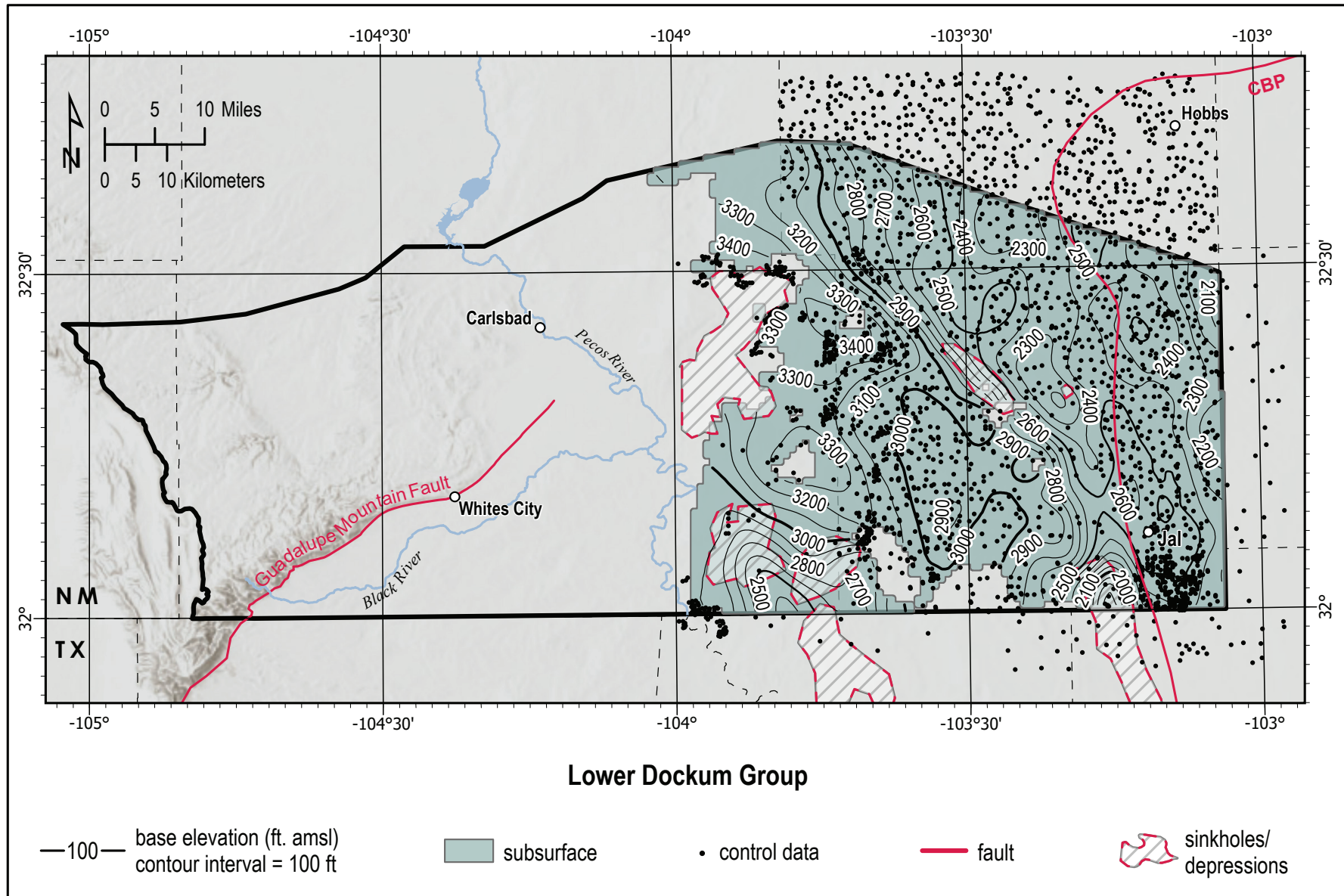
Lower Dockum Group

Figure 20. The base elevation of the Santa Rosa Formation/lower Dockum Group, which includes the Tecovas and Santa Rosa Formations. Santa Rosa base elevation control points shown. CBP: Central Basin Platform.
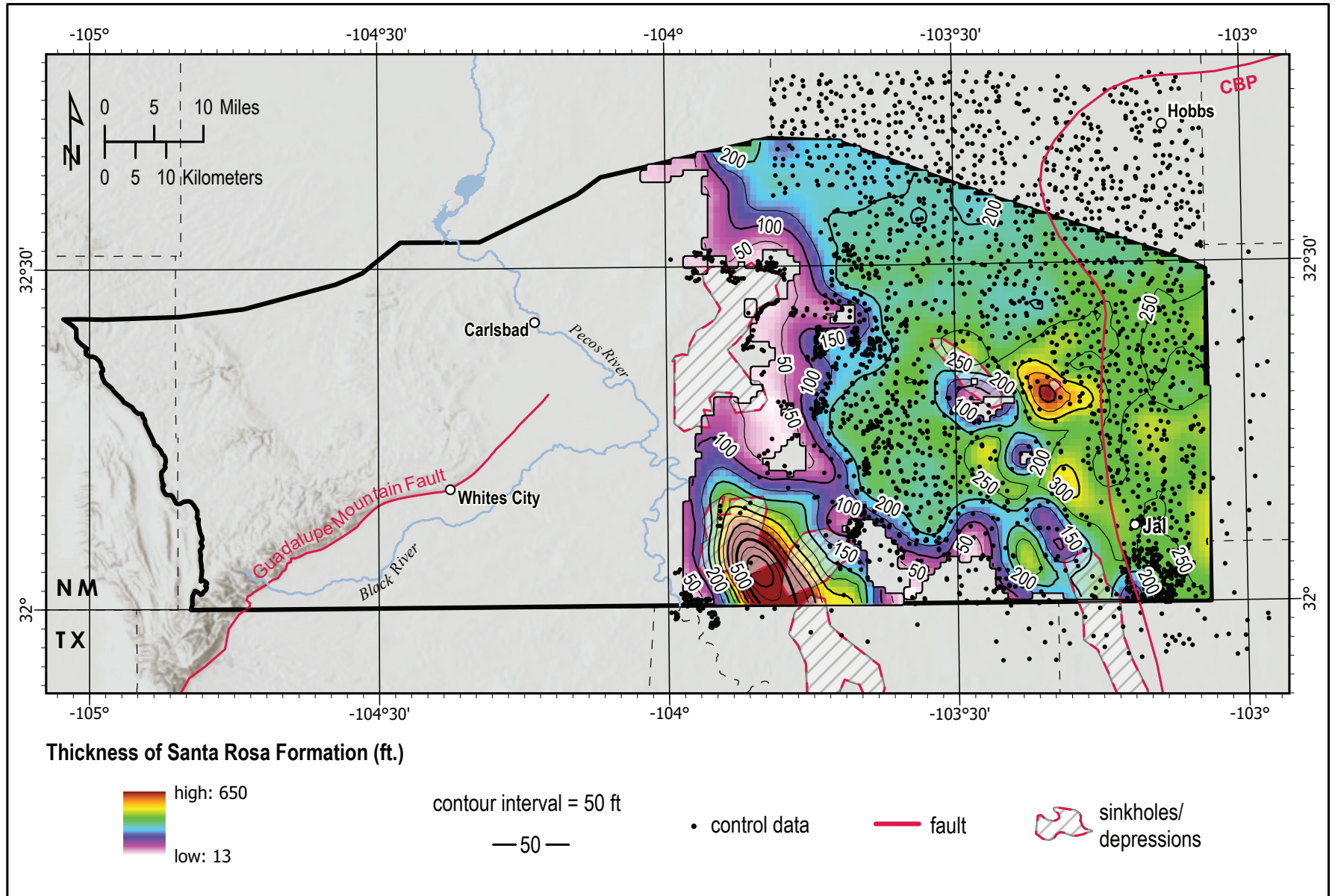
Figure 21. Isopach map showing Santa Rosa Formation thickness. CBP: Central Basin Platform.
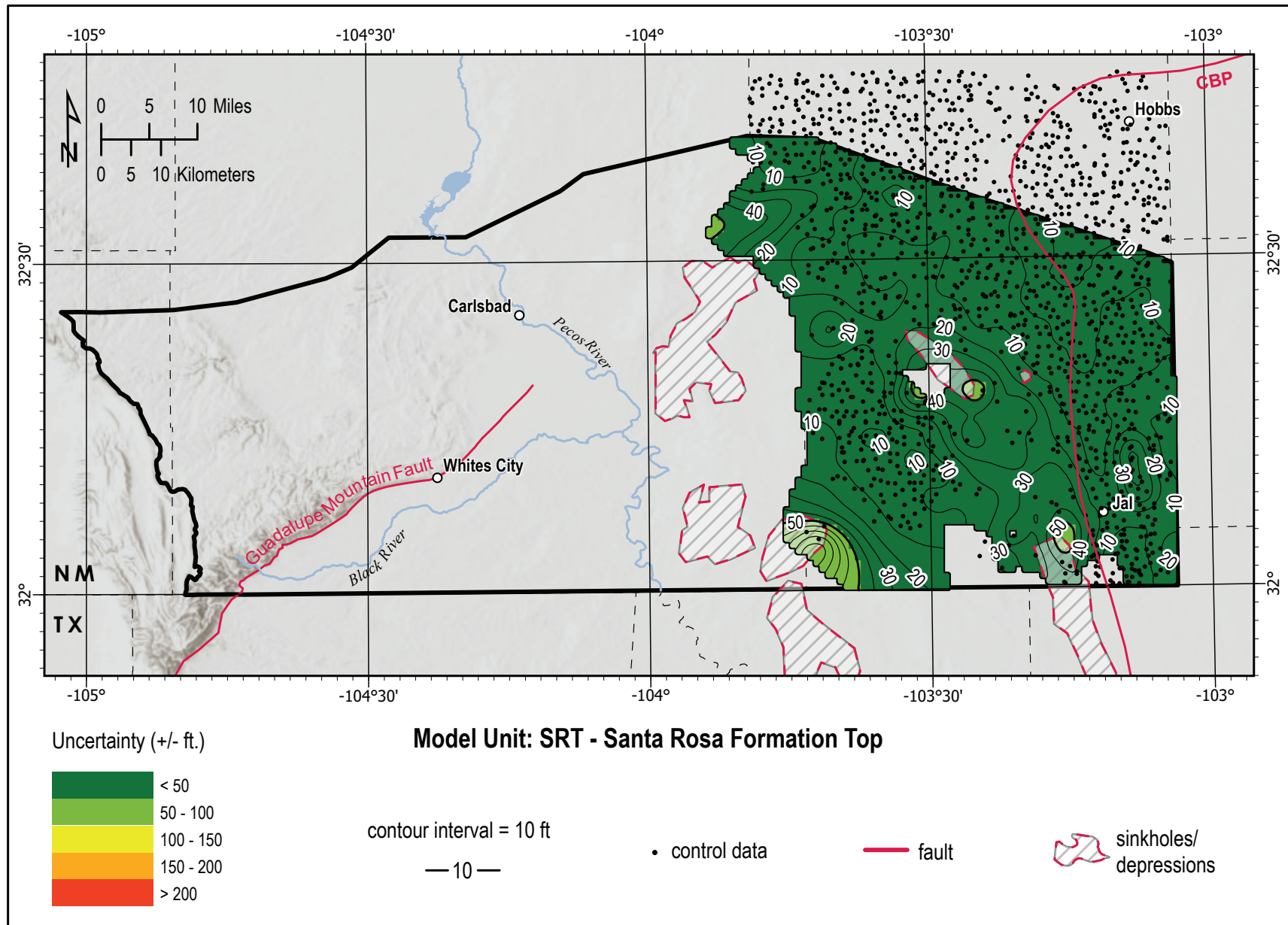
Figure 22. Santa Rosa Formation top elevation uncertainty (this is equivalent to the Tecovas base uncertainty). CBP: Central Basin Platform.
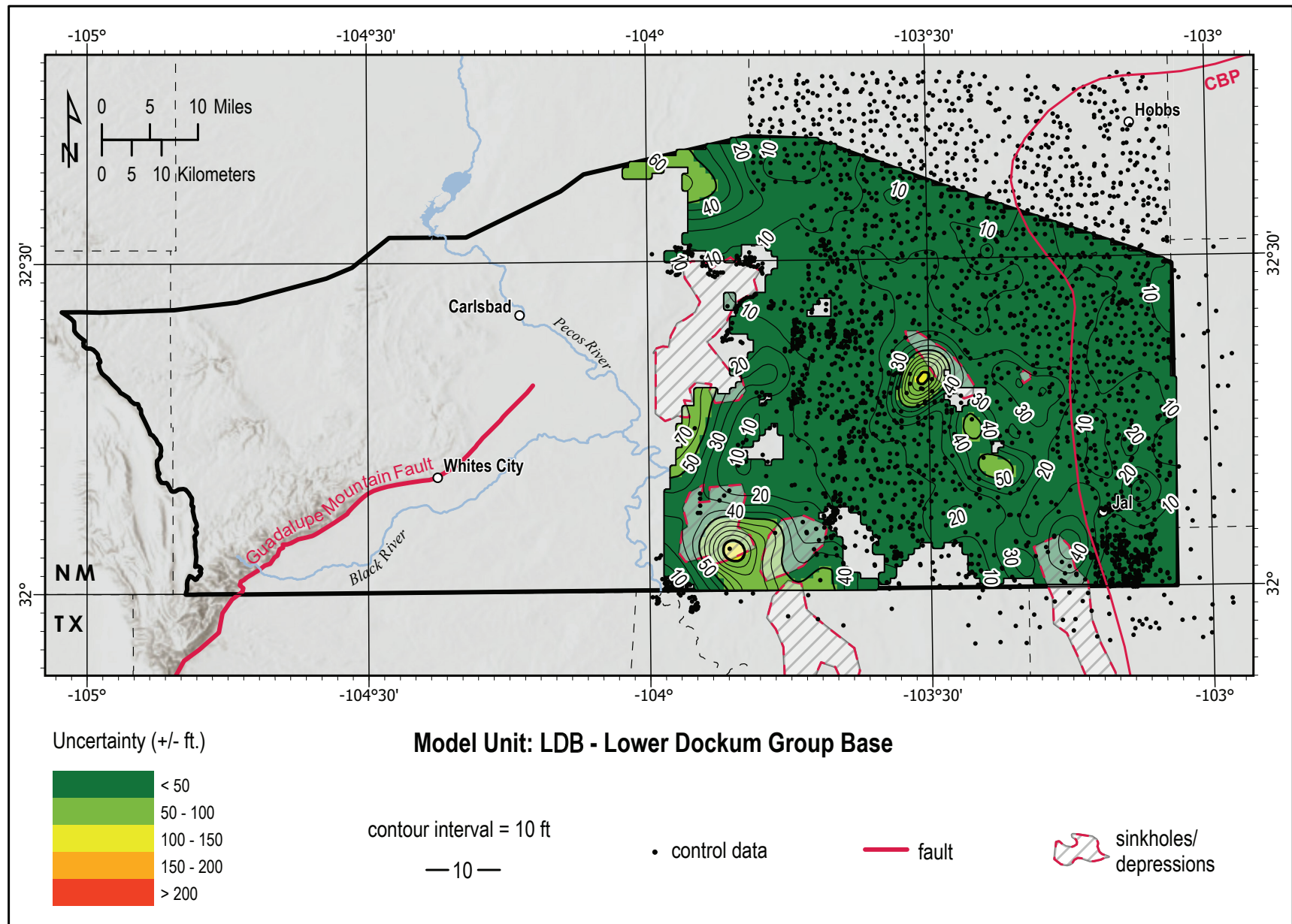
Figure 23. The calculated uncertainty in the Santa Rosa Formation base (base of the lower Dockum Group) elevations. Santa Rosa base elevation control points shown. CBP: Central Basin Platform.

Dewey Lake Formation Base

— 100 — base elevation (ft. amsl) contour interval = 100 ft   outcrop   subsurface   • control data   — fault   sinkholes/ depressions
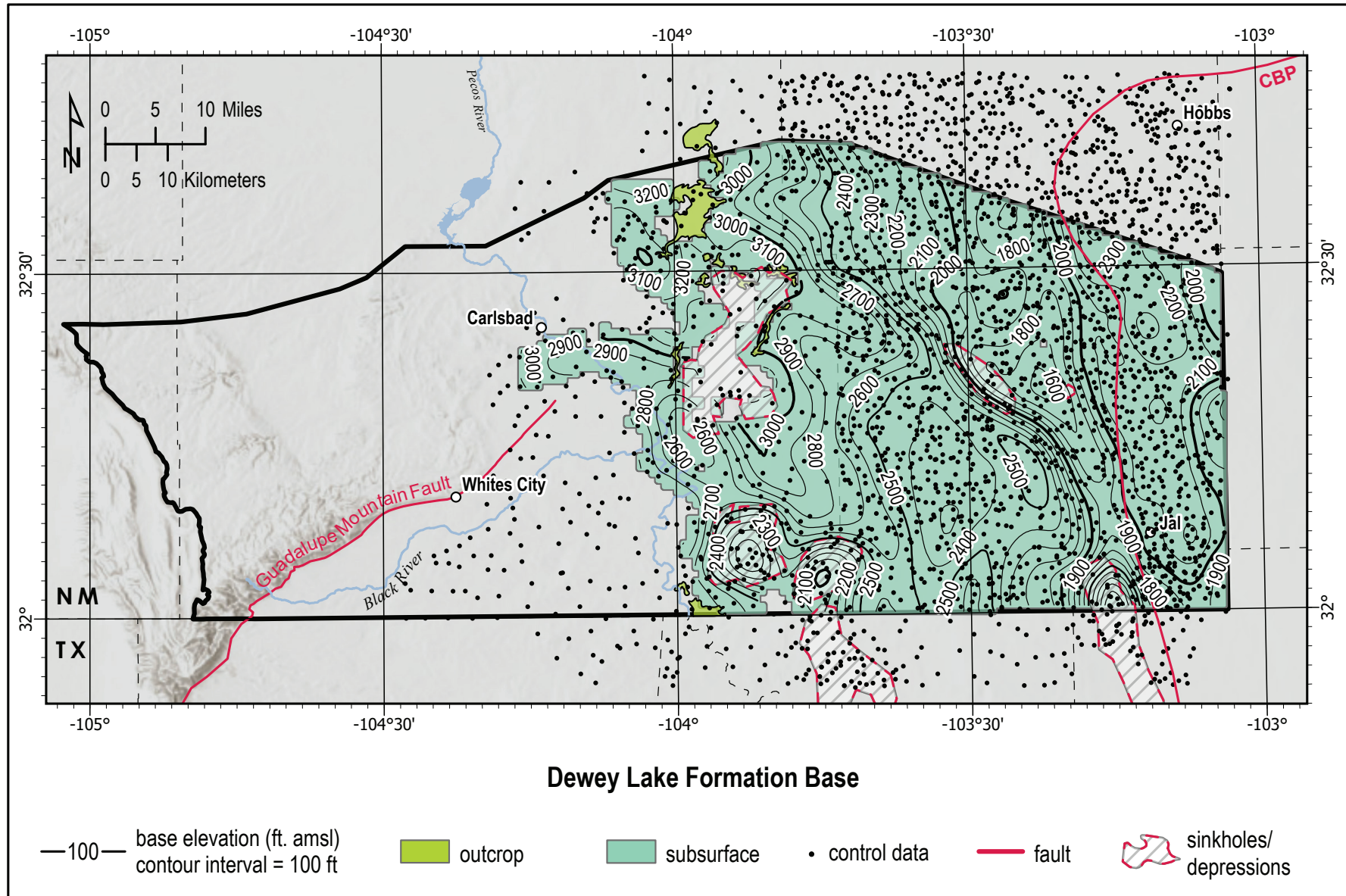
Figure 24. Dewey Lake Formation base (DLB) elevation structure contours. CBP: Central Basin Platform.

Thickness of Dewey Lake Formation (ft.)

high: 873
low: 45

contour interval = 50 ft

— 50 —

• control data

— fault

sinkholes/depressions
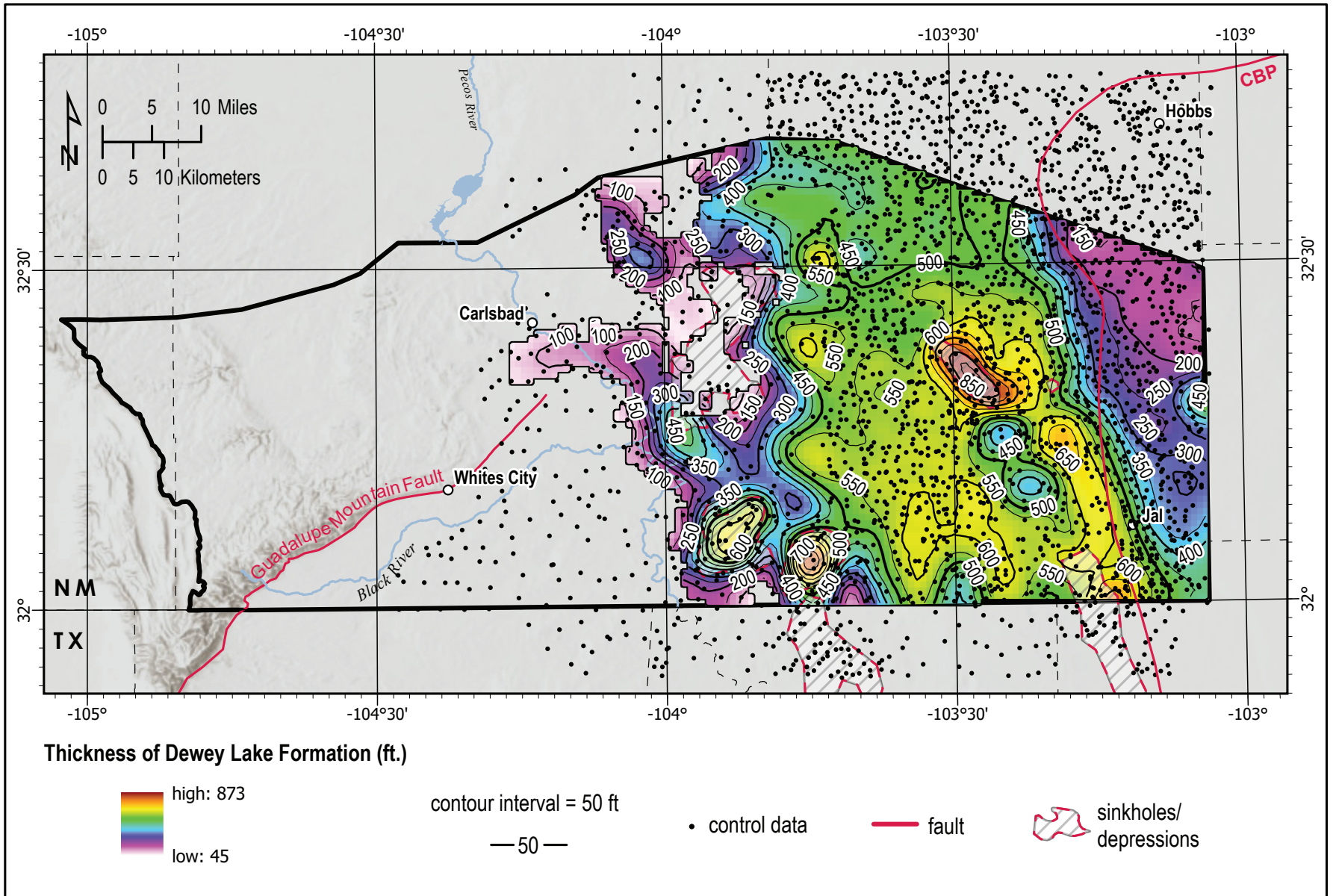
Figure 25. Isopach map showing Dewey Lake Formation thickness. CBP: Central Basin Platform.
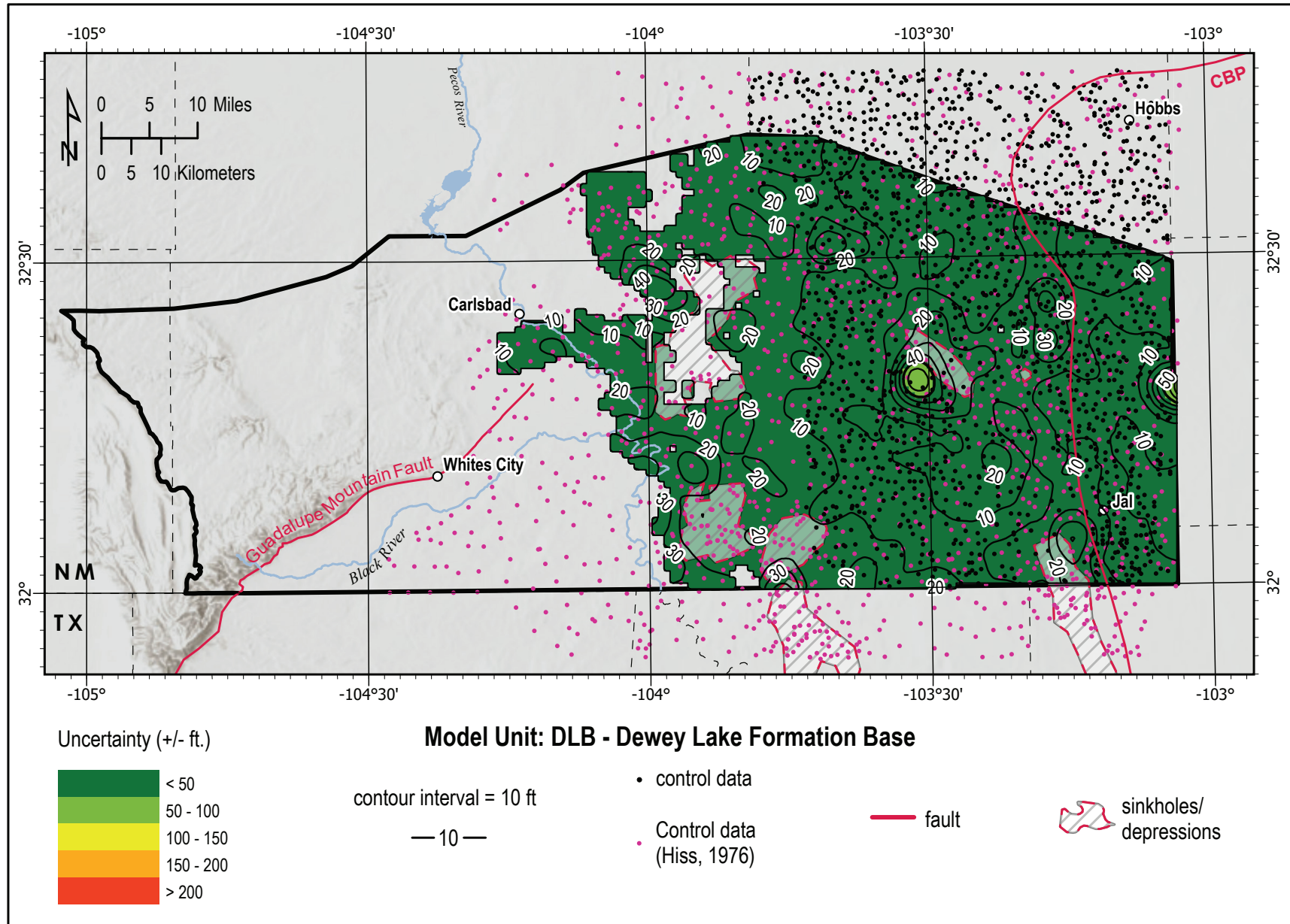
Figure 26. Dewey Lake Formation base uncertainty map. Due to the dense dataset used to generate this surface, the mean uncertainty is ± 18.3 ft. CBP: Central Basin Platform.

Rustler Formation

base elevation (ft. amsl) contour interval = 100 ft — —100— —

outcrop

subsurface

• control data

fault

sinkholes/ depressions
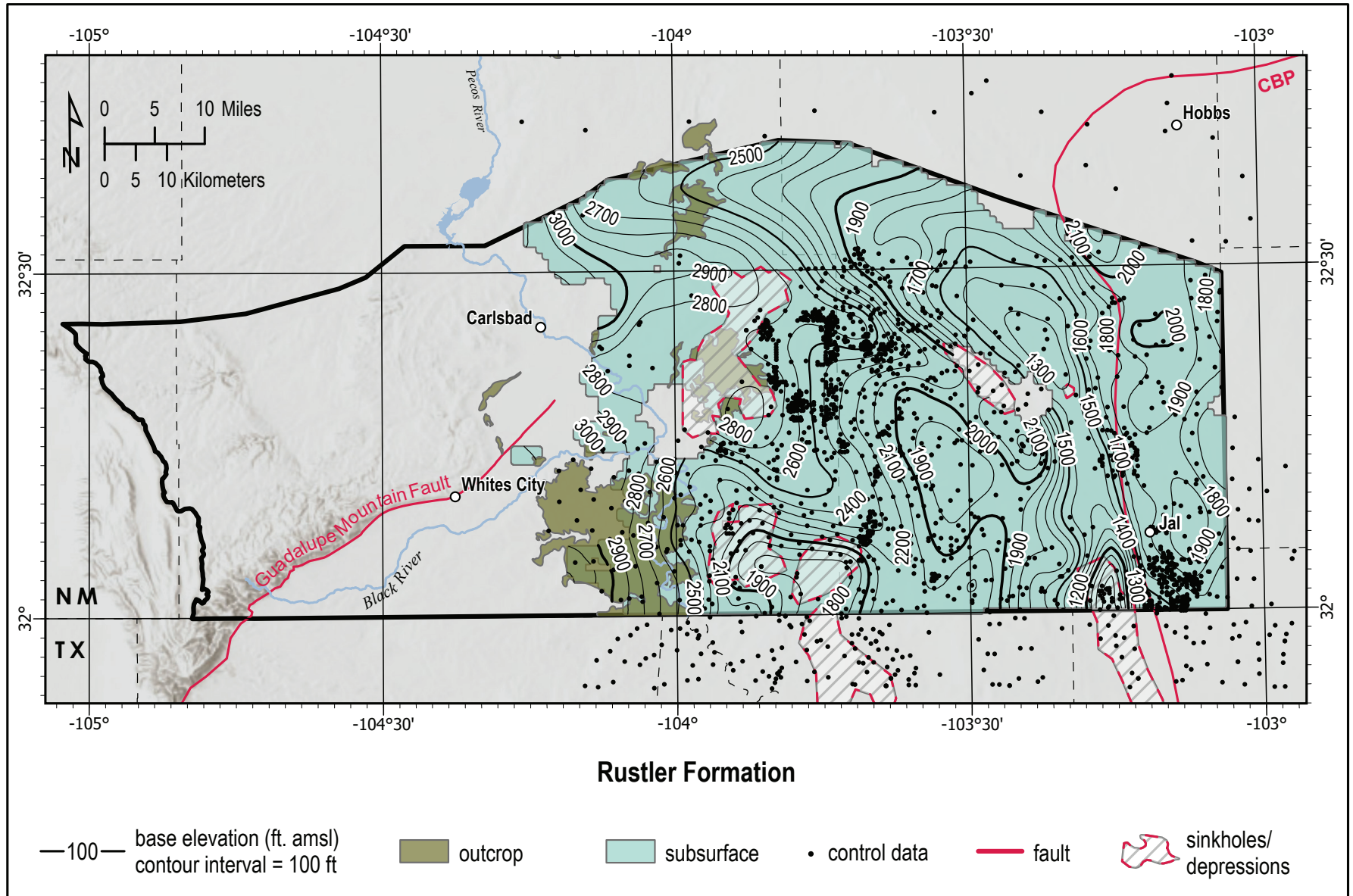
Figure 27. Rustler Formation base (RB) elevation structure contour map. CBP: Central Basin Platform.
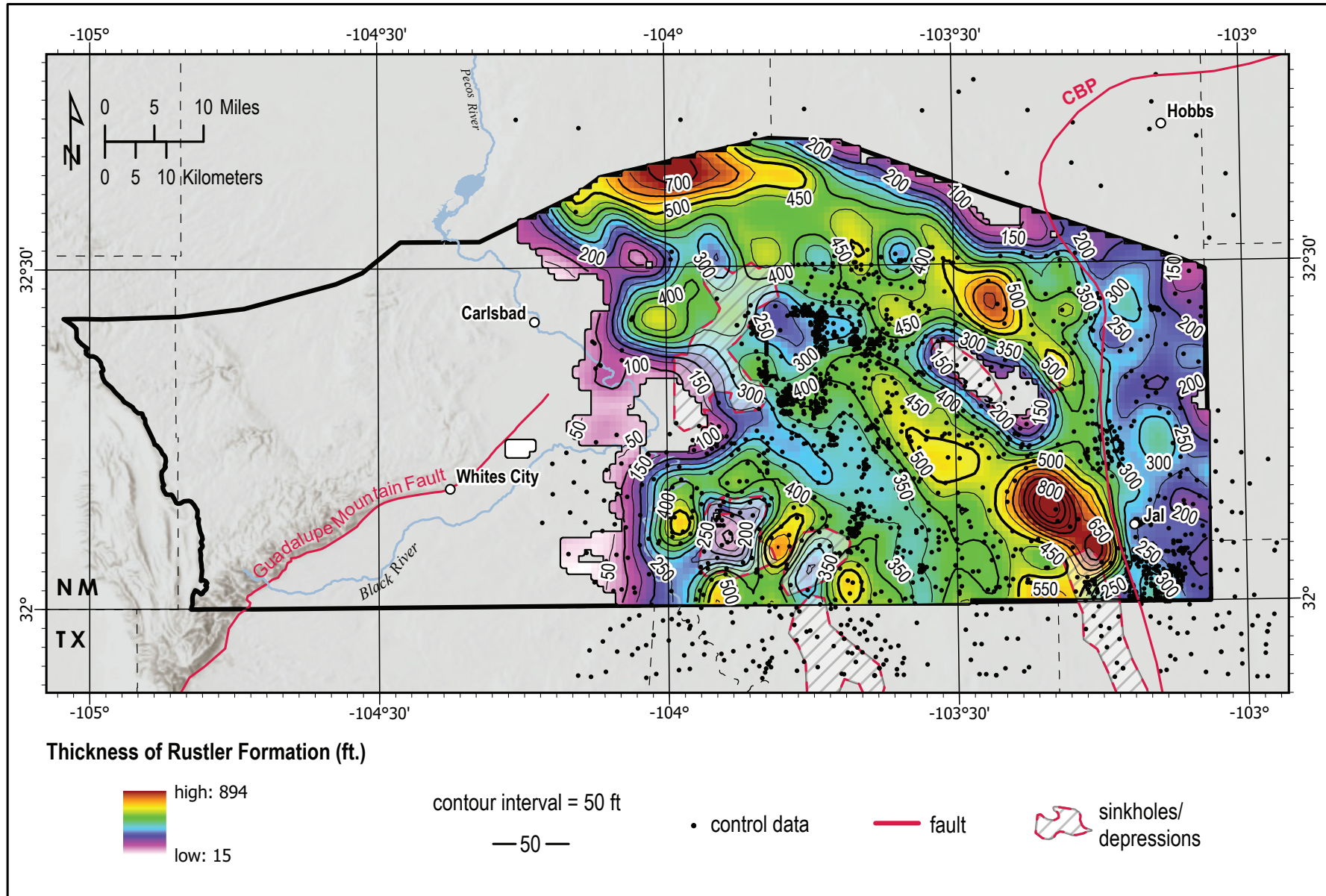
Figure 28. Isopach map showing Rustler Formation thickness. CBP: Central Basin Platform.
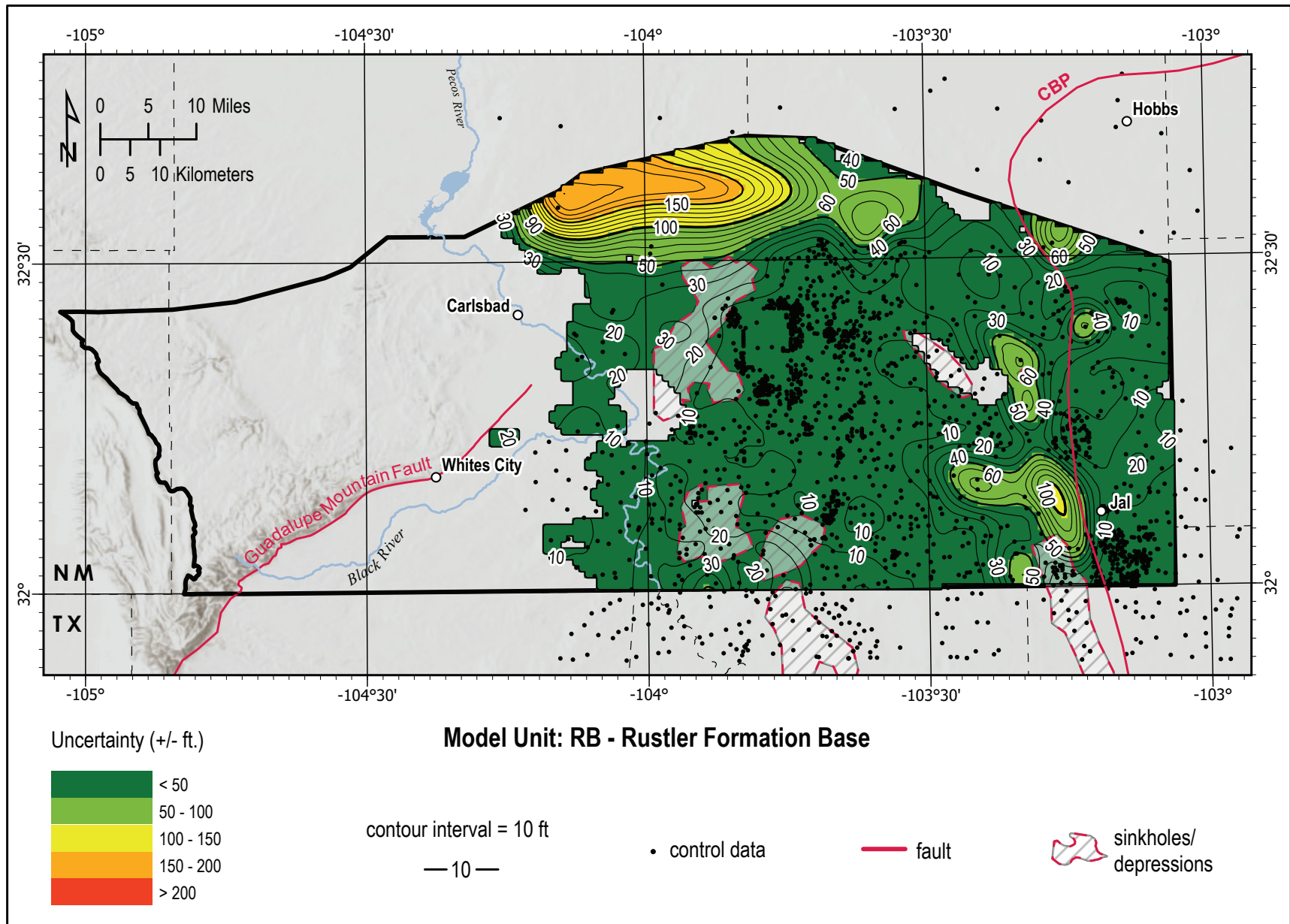
Figure 29. Rustler Formation base uncertainty map. CBP: Central Basin Platform.

Lower Ochoan Formations

base elevation (ft. amsl) contour interval = 100 ft — —100— —

outcrop

subsurface

• control data

fault

sinkholes/ depressions
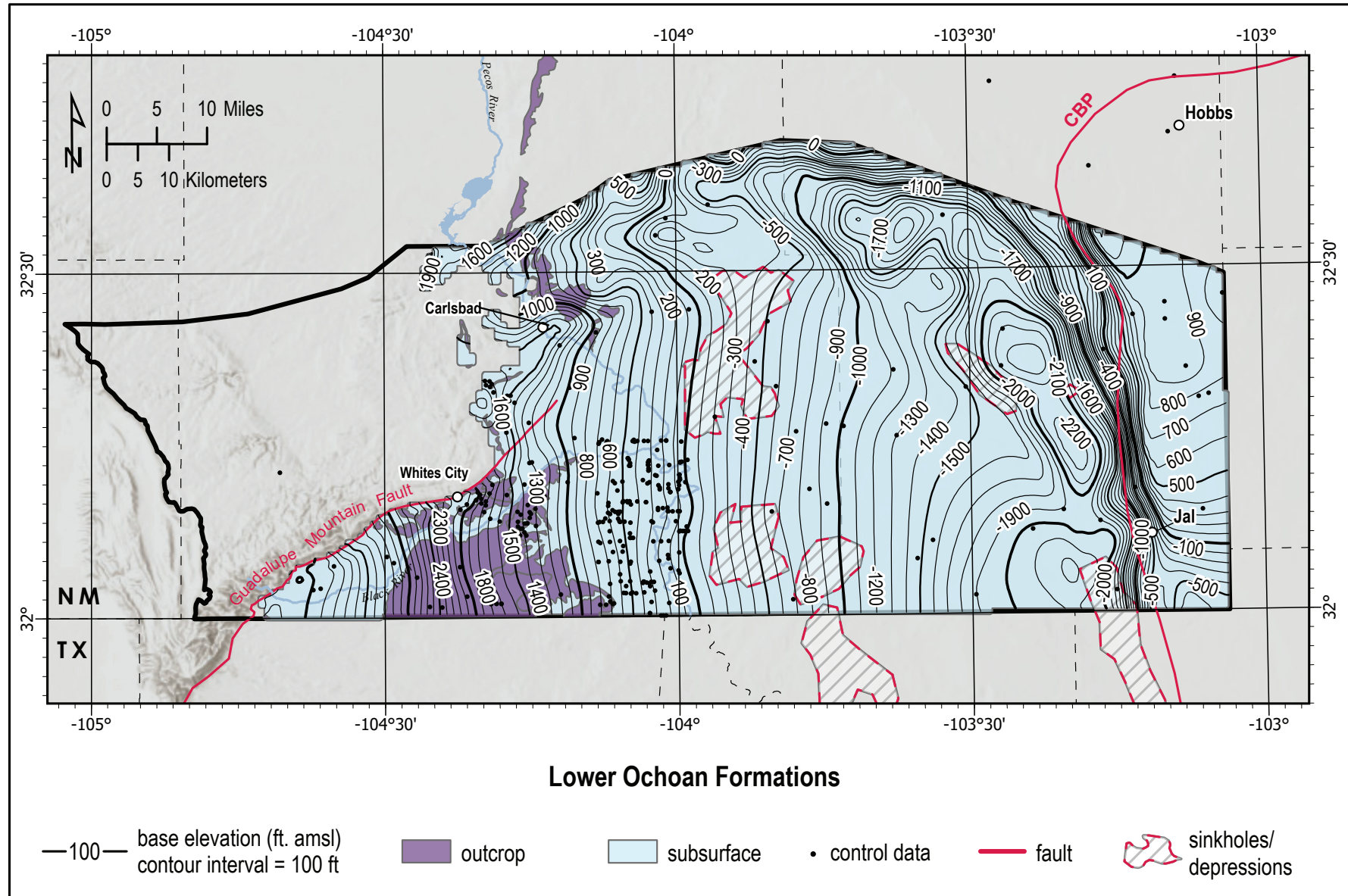
Figure 30. Lower Ochoan formations (Salado and Castile Formations) base (LOB) elevation structure contour map. CBP: Central Basin Platform.

Thickness of Lower Ochoan Formations, undivided (ft.)

high: 4,115

low: 133

contour interval = 50 ft

—50—

• control data

— fault

sinkholes/depressions
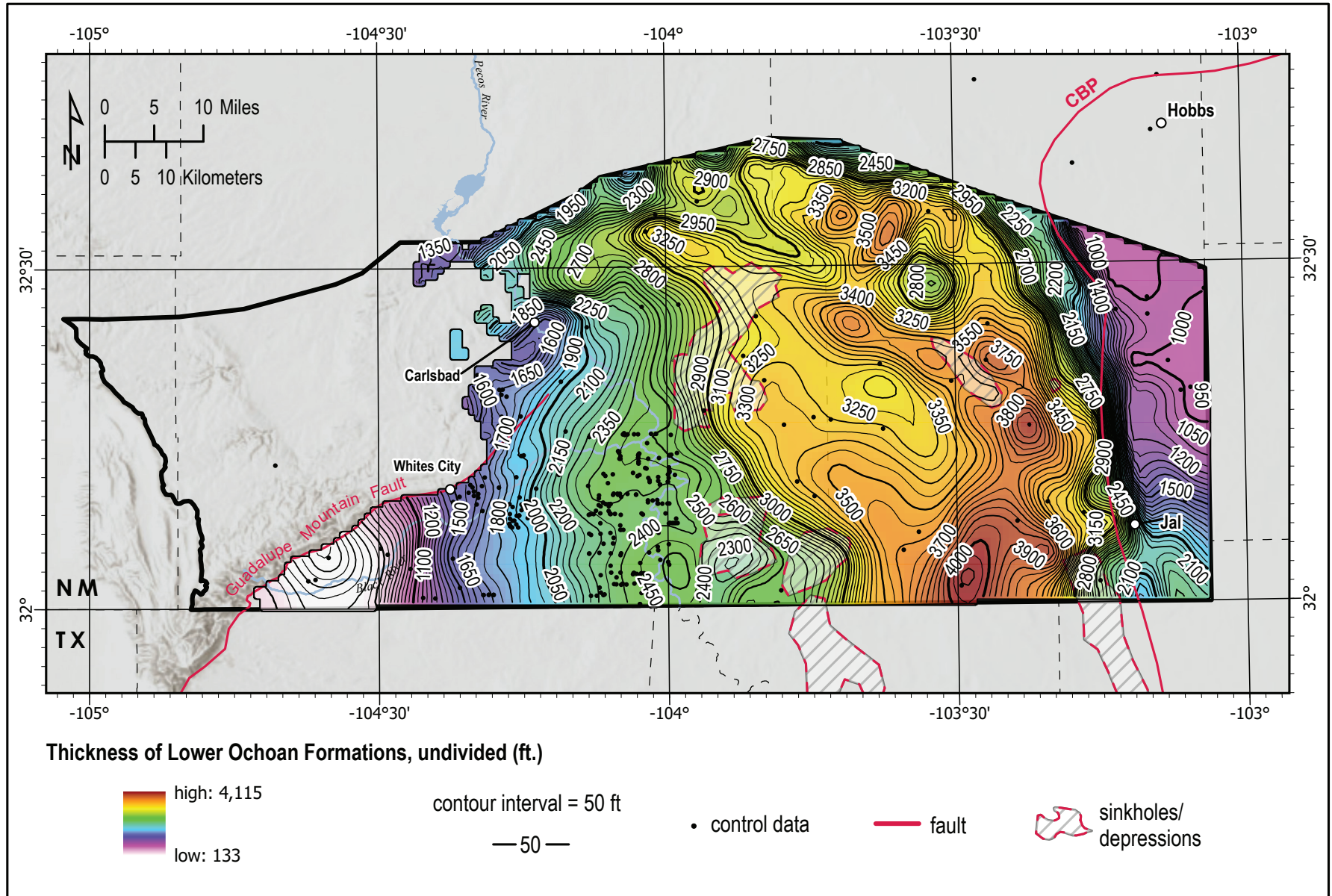
Figure 31. Isopach map showing lower Ochoan series thickness, undivided (Salado and Castile Formations). CBP: Central Basin Platform.
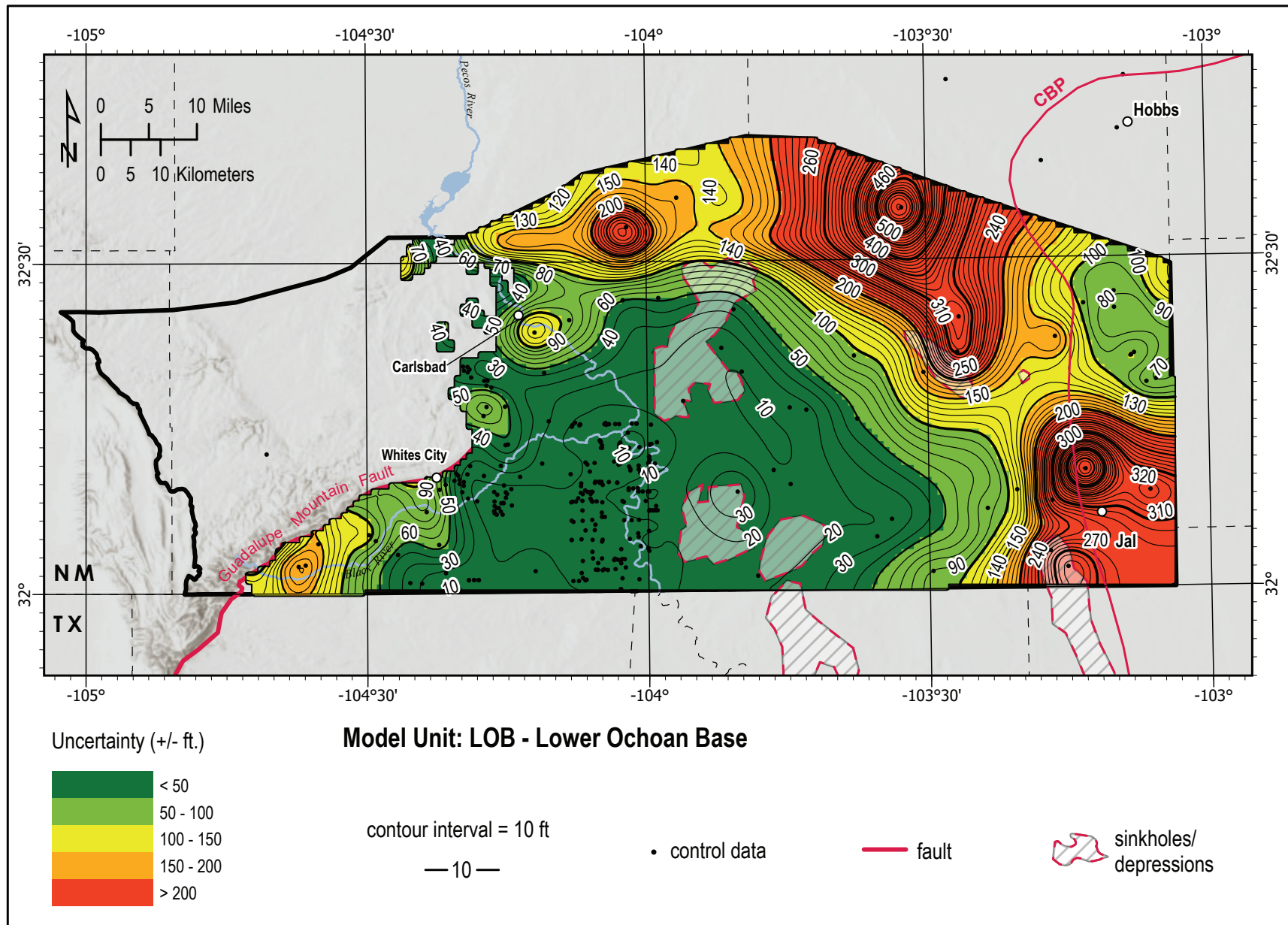
Figure 32. Lower Ochoan series uncertainty map. CBP: Central Basin Platform.

Artesia Formation

Legend: —100— base elevation (ft. amsl) contour interval = 100 ft | outcrop | subsurface | • control data | — fault | sinkholes/depressions
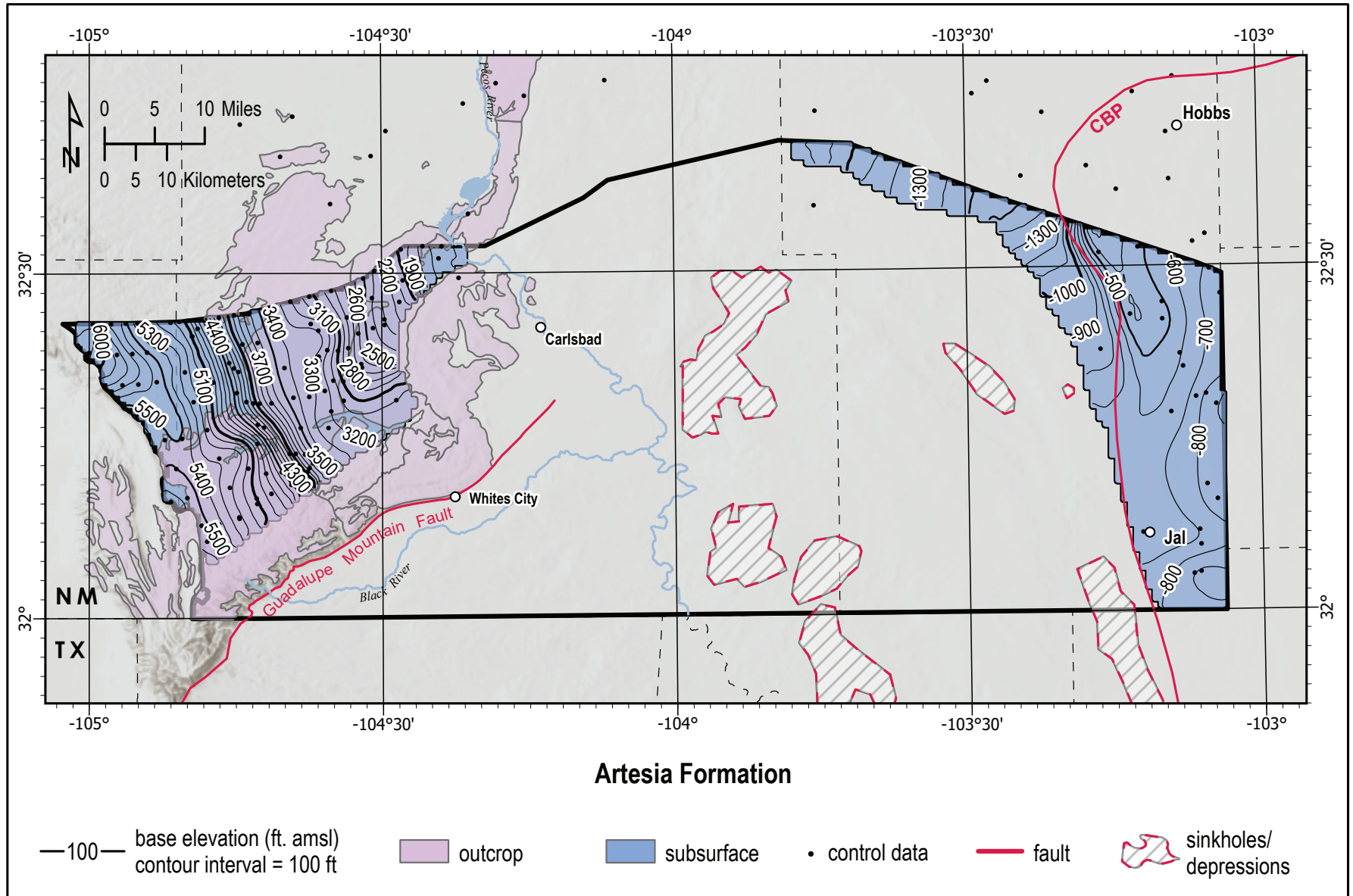
Figure 33. Artesia Group base (AGB) elevation structure contour map. Base elevation not interpolated where the Artesia Group overlaps with the Capitan Reef. CBP: Central Basin Platform.
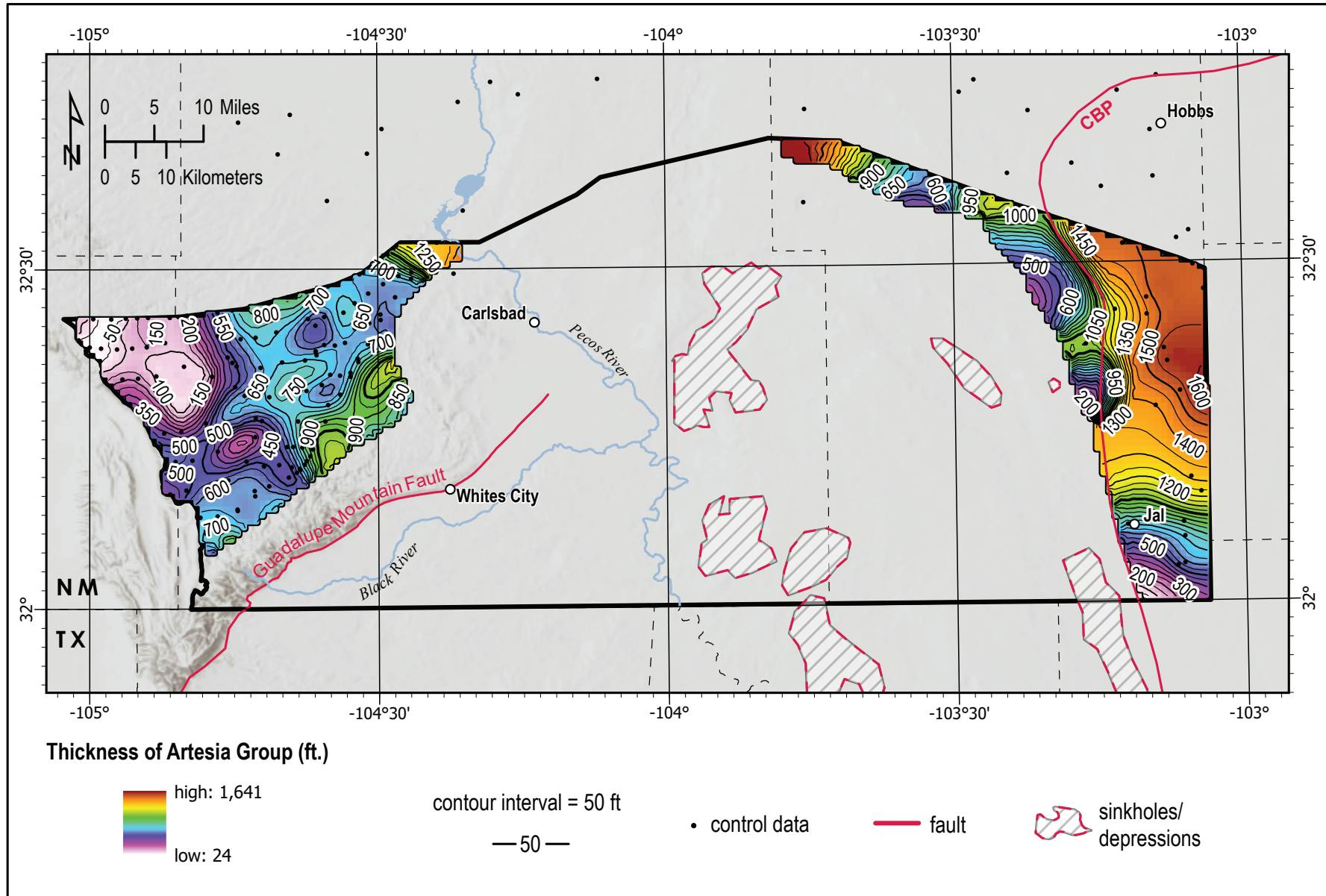
Figure 34. Isopach map showing Artesia Group thickness. CBP: Central Basin Platform.

Model Unit: AGB - Artesia Group Base

Uncertainty (+/- ft.)

- < 50
- 50 - 100
- 100 - 150
- 150 - 200
- > 200

contour interval = 10 ft

— 10 —

• control data

—— fault

sinkholes/ depressions
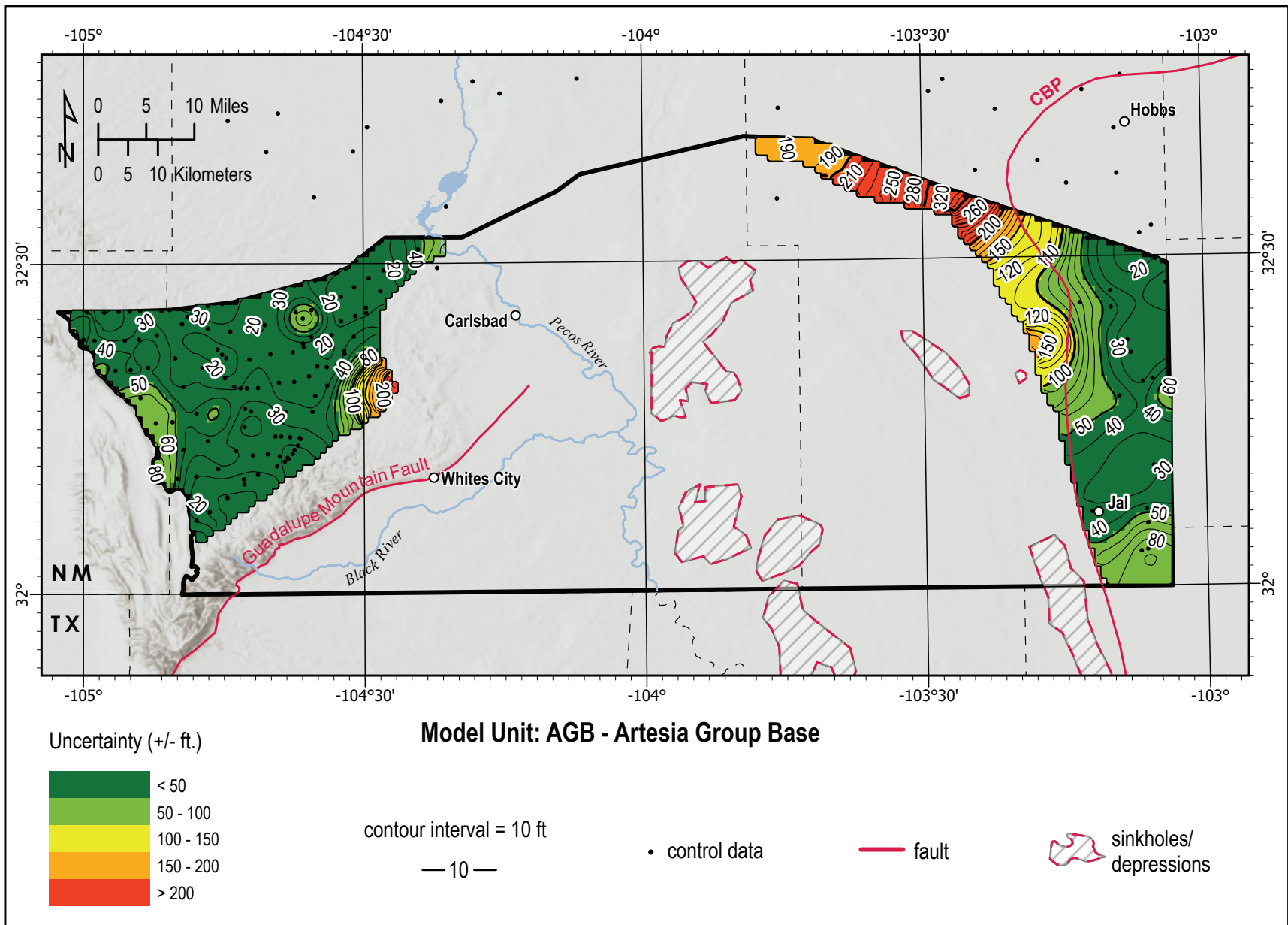
Figure 35. Artesia Group base uncertainty map. CBP: Central Basin Platform.

Figure 36. Capitan Formation outcrops and subsurface extent in New Mexico and Texas.

Capitan Formation

—100— base elevation (ft. amsl) contour interval = 250 ft	outcrop	subsurface	• control data	—— fault	sinkholes/depressions
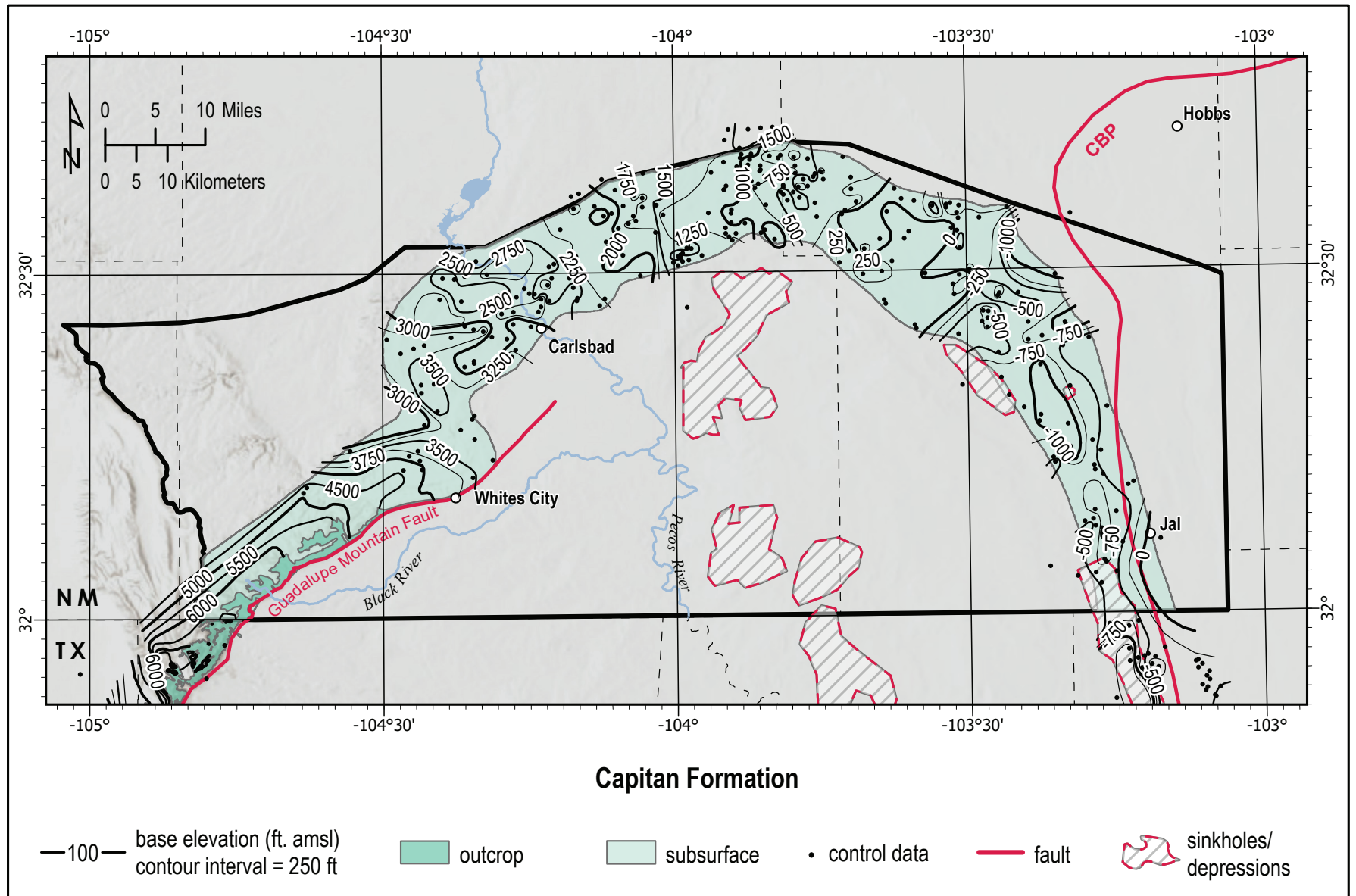
Figure 37. Capitan Formation top (CT) elevation structure contour map. Base elevation not interpolated where the Artesia Group overlaps with the Capitan Reef. CBP: Central Basin Platform.

Capitan Formation Isopach

base elevation (ft. amsl) contour interval = 250 ft — outcrop — subsurface — control data — fault — sinkholes/depressions

Figure 38. Isopach map showing Capitan Formation thickness. Base elevation not interpolated where the Artesia Group overlaps with the Capitan Reef. CBP: Central Basin Platform.

RESULTS: 3D HYDROLOGIC MAP DATA

This section provides a model of the regional shallow subsurface geologic framework of the Delaware basin region of southeastern New Mexico. Its construction involved compiling a variety of input datasets, including well data, surface geologic mapping, geologic cross sections, and structure contours; evaluating the input data using geostatistical methods; and then interpolating contact surfaces between control point locations. The model is intended to be a "framework" model to be used for illustrative purposes, with a target horizontal resolution of no better than 1 km by 1 km and a target vertical resolution of no better than 100 ft. The final, total uncertainty in each contact surface as a function of location was estimated by combining the uncertainties from the interpolation methods used an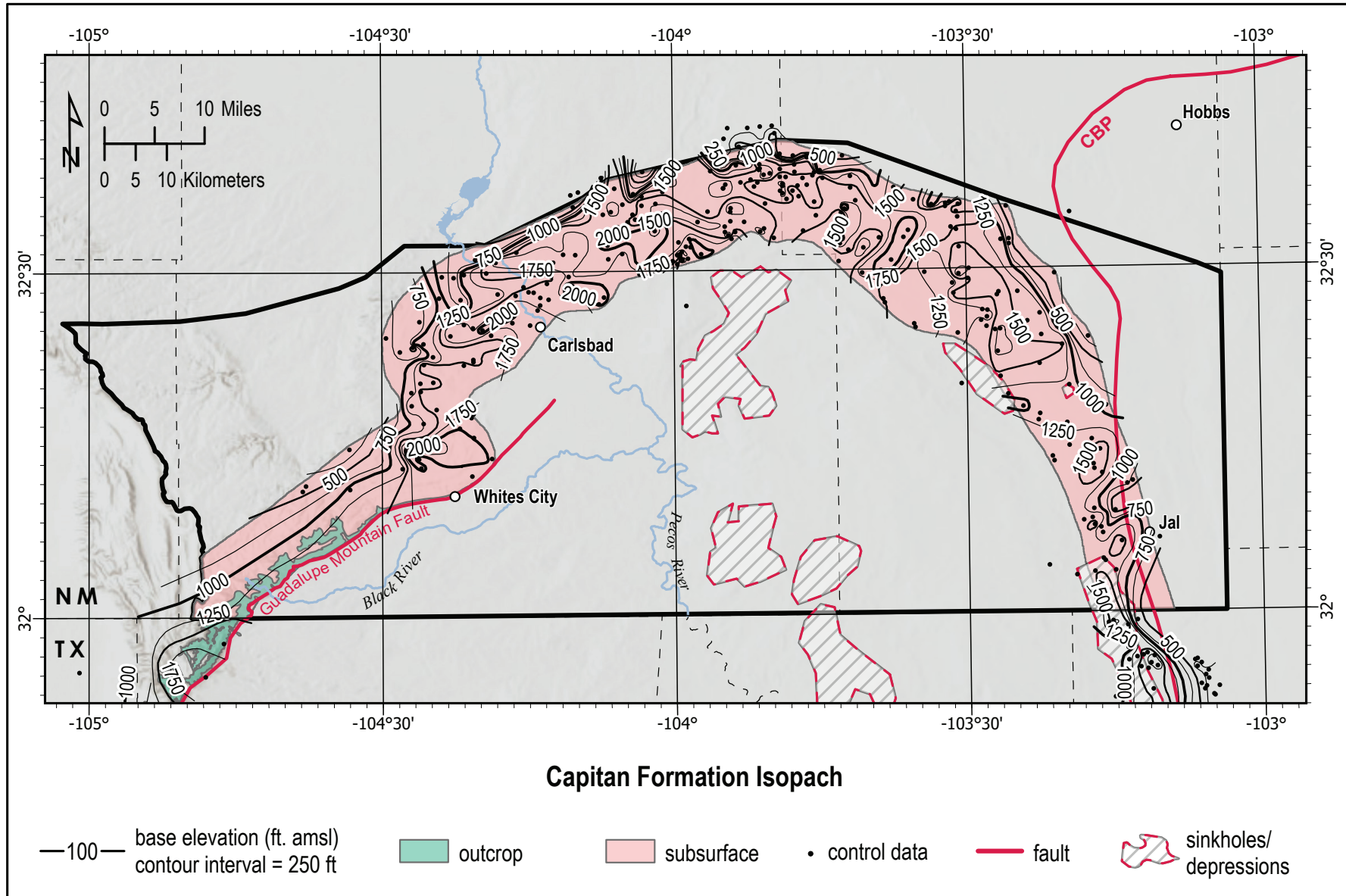d an n-fold cross-validation approach to evaluating dataset uncertainty. Any enlargement of this map could cause misunderstanding in the detail of mapping and may result in erroneous interpretations. Site-specific conditions should be verified by detailed surface mapping or subsurface exploration. Digital data descriptions are as follows.

<aquifer system>Group layer: Contains aquifer system extent, model data, potentiometric surface, depth-to-water map, maximum saturated thickness, base elevation, and water quality data.

<aquifer system>Extent: 2D extent of aquifer system. Determined by study area boundaries and geologic formation extents. Type: polygon.

<aquifer system>ModelData: Water level elevation data for wells within aquifer system. The majority of wells were measured after 2010, except in cases where data were so sparse that older water levels were needed. Exceptions explained in this section. Type: point.

<aquifer system>DepthToWater_ftbgs: Water depth recorded in feet below ground surface. Type: raster; grid size: 1,000 × 1,000 m.

<aquifer system>WaterTableElev_ftamsl: Potentiometric surface elevation above mean sea level. Water level measurements can contain both confined (artesian) and unconfined conditions in this region. Type: raster; grid size: 1,000 × 1,000 m.

<aquifer system>WaterTableFlowLines: Lines indicating direction of groundwater flow. Type: polyline.

<aquifer system>SaturatedThickness_ft: Vertical thickness of water-bearing units defined as difference between water level surface and aquifer base. Type: raster; grid size: 1,000 × 1,000 m.

<aquifer system>BaseElevation_ftamsl: Elevation above mean sea level of the bottom-most geologic formation of the aquifer. Type: raster; grid size: 1,000 × 1,000 m.

<aquifer system>WaterQuality: Wells with available water quality data, including historical datasets. Recent data were defined as water level or water quality measurements reported after the year 2010. TDS maps provided indicate values below 10,000 mg/L as good water quality and above as bad water quality. Type: point.

DELAWARE BASIN AQUIFER SYSTEM

Hydrologic description

The Delaware Basin Aquifer System (DBAS) contains several generally recognized water-bearing units: the Pecos River valley alluvium and other Cenozoic deposits, the Culebra and Magenta Members of the Rustler Formation, and the Santa Rosa Formation of the lower Dockum Group (Fig. 4; Hale, 1945; Henderson and Jones, 1952; Bjorklund and Motts, 1959; Nicholson and Clebsch, 1961; Richey et al., 1985). Other units, such as the late-Permian Dewey Lake Redbeds and Triassic upper Dockum Group/ Chinle Formation, may be present and possibly provide marginal water resources (Mercer, 1983;

Richey et al., 1985). These units are not present everywhere in the aquifer system, but there are likely substantial interactions between them where they spatially coincide, and there is agreement in the general movement of groundwater among them (Henderson and Jones, 1952; Nicholson and Clebsch, 1961). For the purposes of this study, we mapped the aquifer units as a single aquifer system (Fig. 11). We acknowledge that the aquifer units exhibit varying degrees of hydrologic confinement and connection across the study area; however, the resolution of this data from driller's logs is not high enough to quantitatively resolve the complex relationships between specific units. Site-specific studies are encouraged to resolve hydrologic connections within smaller map areas.

Digital data

< DBAS > *Extent*

In this study, the DBAS is composed of basin fill bound on the west and northwest by the Guadalupe Mountains and the Capitan Reef Aquifer System (Fig. 39). The northern boundary is the Roswell basin aquifer system. The northeastern limits are where the study area meets the boundaries of a previously developed Pecos Slope hydrogeologic model. The southern and eastern boundaries are marked by the New Mexico-Texas state line. The areas south of Carlsbad and west of the Pecos River are predominantly alluvial fill, but they also include the Rustler Formation where it crops out and is in connection with the Pecos River. West of that, we determined from detailed 1:24,000 geologic maps, satellite imagery, and the location of water wells that there are several isolated pockets of groundwater along channels, but not enough to connect them. Elevations in the aquifer system range from 7,457 ft amsl in the Guadalupe Mountains to 2,812 ft amsl in the Pecos River valley near the New Mexico-Texas state line.

< DBAS > *Model Data*

There was a total of 353 wells with water levels measured after 2010 used to calculate hydrologic surfaces in the DBAS. Hydrographs examining water level changes over this time period reveal fairly stable water table elevations, with an equal number of wells showing rising and falling trends. One well with a water level from 1998 was used to expand the interpolated area to the reef escarpment in the west.

These depth-to-water measurements were reported by NMBGMR, Sandia National Laboratories, NMOSE, NM EMNRD OCD, TWDB/BRACS, and USGS. The highest spatial concentration of wells is generally found in areas with thick alluvial and bolson deposits, as well as the Monument dissolution trough in the southeastern part of the study area that extends outside the model area (Fig. 39). Other areas with high data densities are population centers like Carlsbad, Hobbs, and Jal. Given the poor quality and quantity of water in many areas, along with sparse population, there are some spatial gaps in the data. One area with especially poor data density is western Lea County, where the alluvium is very thin and water in the underlying strata is highly mineralized. The southern Guadalupe Mountains in the study area also generally lack wells with water level measurements.

< DBAS > *Depth to Water in feet below ground surface*

Depth to water and groundwater elevations were calculated based on water level measurements from 2010 to the present (also described in the *3D Aquifer Mapping Methods* section above). The depth-to-water surface was calculated by subtracting the water level elevation surface values from the land surface elevation values of a 4.5-m digital elevation model. The final resolution of the depth-to-water surface was 1 km. When interpreting this surface, keep in mind that wells could be drawing water from multiple water-bearing units—either by design or through the degradation of the well casing—or the artesian pressure in a well could give the false impression of a shallow depth to water. Depth to water and potential saturated thickness values should always be considered in the context of the local geology.

The extent of the system was discontinuous due to interpolated water level elevation values rising above the land surface where groundwater discharges to the surface in the form of springs. The calculated depth to water in the DBAS ranges from about 20 ft below ground surface (bgs) to almost 1,254 ft bgs (Fig. 39). Due to confined conditions in regions of the aquifer system, the depth-to-water map may reflect artesian values where the water level has risen above the formation depth after drilling. Caution should be used when interpreting these values for estimated well drilling depths. The shallowest depths to water were calculated in the northeastern part of the aquifer system where groundwater is likely entering the basin

from the Ogallala Formation of the High Plains, driven by the southwest-trending topography in the area. Water is deepest along the reef escarpment and transitions from the Capitan Reef system to the DBAS, where significant topographic relief exists. Areas of relatively deep water also exist in southeastern Eddy County east of Malaga Bend, and in southwestern Lea County south of Laguna Plata (Fig. 39). The notably deeper groundwater in these areas coincides with a slight north-south-running ridge in southwestern Lea County with exposures of the Ogallala Formation. The significant water-bearing stratum in these areas is the Santa Rosa Sandstone of the Dockum Group, which occurs at about the same depth as the depth-to-water contours as indicated by the geologic surfaces (Fig. 20).

< DBAS > Potentiometric surface in feet above mean sea level

Groundwater elevations range from more than 4,200 ft amsl at the base of the reef escarpment of the Guadalupe Mountains to less than 2,800 ft amsl in the southeastern corner of the study area on the state line where a large collapse structure has been filled in (Fig. 40). High water level elevations coincide with primary recharge areas in the Guadalupe Mountains and a topographic high in western Lea County, just west of San Simon Swale. In Eddy County, most of the fresh water originates as precipitation in the Guadalupe Mountains, percolates into the carbonate rocks, then flows east along the topographic gradient and through fractures, bedding planes, and submerged limestone caverns until it ends up in the DBAS (Hale, 1945; Henderson and Jones, 1952). This eastward movement is restricted by a change to evaporite and silt/sandstone facies just east of Carlsbad, and groundwater is discharged to the surface and Cenozoic deposits (Motts, 1968). The topographic high west of San Simon Swale is an area of concentrated recharge occurring primarily during large precipitation events, where sinkholes filled with sediment allow for accumulation and more focused recharge to underlying Triassic and Permian substrates (Nicholson and Clebsch, 1961; NMOSE, 2016a). Groundwater moves out from this recharge area in all directions, but is especially captured by dominant flow paths to the southwest toward the Pecos River, likely through the Santa Rosa and Rustler Formations, and to the southeast toward the large collapse structure on the New Mexico-Texas state line. These dominant flow paths could result

from increased permeability in collapse structures to the southwest of the recharge area and/or the slightly sloping topography toward the Pecos River. In eastern Lea County near the New Mexico-Texas state line, groundwater flow is predominantly north-south through Monument Draw. The groundwater that flows through this portion of the system likely originated from the Ogallala Formation to the north of the Laguna Valley area (Fig. 2), moving south and southeast through Cenozoic deposits, including the Ogallala Formation (Nicholson and Clebsch, 1961).

< DBAS > Saturated Thickness feet

The calculated saturated thickness takes into account the potentiometric surface of the aquifer system and the base of the Rustler Formation, and does not differentiate individual geologic units within the DBAS. The thickness of the aquifer is largely driven by the base of the Rustler, where large collapse structures created by dissolution in the underlying evaporites have been filled in with overlying Permian- and Triassic-age formations. An estimate of the saturated thickness in the Delaware basin aquifer is presented in Figure 41 and ranges from less than 3 ft to greater than 2,246 ft.

Caution should be used in applying this estimate to regional volume calculations or drilling estimates because, as discussed above, large unsaturated zones exist within the overall DBAS (see Fig. 4). Values east of the Pecos River become increasingly misleading as the most important water-bearing geologic units become more confined, isolated, and deeper under the surface, moving east across the system. The most significant saturated zones are the Magenta and Culebra Members of the Rustler Formation, the Santa Rosa Sandstone of the Dockum Group, and pockets of the Pecos River valley alluvium. Places with the lowest saturated thickness values occurred in the western half of the basin system where the aquifer is more intermittent, and also around the Pecos and Black Rivers. An area of elevated thickness was calculated at Bell Lake west of San Simon Sink, where a "mound" of groundwater has been historically observed and noted as a recharge area for the system (Henderson and Jones, 1952; Nicholson and Clebsch, 1961). Places with the highest saturated thickness values coincided with likely recharge areas, especially in the area of Laguna Valley where the Ogallala Formation of the High Plains aquifer is probably contributing to the basin aquifer (Fig. 2).

< DBAS > Base Elevation in feet above mean sea level

The base aquifer elevation was determined using the base of the Rustler/top of the Salado, below which potable water is not found in the system where the Salado is present (Fig. 42; Henderson and Jones, 1952; Nicholson and Clebsch, 1961). To make the aquifer base surface, raster surfaces representing the bases of the Rustler and Dewey Lake Formations and alluvium are combined into one surface using the Esri Mosaic tool. The basal surface of the system is characterized by a high degree of topographic variation, with an overall west-to-east-trending slope. Irregularities in the base of the aquifer are largely interconnected depressions created by the collapse of strata overlying areas where deeper evaporites and carbonate units were removed by dissolution (Anderson, 1981). Extensive areas of dissolution and collapse are found in the eastern area of the basin, where the north-south-oriented Monument dissolution trough runs through the study area over the eastern arm of the Capitan Reef. Faulting and flexing at depth along the eastern arm of the reef margin likely facilitated contact between evaporites and deeper groundwater, dissolving the salts and leading to collapses that sometimes extend to the surface through breccia pipes (e.g., San Simon Sink; Anderson, 1981).

Water quality

< DBAS > Water Quality

Spatial variability of TDS in groundwater

Table 4 shows selected constituents (pH, TDS, and major cations and anions), the number of samples with that specific constituent, the range of data, and the mean and standard deviation for each constituent within the DBAS. The large range of concentrations and standard deviations demonstrates the complexity of the groundwater system. Figure 43 shows the spatial variability for TDS for 583 samples collected from different wells within the DBAS over the last 70 years. The best-quality groundwater, with TDS concentrations less than 1,000 mg/L (small green points), occurs on the western edge of the DBAS, the southeastern corner of Eddy County, and sparsely throughout Lea County. Groundwater with TDS concentrations between 1,000 and 3,000 mg/L (yellow points) is typically observed in the

northeastern corner of the DBAS. In addition, wells that produce these waters are sparsely distributed throughout the rest of the DBAS. While groundwater with TDS concentrations greater than 3,000 mg/L (orange and red points) appears to occur throughout the DBAS, the majority of wells that produce these poor-quality waters are located approximately in the center of the DBAS in eastern Eddy County.

Figure 44 shows data for wells for which both TDS and an estimate of the total well depth below the surface were known. As is evident when comparing Figures 43 and 44, water quality data are often lacking the well depth, which is needed to more precisely map water quality in three dimensions. The colors of the points indicate the TDS range, and the sizes of the points are proportional to the total well depth. With the limited data available, it appears that TDS concentrations are not correlated with depth. On the western edge of the DBAS, good-quality groundwater (<1,000 mg/L, green points) is produced from wells that are completed 500 to 1,000 ft bgs, and this is the deepest that this high-quality water is observed. Similarly, wells that produce water with TDS concentrations ranging from 1,000 to 3,000 mg/L (yellow points) are mostly not observed to be deeper than 1,000 ft bgs. The one exception is the well in the southwestern corner of the DBAS, which is completed at about 1,200 ft bgs. Wells that produce water over 3,000 mg/L are observed to be completed in the full range of depths, from less than 200 to about 8,000 ft bgs.

Table 4. Statistics for selected analytes. Except for pH, units are mg/L.

Analyte	Number of samples	Concentration range (mg/L, except pH)	Mean (standard deviation)
Total dissolved solids (TDS)	627	21–412,000	14,140 (52,614)
Calcium (Ca^{2+})	468	2.6–31,000	650.6 (2,228)
Magnesium (Mg^{2+})	416	2.1–82,000	1,059 (6,556)
Sodium (Na^+)	235	0.3–130,000	8,486 (22,841)
Potassium (K^+)	202	0.2–21,000	745 (2,736)
Bicarbonate (HCO_3^-)	441	1–2,310	225 (179)
Chloride (Cl^-)	740	0.25–290,000	8,750 (33,233)
Sulfate (SO_4^{2-})	535	6–222,000	1,658 (9,715)
pH	198	5.8–9.3	7.4 (0.52)

Assessment of water sources and geochemical processes

Figure 45 shows a log/log plot of TDS concentration as a function of Cl⁻ concentrations for 515 wells that had both TDS and Cl⁻ data available. There is a clear, direct linear correlation between these two measurements that shows Cl⁻ to be a good proxy for TDS concentrations for Cl⁻ concentrations greater than 1,000 mg/L. For water with Cl⁻ concentrations less than 1,000 mg/L, TDS concentrations can range from about 300 to over 2,000 mg/L. Figure 46 shows spatial variations in TDS and Cl⁻ concentrations for groundwater in the DBAS. Again, TDS values are represented by the colors of the points, and the size of the point is proportional to Cl⁻ concentrations, ranging from 0.25 to 290,000 mg/L. For all waters that exhibit TDS concentrations greater than 10,000 mg/L (red points), Cl⁻ concentrations are also high (Cl⁻ >3,000 mg/L). However, for all waters with TDS values less than 10,000 mg/L (orange, yellow, and green points), Cl⁻ concentrations can vary greatly. Again, wells producing the highest TDS and Cl⁻ concentrations are most abundant in the approximate center of the model domain near the boundary between Eddy and Lea Counties.

Three mixing end members can be identified in Figure 47, which shows TDS concentrations plotted as a function of relative SO_4^{2-} concentrations, with the size of data points being proportional to Cl⁻ concentrations. The data points with the lowest Cl⁻ concentrations (smallest points) plot on a mixing line between a low-TDS, HCO_3^- water type and an intermediate-TDS, SO_4^{2-} water type. Any increase in Cl⁻ concentration appears to be associated with mixing with a high-TDS Na-Cl brine. The major chemistry for all groundwater samples can be explained as being a mixture of these three end members.

Figure 48 shows groundwater chemistry data for groundwater with TDS concentrations less than 3,000 mg/L plotted on a Piper diagram. Green points (TDS <1,000 mg/L) and open squares (TDS 1,000–3,000 mg/L) correlate with green and yellow points, respectively, in Figures 43, 44, and 46. These wells are located throughout the DBAS, mostly at shallow depths (Fig. 44). However, some wells are observed to be between 500 and 1,000 ft bgs. The data seen in Figure 48 look similar to those plotted on Piper diagrams in Figures 7 and 8, which

represent groundwaters from the aquifers in the upper Dockum Group and Cenozoic alluvium, respectively. The deeper wells are likely completed in the lower Dockum Group. The green wells on the western boundary of the DBAS that are between 500 and 1,000 ft bgs are completed in the Capitan Reef limestone. Shallower wells that produce water with TDS concentrations less than 3,000 mg/L are completed in the alluvial aquifers.

The Piper diagram in Figure 49 shows water chemistry for wells with TDS concentrations greater than 3,000 mg/L. The orange points (TDS 3,000–5,000 mg/L) and pink points (TDS 5,000–10,000 mg/L) correlate to orange and pink points, respectively, in Figure 43, but correlate to just orange points (TDS 3,000–10,000 mg/L) for Figures 44 and 46. The red points (TDS >10,000 mg/L) correlate to red points in Figures 43, 44, and 46. The data shown in Figure 49 look very similar to those shown in Figure 6, which shows water chemistry data for groundwater from the Rustler Formation and the Dewey Lake Formation. Most of the wells that produce water with TDS concentrations between 3,000 and 10,000 mg/L are relatively shallow and located in areas of Eddy County where the Rustler Formation crops out or is very shallow in the subsurface (Fig. 44). Most wells that produce water with TDS values greater than 10,000 mg/L are located near Rustler outcrops and are relatively deep, indicating that they are likely completed in the lower Rustler Formation or underlying Ochoan strata.

Groundwater samples collected by NMBGMR for this study exhibit TDS concentrations ranging from 486 to 4,220 mg/L (Fig. 50). The Piper diagram in Figure 51 shows these data. Wells producing water with TDS concentrations between 500 and 2,000 mg/L (black, dark-green, and light-green points) are likely fairly shallow and completed in the Cenozoic Pecos River valley alluvium. Most wells producing water with TDS concentrations greater than 2,000 mg/L (blue and red points) exhibit a Ca-SO₄ water type and therefore likely produce water from the Rustler Formation (Facies B).

Environmental tracers

In addition to general water chemistry (major cations and anions) and trace metals, water samples collected by NMBGMR researchers in 2021 (purple diamonds, Fig. 12) were analyzed for the stable isotopes of

water, carbon-14 (^{14}C), and tritium to assess water sources and ages. The following discussion describes important concepts and how these data are used and interpreted.

The stable isotopes of oxygen and hydrogen are useful tools for tracing the hydrologic cycle. The isotopic composition of a water sample refers to the ratio of the heavier isotopes to the lighter isotopes (R) for the hydrogen and oxygen that make up water molecules. Because these stable isotopes are part of the water molecule, small variations in these ratios act as labels that allow tracking of waters with different stable isotopic signatures. All isotopic compositions in this report are presented as relative concentrations (R), or the per mil deviation of R of a sample from the Vienna Standard Mean Ocean Water (VSMOW) R as shown in the equation below:

$$\delta = \frac{R_{sample} - R_{standard}}{R_{standard}} * 1000‰$$

It is useful to plot stable isotope data on a δD vs. δ^{18}O graph, as shown Figure 52. In general, most precipitation plots on or near the global meteoric water line (GMWL) with a slope of 8 and a deuterium excess (y-intercept) of 10, as demonstrated by Craig (1961). Stable isotopes of water can also be useful for identifying water that has undergone evaporation. Isotopically lighter water molecules evaporate at a slightly higher rate than isotopically heavier water molecules, resulting in isotopic fractionation and thus causing the residual water to become heavier and evolve along an evaporation line that usually has a slope between 4 and 6. Mixing of waters with different isotopic compositions can also be assessed.

The stable isotopic composition of groundwater in the study area has been studied extensively by researchers assessing the hydrogeologic conditions of the Rustler Formation at the WIPP site (Chapman, 1986). Stable isotope data plotting along the GMWL (Fig. 52) do not appear to be associated with the mixing line observed for water at the Rustler/Salado interface or the evaporation line defined by Chapman (1986). The mixing line is a result of meteoric water mixing with isotopically heavy brines from the lower Ochoan strata (Salado and Castile Formations). The evaporation line is due to the evaporation of

water from the Rustler Formation through the thin vadose zone in the area near Nash Draw. These data indicate that the different aquifers in this system (Rustler Formation, Dewey Lake Formation, Dockum Group, and Cenozoic alluvium; see Fig. 4) are being recharged by precipitation under the current climatic conditions and not during wetter conditions in the Pleistocene.

Tritium and carbon-14

Tritium (^{3}H), a radioactive isotope of hydrogen with a half-life of 12.4 years, is produced naturally in the atmosphere by cosmic radiation and enters the hydrologic cycle via precipitation as part of water molecules. Tritium concentration is measured in tritium units (TU), where one TU indicates a tritium:hydrogen atomic ratio of 10^{-18}. The tritium content of precipitation varies spatially and temporally, with average values in the U.S. Southwest and Mexico ranging from 2 to 10 TU (Eastoe et al., 2012). Newton et al. (2012) observed tritium concentrations in precipitation in the Sacramento Mountains in southern New Mexico to range from 3 to 10 TU. For groundwater samples collected over the last 20 years or so, the general interpretation of tritium in groundwater is (1) tritium concentrations between 5 and 10 TU represent modern water that is less than 10 years old; (2) tritium concentrations between 1 and 5 TU indicate a mixture of modern recharge and older, "tritium dead" water that is more than 50 years old or so; and (3) groundwater with tritium concentrations of 1 TU or less indicates that most recharge is more than 50 years old. Due to testing of thermonuclear weapons beginning in 1953, tritium concentrations in precipitation increased drastically above background levels, with concentrations peaking in 1962 and 1963 (>3,000 TU; Solomon et al., 1991). Since then, tritium concentrations in precipitation have decreased back to pre-1953 levels. For many years after this increase in tritium activity in precipitation, the "bomb pulse" could be detected in groundwater. These days, the bomb pulse cannot be detected in groundwater due to radioactive decay of tritium.

Atmospheric carbon dioxide gas, which has an approximate ^{14}C activity of 100 percent modern carbon (Clark and Fritz, 1997), is incorporated into the groundwater system (as bicarbonate, H^{14}CO$_3^-$) during infiltration of recharge through the vadose zone (Kalin, 2000). As the infiltration crosses the

water table, the dissolved inorganic carbon is isolated from the modern ^{14}C input from the atmosphere and soil zone reservoirs. As the water travels along a flow path in the aquifer system, the ^{14}C decays with time. As a result, the amount of ^{14}C measured in the groundwater along a flow path gives an age or the approximate amount of time that has passed since the water recharged the aquifer system. In general, lower percent modern carbon indicates older groundwater. However, to properly quantify groundwater age, it is usually necessary to correct the measured ^{14}C activity to account for hydrogeologic processes, such as carbonate dissolution, isotopic exchange, and mixing of older and younger waters (Clark and Fritz, 1997).

Figure 53 shows uncorrected ^{14}C results plotted on the map, with the size of data point being proportional to the apparent age of the groundwater. Apparent ^{14}C ages range from 90 to 3,190 years before present. These are relatively young ages, especially for being uncorrected ages. Correction for the dissolution of calcite and other processes will likely decrease these apparent groundwater ages. The bold numbers beside each point in Figure 53 are tritium concentrations in TU. Negative numbers are interpreted to be zero. Most groundwater samples show zero tritium or tritium concentrations less than 1 TU, indicating that the groundwater is more than 50 or 60 years old. The highest tritium concentration is 2.46 TU, indicating a mixture of modern water and older water. These results agree with the stable isotope data. While most groundwater in the area is more than 50 or 60 years old, the groundwater system is being recharged by precipitation under modern climatic conditions.

Water quality discussion

While we can clearly identify mixing end members based largely on the lithology and mineralogy of the aquifers (Fig. 47), it is difficult to use major ion chemistry to identify the specific aquifer from which water is being produced. Water chemistry for water samples collected in different aquifers exhibits significant overlap when plotted on a Piper diagram. The high variability in water chemistry and TDS concentrations in the study area is related to the spatial variability of permeability of the different aquifers and to what extent the aquifer has been flushed with meteoric water (Rosenau-Davidson, 2003). Fresh meteoric water that enters the aquifer system in the Guadalupe Mountains or locally

through sand dunes in Lea County mixes with and displaces saline water that is likely connate water and in chemical equilibrium with minerals that make up the aquifer. Therefore, aquifers with higher permeability—those that have had more meteoric water flowing through them—typically have lower TDS concentrations. For parts of the aquifer system with lower permeability, there has either been less flushing of connate waters or meteoric water flows have been much slower, increasing residence times and TDS concentrations.

In general, good-quality groundwater with TDS concentrations less than 3,000 mg/L occurs within 1,000 ft of the surface (Fig. 44). Figure 54 shows depths of wells that produce this fresh water, which range from 22 to 1,240 ft bgs. It appears that good-quality groundwater (TDS <3,000 mg/L) occurs throughout most of the DBAS at a variety of depths, with the deepest wells located in western Lea County and eastern Eddy County (with the exception of one well located in the southwestern corner of the DBAS). While it is almost certain that wells completed below 1,000 ft will produce water with TDS well above 10,000 mg/L, there are many wells completed within 1,000 ft of the surface that produce water with TDS values above 10,000 mg/L (Fig. 55). It appears that there is a large area within Lea County where there is no groundwater being pumped from 1,000 ft bgs (or shallower) that exhibits TDS concentrations greater than 3,000 mg/L. While the number of existing wells with a known depth is relatively small, this observation suggests that water tapped at less than 1,000 ft deep will likely exhibit TDS concentrations less than 10,000 mg/L.

CAPITAN REEF AQUIFER SYSTEM

Hydrologic description

In this study, the Capitan Reef Aquifer System (CRAS) comprises the Capitan Reef and the undifferentiated Artesia Group. The Capitan Reef is a shelf-to-basin reef complex made up of massive limestone that is part reef and part reef-talus, up to 2,000 ft thick, and characterized by significant karst development (Hayes, 1964; Hiss, 1975a, 1975b). It is exposed in the Guadalupe Mountains and forms the reef escarpment along the southern border of the reef system, which also contains the elaborate Carlsbad Caverns cave system and hundreds of

other caves (Fig. 2). The formation is an important aquifer because it delivers groundwater along its karst conduits and bedding planes from the Guadalupe Mountains to the Carlsbad area, with the Castile Formation and lower Artesia Group confining groundwater to the formation (Henderson and Jones, 1952; Motts, 1968). Precipitation recharges the Capitan Formation where it crops out in the Guadalupe Mountains, through percolation where it is overlain by permeable material, and from adjacent shelf deposits (Henderson and Jones, 1952; Bjorklund and Motts, 1959). Groundwater from Lake Avalon to the north of Carlsbad has also historically recharged the reef aquifer (Richey et al., 1985). Extensive karst pathways have developed in the reef aquifer, primarily along joints, allowing for specific capacities up to 419 gpm/ft and hydraulic conductivities up to 75 ft/d (Bjorklund and Motts, 1959; Motts, 1968; Jones, 2016). Karst development can be localized, and the yields of wells depend on the quantity and size of voids and pathways intersecting a well hole, though the interconnectedness of the system can be seen in some wells where long-term water levels fluctuate in tandem (Bjorklund and Motts, 1959; Motts, 1968). Artesian conditions can exist in the reef aquifer due to the seemingly random nature of karst development, but confinement of the aquifer is largely in the Carlsbad area where it is overlain by alluvium (Motts, 1968).

In this study, the individual units of the Artesia Group (Grayburg, Queen, Seven Rivers, Yates, and Tansill) are considered a single geologic unit owing to their similar lithology and hydrogeologic characteristics. The Artesia Group in the reef aquifer system of the study area comprises two dominant facies types: (1) carbonate facies with highly variable permeability due to differences in limestone and dolomite subfacies, with limestone subfacies dominating closer to the Capitan Reef and dolomite subfacies dominating shelfward, and (2) evaporite facies composed of gypsum and anhydrite with interbedded sandstone, siltstone, and dolomite, also with a large range in permeability attributed to the variability in the dissolution of gypsum (Motts, 1968). The presence of well-cemented sandstone and siltstone beds in both of the major facies types allows for perched aquifers in the system (Motts, 1968). Facies transition from carbonate to evaporite moving away at right angles from the Capitan Reef trend (Motts, 1968). The highly variable

permeability of both facies types is demonstrated by a range in well yields, from 3 to 4,000 gpm in the carbonate facies and from 25 to 1,000 gpm in the evaporite facies (Motts, 1968). The highest permeabilities in the carbonate facies are near the Capitan Reef, and permeability generally decreases shelfward; the highest permeabilities in the evaporite facies are where significant dissolution of gypsum has occurred (Motts, 1968).

Precipitation recharges the Artesia Group in the Guadalupe Mountains, percolating to semi-impermeable layers before moving downgradient east and northeast (Motts, 1968). The Capitan Reef formation acts as a "huge collection gallery" for groundwater moving eastward along the reef trend, effectively funneling the groundwater along the reef (Motts, 1968, p. 294).

Digital data

< CRAS > Extent

The CRAS extent is defined by where the geologic units exist in the subsurface within the study area in Eddy County and where water levels were measured in the Artesia Group and Capitan Reef formation (Fig. 56). While the geologic units of the aquifer system are present to the west and southwest of the system extent, faulting to the west and southwest of the Guadalupe Mountains has separated them into another aquifer system (Hiss, 1975a, 1975b; Standen et al., 2009). The eastern boundary of the system is limited by available recent water level measurements. Elevations range from about 3,080 ft in the Pecos River valley in the east to almost 7,500 ft in the Guadalupe Mountains in the southwestern portion of the aquifer system.

< CRAS > Model Data

There were 94 wells with water levels measured after 2010 that were used in the CRAS model. One historical (pre-2010) water level from 1968 was incorporated into the dataset due to a lack of recent data in the westernmost area of the model. The sources of water level data in this system were NMOSE and NMBGMR. Water level and water quality data density is highest in the alluvial aquifer of the Carlsbad area and decreases to the west, with the lowest density in the Guadalupe Mountains (Fig. 56). There were no wells completed in the upper San Andres Formation in the dataset used for this

study, so it was not included as a major aquifer unit, but groundwater from the reef system likely enters the San Andres and moves north to the Roswell basin (Motts, 1968).

< CRAS > Depth to water in feet below ground surface

Measured depth to water in the CRAS ranges from 15 to 615 ft bgs, and calculated depth to water ranges from 26 to 1,538 ft bgs (Fig. 56). The shallowest measured depths to water are near the Pecos River, and the shallowest calculated depths to water are found in the vicinity of the Pecos River and also to the east of Last Chance Canyon in the southern tip of the Seven Rivers embayment (Fig. 2). The deepest measured depth to water is in the town of Queen in the Guadalupe Mountains, and the deepest calculated depths to water are in the southern Guadalupe Mountains along Guadalupe Ridge.

< CRAS > Water table in feet above mean sea level

While the general groundwater flow direction of the system follows the topographic east-northeast trend, some water in the system is diverted to the southeast through karst and along bedding planes, discharging to springs in the sharp relief of the canyons of the escarpment (Fig. 57). Some of this diverted groundwater percolates deeper into the system than the escarpment and reemerges farther to the southeast in the Black River drainage of the basin aquifer.

< CRAS > Saturated thickness feet

Subtracting the elevations of the lower surface from the upper surface gave a saturated thickness range of less than 0.1 ft to greater than 2,029 ft (Fig. 58). This thickness is certainly not fully saturated, but it represents the zone in which there would likely be groundwater flow, for example through karst or along bedding planes. The smallest calculated thickness was found in recharge areas in the Guadalupe Mountains, and the thickest areas were calculated east of the Pecos River, where groundwater can be found in shallow alluvial aquifers as well as in the deeper Capitan Reef formation. The saturated thickness of the system is largely controlled by the base elevation of the Capitan Reef formation. The base elevation of the Capitan Reef descends in elevation from west to east with a steeper slope than the potentiometric

surface, and so the thickness of the aquifer increases to the east.

< CRAS > Base elevation in feet above mean sea level

The CRAS base elevation values range from 539 to 5,083 ft amsl, with an average elevation value of 2,755 ft amsl (Fig. 59). The conceptual aquifer base was constructed by the same methods as the DBAS basal elevation surface. The lower Ochoan and Artesia geologic formation base surfaces were combined by clipping, mosaic, and smoothing tools in Esri.

Water quality

< CRAS > Water Quality

There are several zones of water quality described by Bjorklund and Motts (1959) where TDS in the CRAS increases from the Hackberry Hills in the west to La Huerta in the east as the reef aquifer interacts with the alluvial aquifer. The TDS of the reef aquifer increases from generally less than 700 mg/L under Hackberry Hills to 700 to 1,700 mg/L starting at about Hackberry Draw in Happy Valley, where it has some interaction with alluvium containing "residue" from the Salado and Rustler Formations (Bjorklund and Motts, 1959). This mixed-water zone extends underneath the Pecos River valley alluvium aquifer and east of the Pecos River before TDS concentrations reach 1,700 to 3,500 mg/L in the reef aquifer.

There were 270 wells with water quality measurements that were mapped in the CRAS. The TDS values ranged from 9.5 to 39,600 mg/L (Fig. 60). Data are sparse in the Guadalupe Mountains, with an extensive gap from Queens Highway to Hackberry Hills and Frontier Hills west and southwest of Carlsbad. The water with the lowest TDS concentrations is found in carbonate rocks of this system, especially in recharge areas in the Guadalupe Mountains (Bjorklund and Motts, 1959; Hiss, 1973; Richey et al., 1985; NMOSE, 2016b). Water found in evaporite facies of this system can also be of acceptable quality for livestock and irrigation, though it is high in Ca^{2+} and SO_4^{2-} (Henderson and Jones, 1952). Groundwater in this system east of the Pecos River is of poor quality, with TDS ranging from 10,000 to 30,000 mg/L as it mixes with mineral-rich groundwater upwelling from Ochoan strata (Bjorklund and Motts, 1959; Motts, 1968; Richey

et al., 1985). Water quality is generally available for domestic use where wells tap into carbonate facies of the Artesia Group, but wells tapping into evaporite facies are generally only useful for stock watering (Bjorklund and Motts, 1959). The highest TDS values measured in wells in this system can be found just east of Lake Avalon, where concentrations of 25,284 to 28,000 mg/L were measured in 2016.

While there are some high-TDS waters in this system, Figure 61 shows that most wells produce water with TDS concentrations less than 3,000 mg/L, which is produced at a variety of depths (green and yellow points in Fig. 60), ranging from 22 to 1,000 ft bgs. Waters with higher TDS, located to the northeast, occur at the same range of depths. Figure 62 shows water chemistry for the few samples that had enough chemistry data to plot on a Piper diagram, which includes samples collected by NMBGMR in 2021. The low-TDS Ca-HCO$_3$ water types are due to dissolution of limestone and dolomite. A mixing trend between Ca-HCO$_3$ water and Ca-SO$_4$ water from the Artesia Group is observed, and the water sample with the highest TDS concentration appears to be the high-Cl brine from the Ochoan strata.

Stable isotopic compositions for water samples collected from the CRAS (data are not shown) are similar to those shown for the DBAS in Figure 52, indicating that the groundwater system is recharged by meteoric water under modern climatic conditions. This conclusion is supported by ^{14}C and tritium data, shown in Figure 63. Apparent ^{14}C ages range from less than 500 to 1,700 years before present. These uncorrected ages are very young, and would be younger still after corrections. Tritium concentrations agree with the ^{14}C dates, with the oldest water having less tritium. Tritium concentrations range from 0.14 to 1.58 TU, indicating that most groundwater is more than 50 or 60 years old, but there is a very small component of modern recharge (<50 years old).

INTERMITTENT AQUIFER

There are 14 wells with water levels measured after 2010 that were used to characterize the intermittent aquifer system (Fig. 64). The sources of water level data in this system were the NM EMNRD OCD reports. Depth-to-water measurements range from 7 to 73 ft bgs, and water level elevation ranges

from 3,094 to 3,491 ft amsl. Exposures of Ochoan formations where useful sources of water would be sporadic in space and time were used to designate wells in this system. The primary geologic units found in the intermittent aquifer system (from oldest to youngest) are the Salado, Castile, and Rustler Formations of Permian age, and Cenozoic alluvium, bolson fill, and eolian deposits. The Castile Formation is considered the primary aquifer in this area, though areas of alluvium are connected to and exchange water with the Castile; karst development provides localized aquifers and likely connections to and between alluvium deposits (Henderson and Jones, 1952; Stafford, 2013). Water quality in the system is highly variable, but generally contains lower concentrations of dissolved solids in the west than the east due to the dissolution of gypsum as groundwater moves through the system (Stafford, 2013).
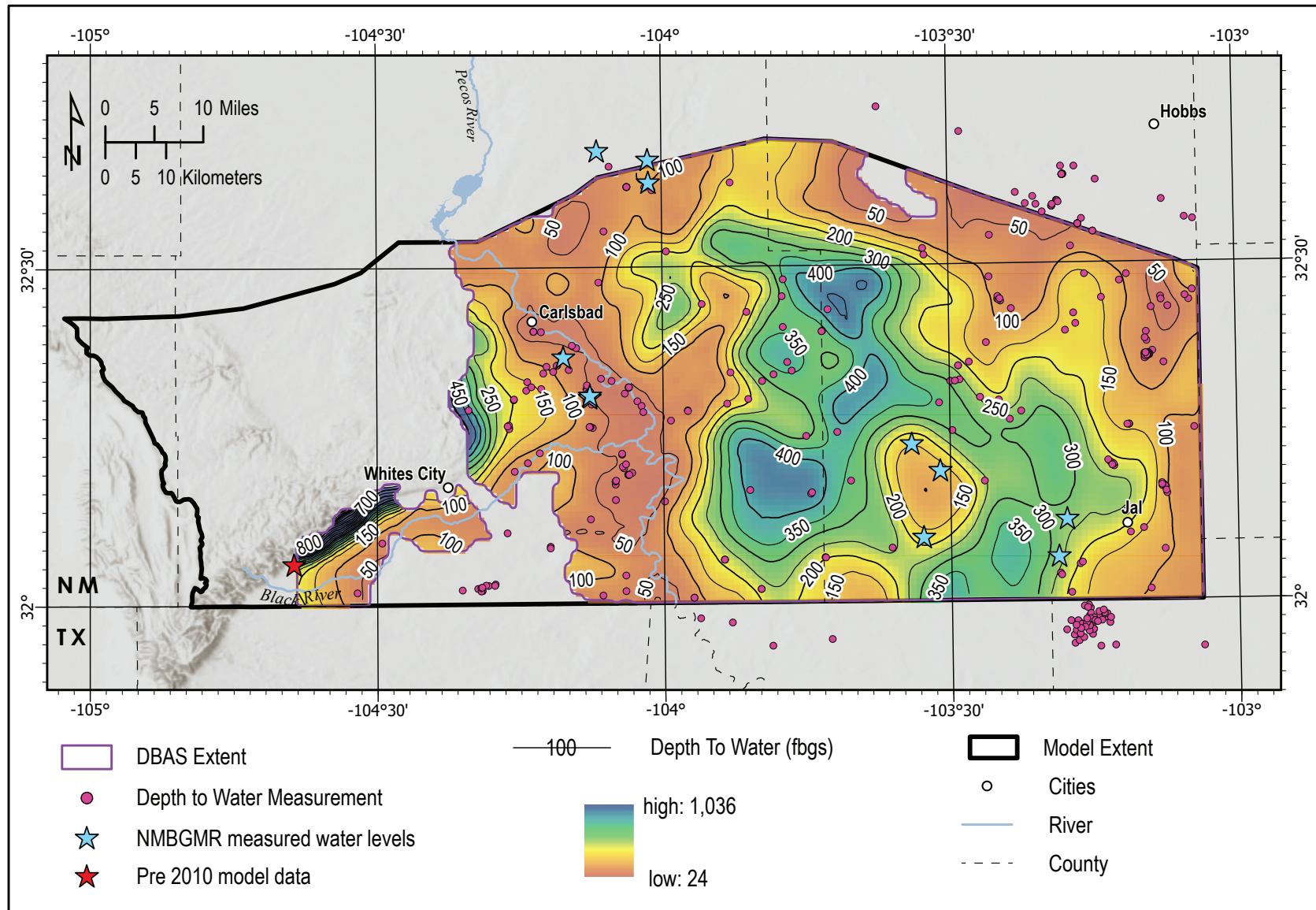
Figure 39. Estimated depth to water in the DBAS, showing the extent and locations of wells with data used to make the water level surface and contours. Measurements were not used if the well depth was unknown, or if the measurement was taken before 2010 (with one exception noted by a red star). Due to confined conditions in regions of the aquifer system, the depth-to-water map may reflect artesian values where the water level has risen above the formation depth after drilling. Caution should be used when interpreting these values for estimated well drilling depths. The extent of the system was discontinuous due to interpolated water level elevation values rising above the land surface where groundwater discharges to the surface in the form of springs.
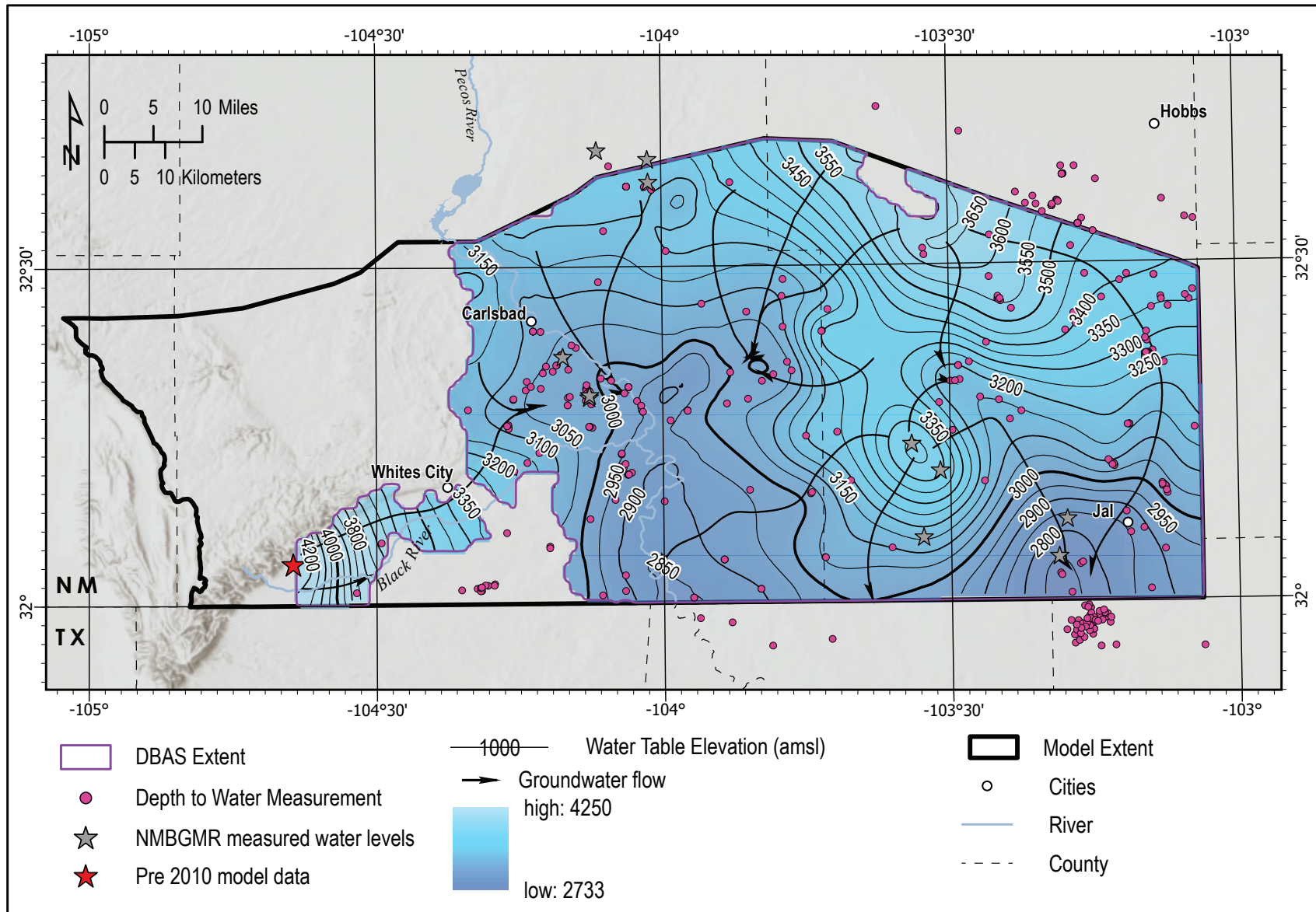
Figure 40. DBAS interpolated water level elevation surface, elevation contours, and groundwater flow lines. Groundwater flow lines were created with the Esri Steepest Path function, then adjusted manually. San Simon Swale is a large collapse feature that catches groundwater from adjacent potentiometric highs. The potentiometric highs at about 103°30' W form a groundwater divide; on the western side of the divide the groundwater generally flows toward the Pecos River, and on the eastern side the water generally flows south-southeast.
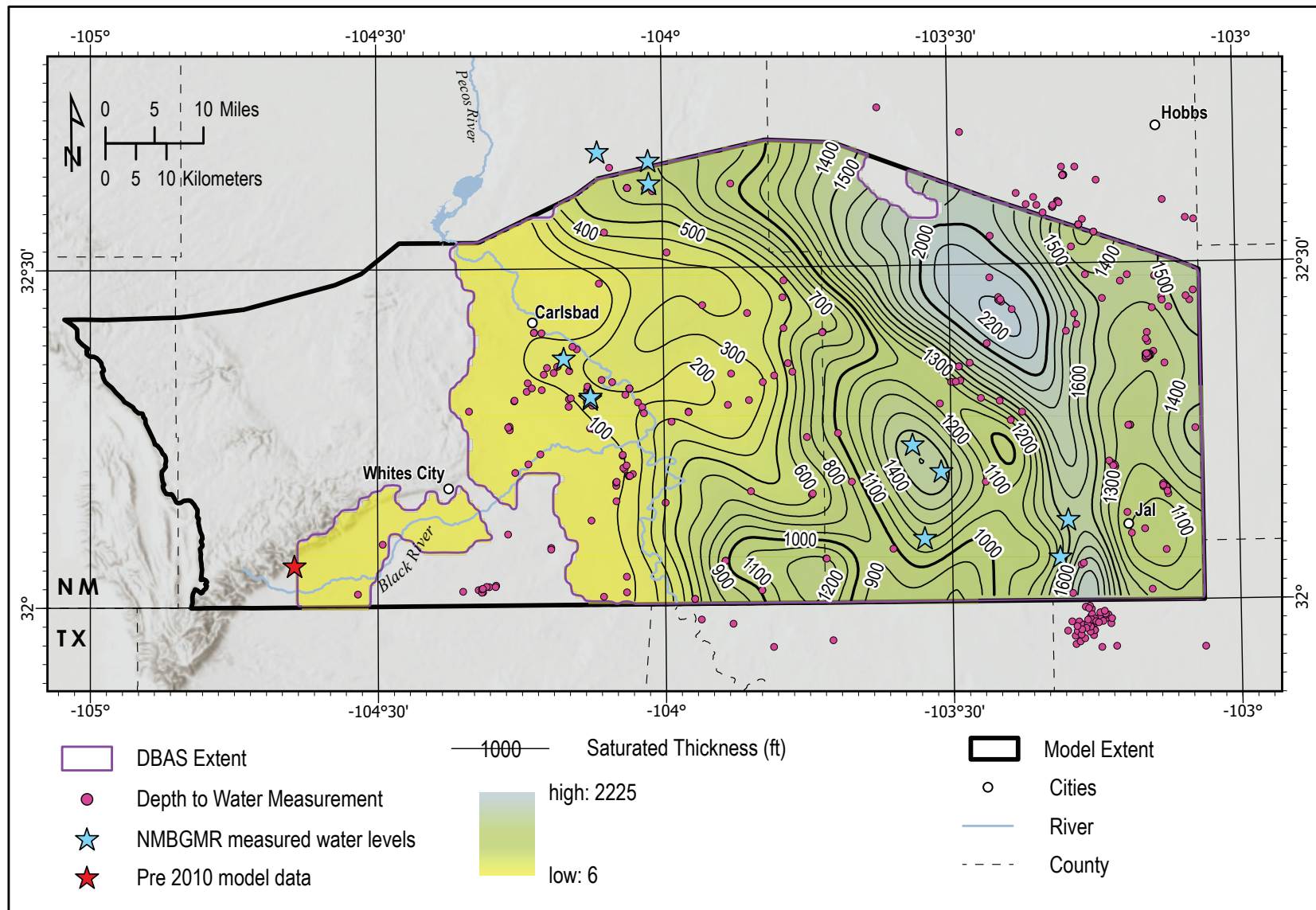
Figure 41. The DBAS potential saturated thickness map was created by subtracting the aquifer system base elevation values from the water level elevation values (or potentiometric surface). As the name implies, the DBAS is an aquifer system and not one continuous aquifer body; as such, this estimate represents the maximum thickness of a series of perched aquifers with varying levels of connectivity and saturation and should not be used for aquifer volume calculations. The largest potential saturated thickness values just east of 103°30' W were driven by the base elevation of the aquifer system, which formed a large, deep trough created by dissolution and collapse structures.
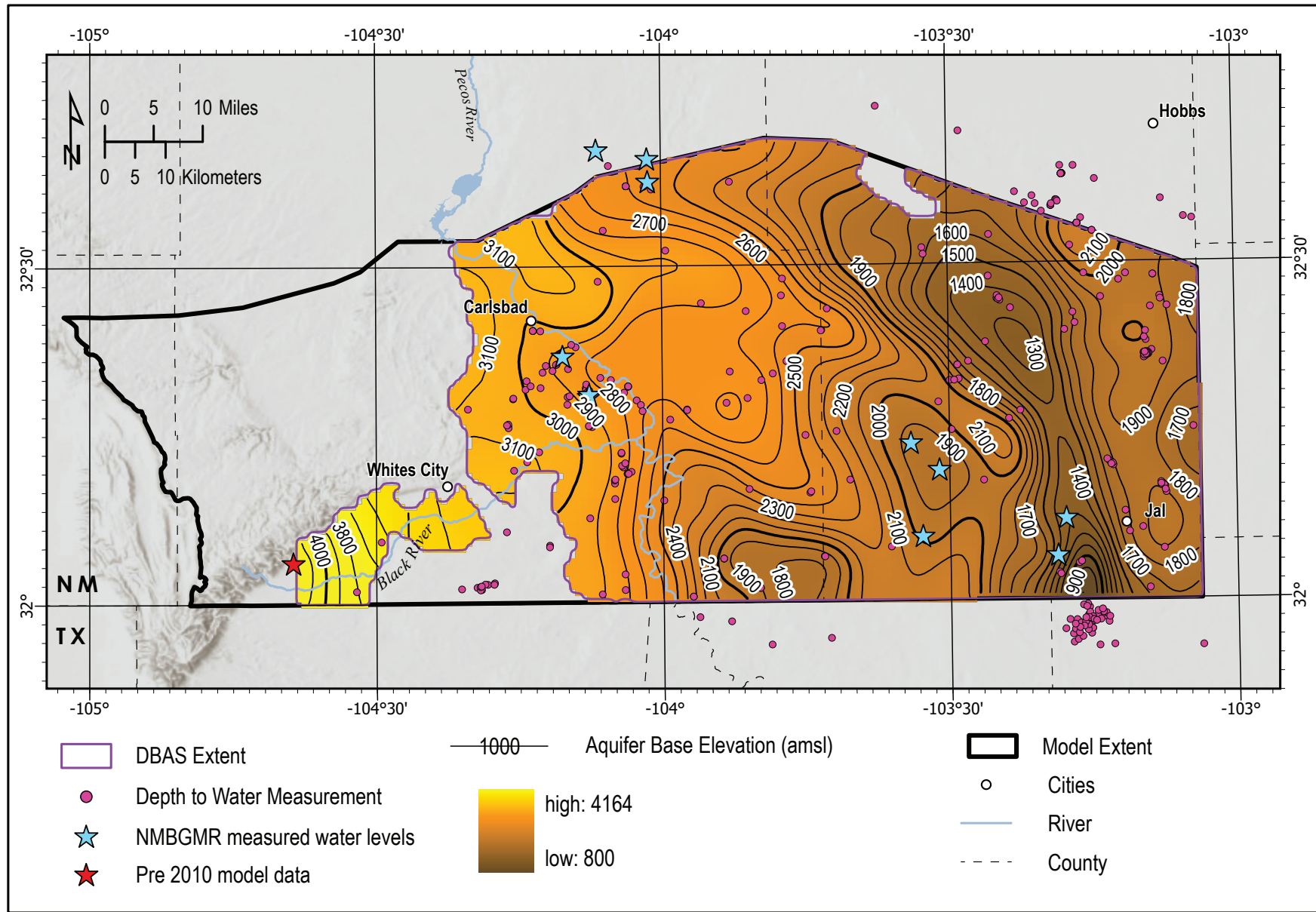
Figure 42. DBAS base elevation (elevation contours in ft). The base elevation surface of the aquifer system was created by combining the alluvium and upper Ochoan base elevation surfaces and smoothing the result with Esri Focal Statistics.
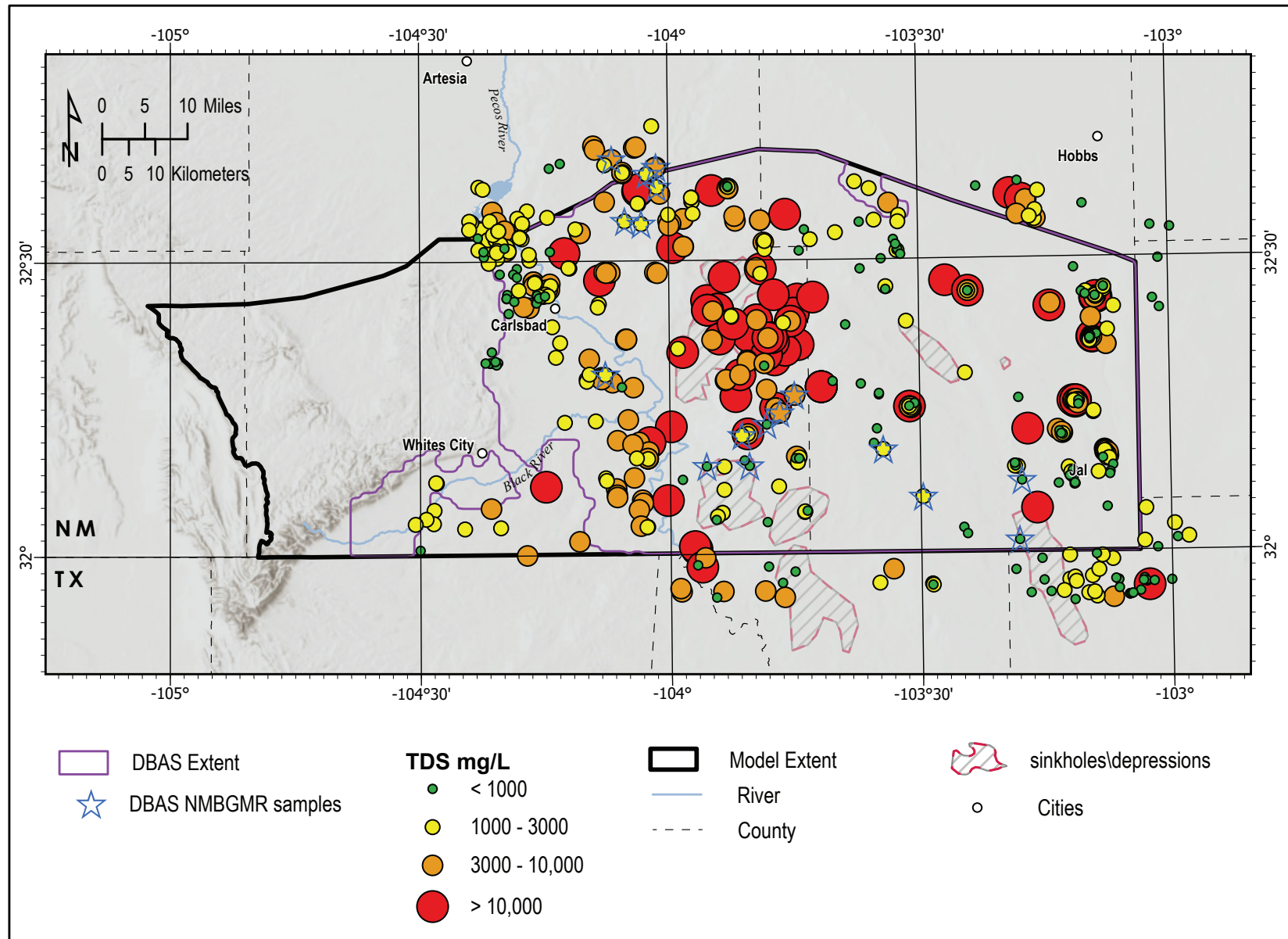
Figure 43. TDS concentrations for water produced from wells in the DBAS. Wells sampled by NMBGMR are indicated by red stars. USGS classifies fresh water as less than 1,000 mg/L TDS, slightly saline as 1,000–3,000 mg/L TDS, moderately saline as 3,000–10,000 mg/L TDS, and highly saline as 10,000–35,000 mg/L TDS. For comparison, the TDS is of seawater is typically 35,000 mg/L.
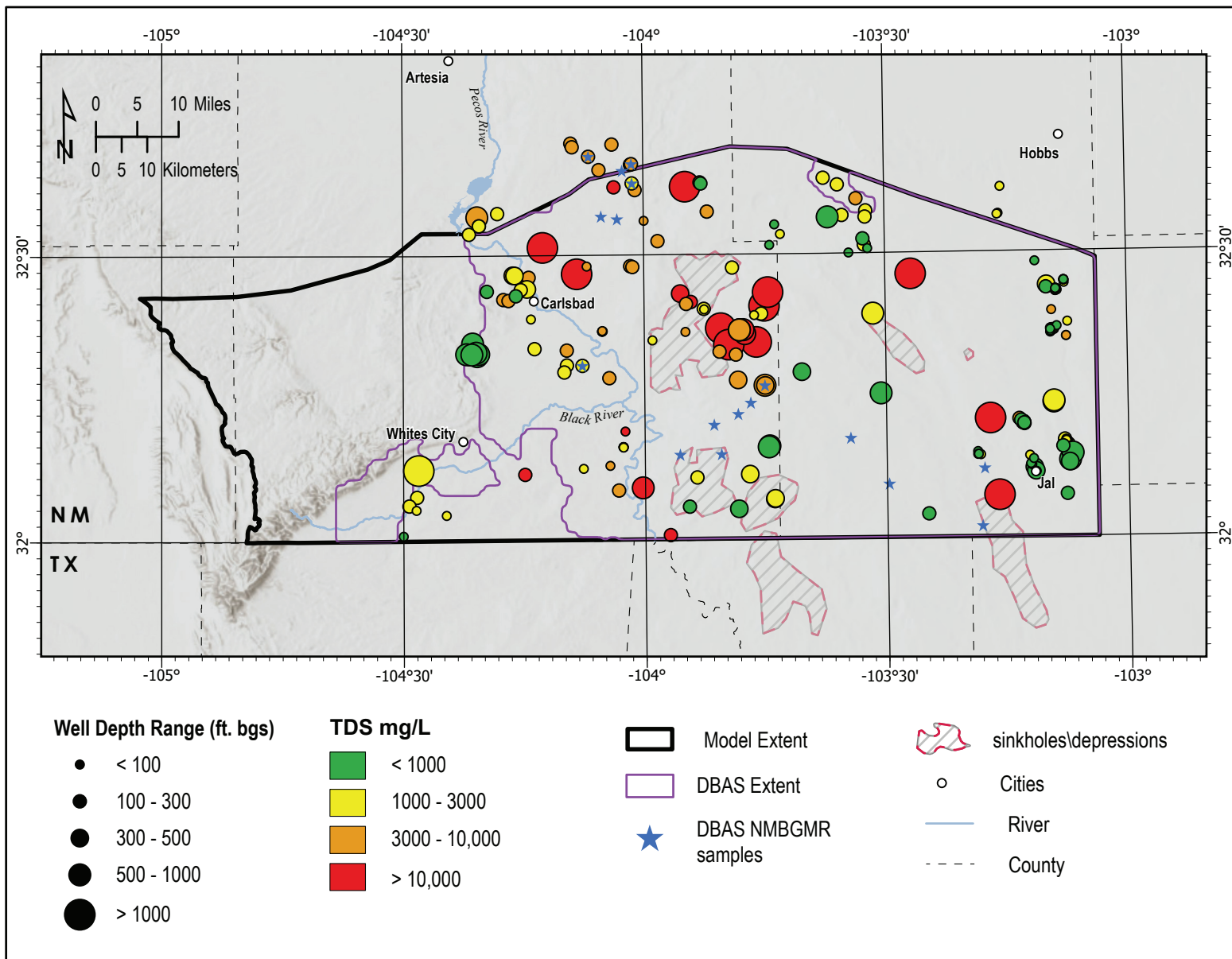
Figure 44. Wells with both TDS and well depth information. The size of the point is proportional to the total well depth, ranging from 22 to 8,000 ft bgs. Colors represent TDS concentrations; green: less than 1,000 mg/L, yellow: 1,000–3,000 mg/L, orange: 3,000–10,000 mg/L, red: greater than 10,000 mg/L.
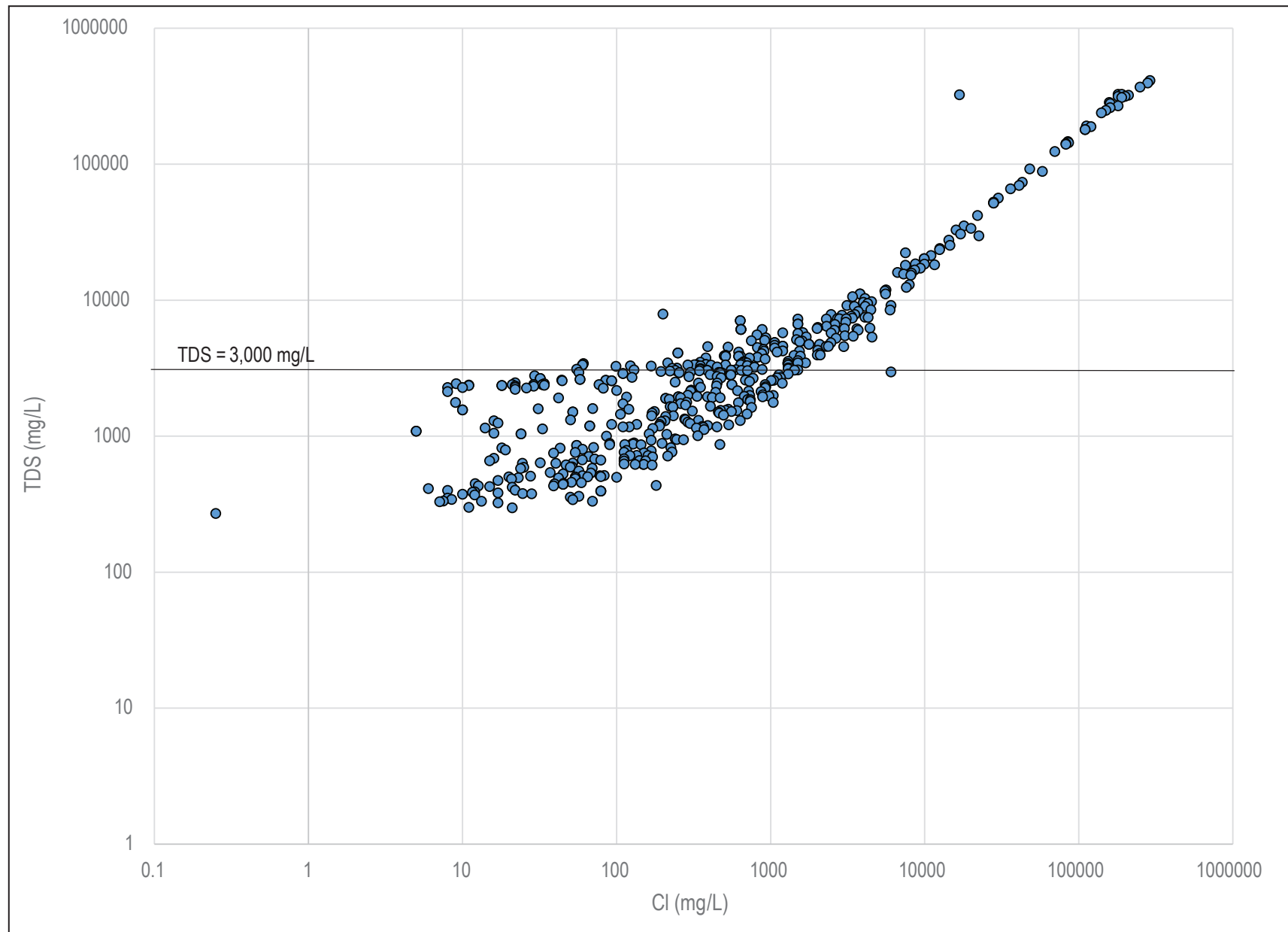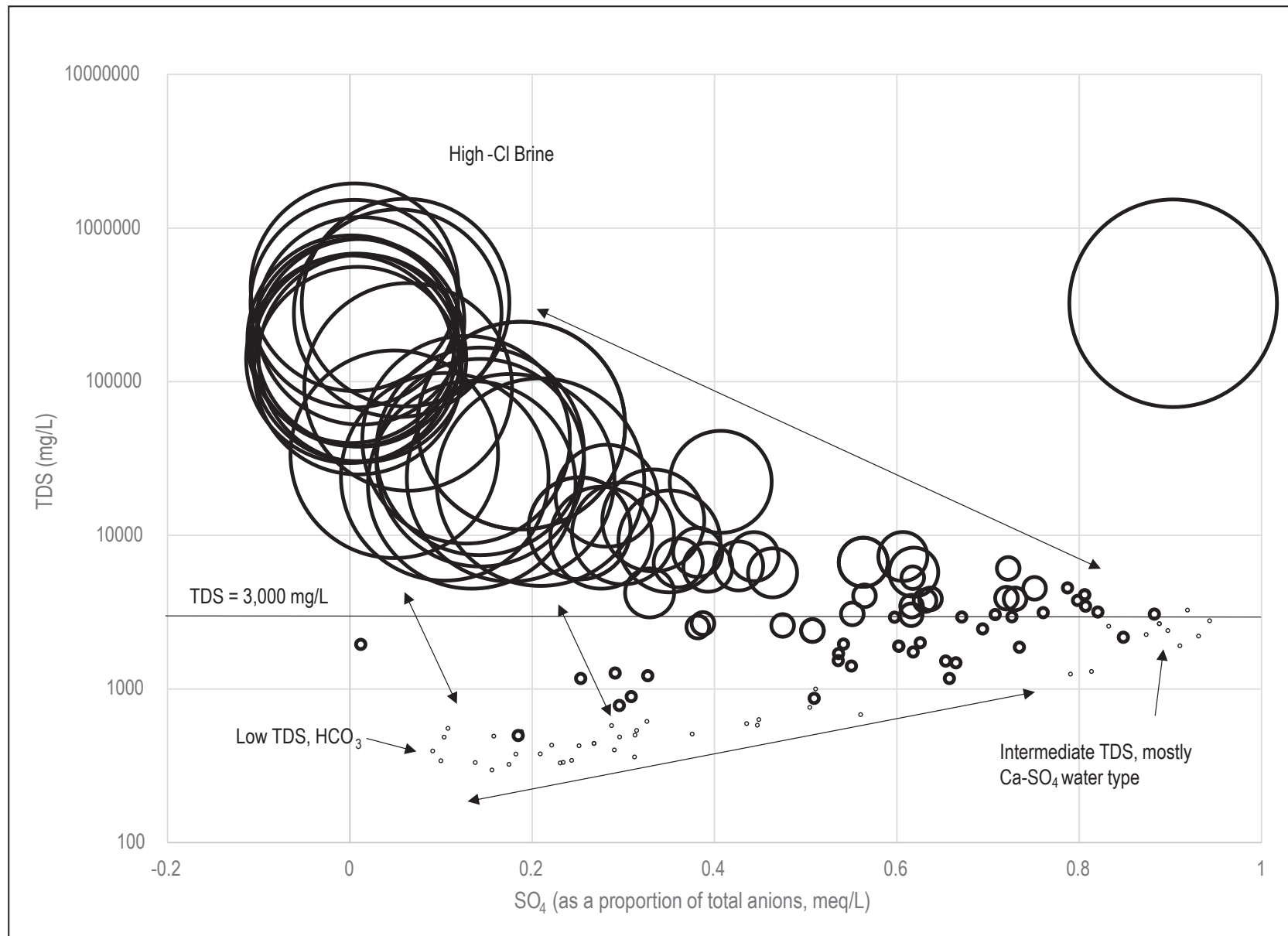
Figure 45. TDS concentrations plotted as a function of Cl. Above 1,000 mg/L TDS, there appears to be a linear correlation between Cl and TDS.
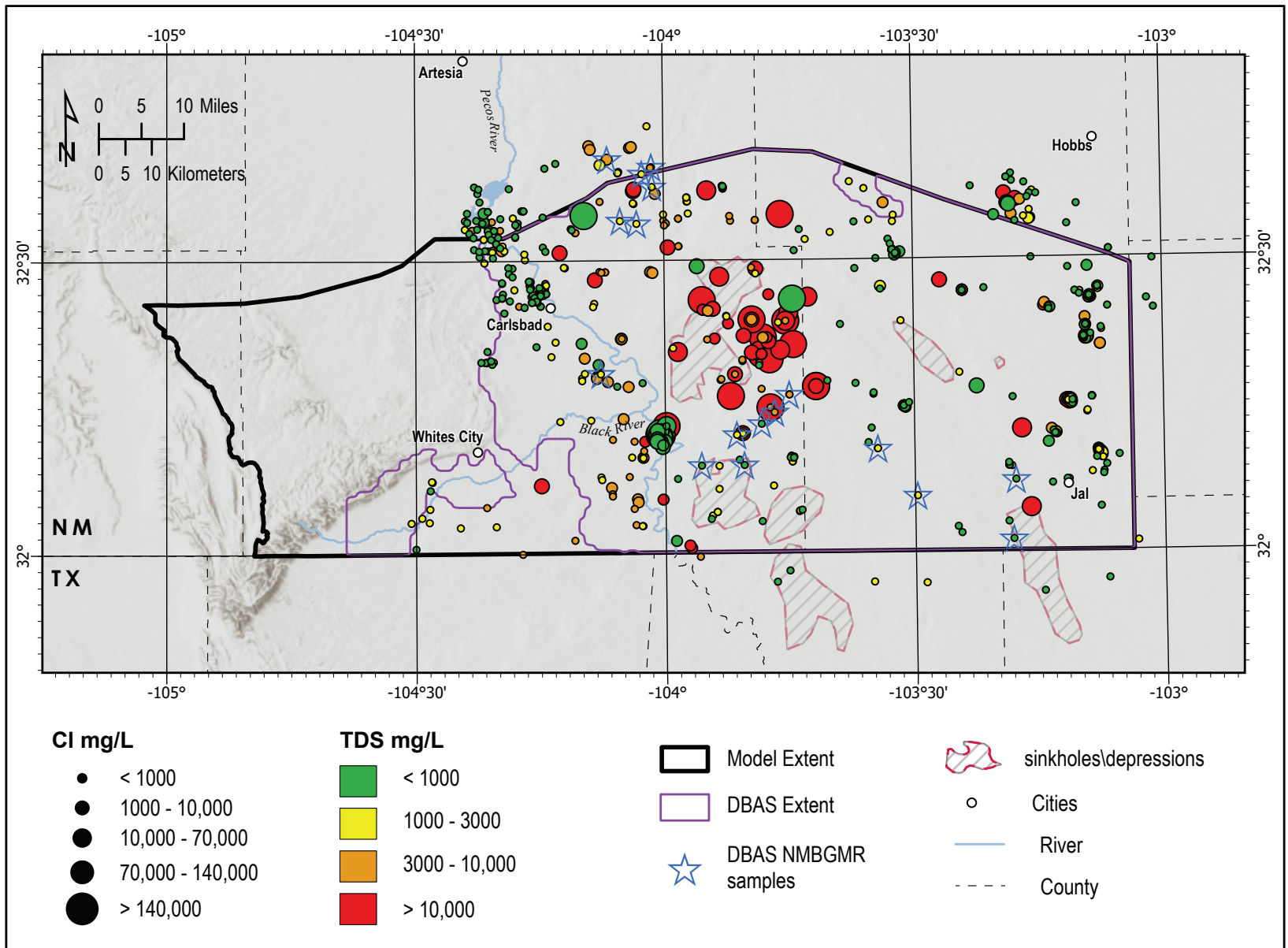
Figure 46. Wells with both TDS and Cl concentration data available. The size of the point is proportional to the total Cl concentration, ranging from 0.25 to 290,000 mg/L. Colors represent TDS concentrations; green: less than 1,000 mg/L, yellow: 1,000–3,000 mg/L, orange: 3,000–10,000 mg/L, red: greater than 10,000 mg/L.

Figure 47. TDS plotted as a function of relative SO$_4$ concentrations. The sizes of data points are proportional to Cl concentrations, which range from 21 to 290,000 mg/L. The y-axis is exponential to better fit all the data on one graph. Double arrows indicate mixing.
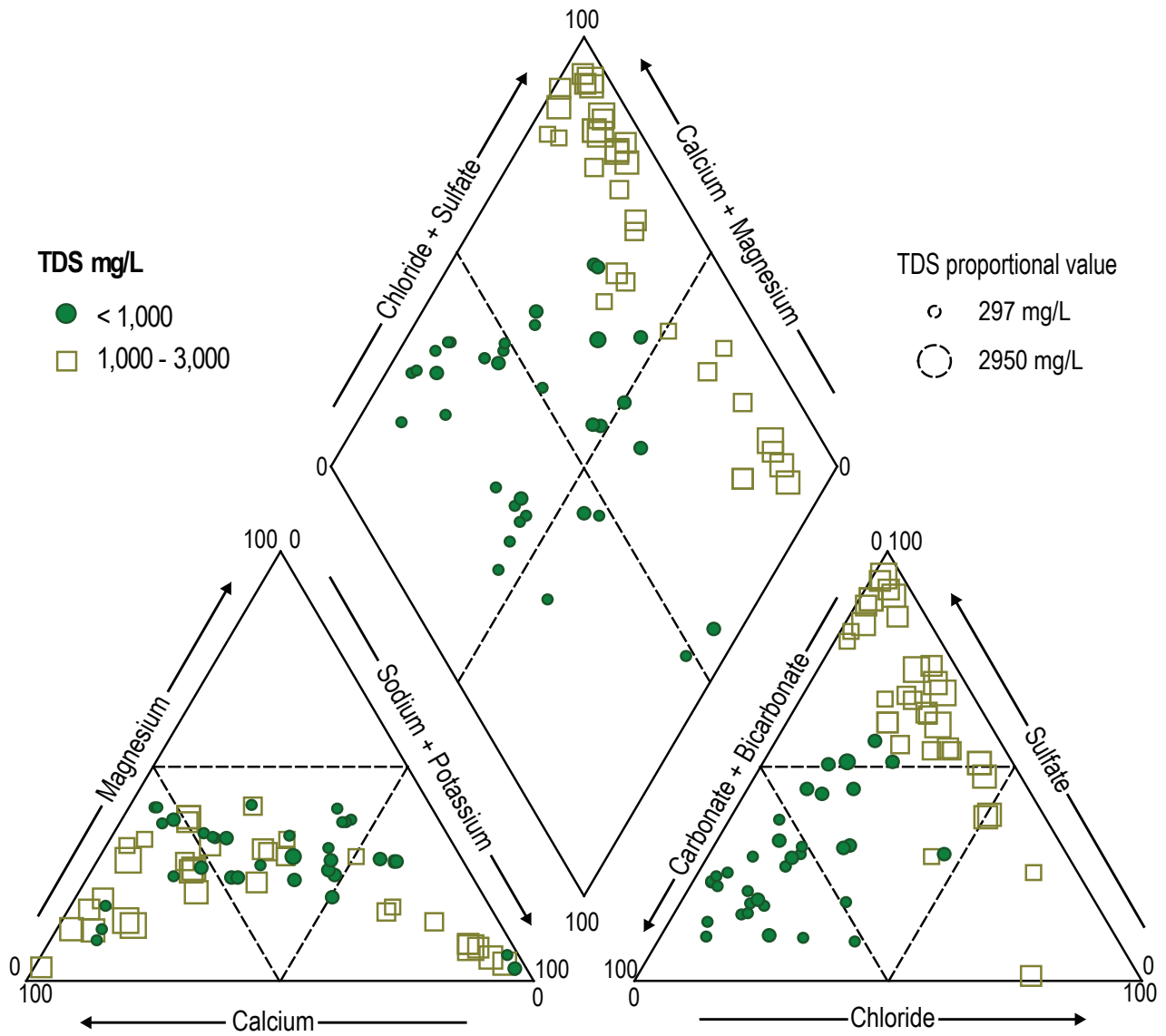
Figure 48. Piper diagram for water samples in DBAS with TDS concentrations less than 3,000 mg/L. The sizes of data points are proportional to TDS concentrations; however, many of the data points fall within a similar range of concentrations..
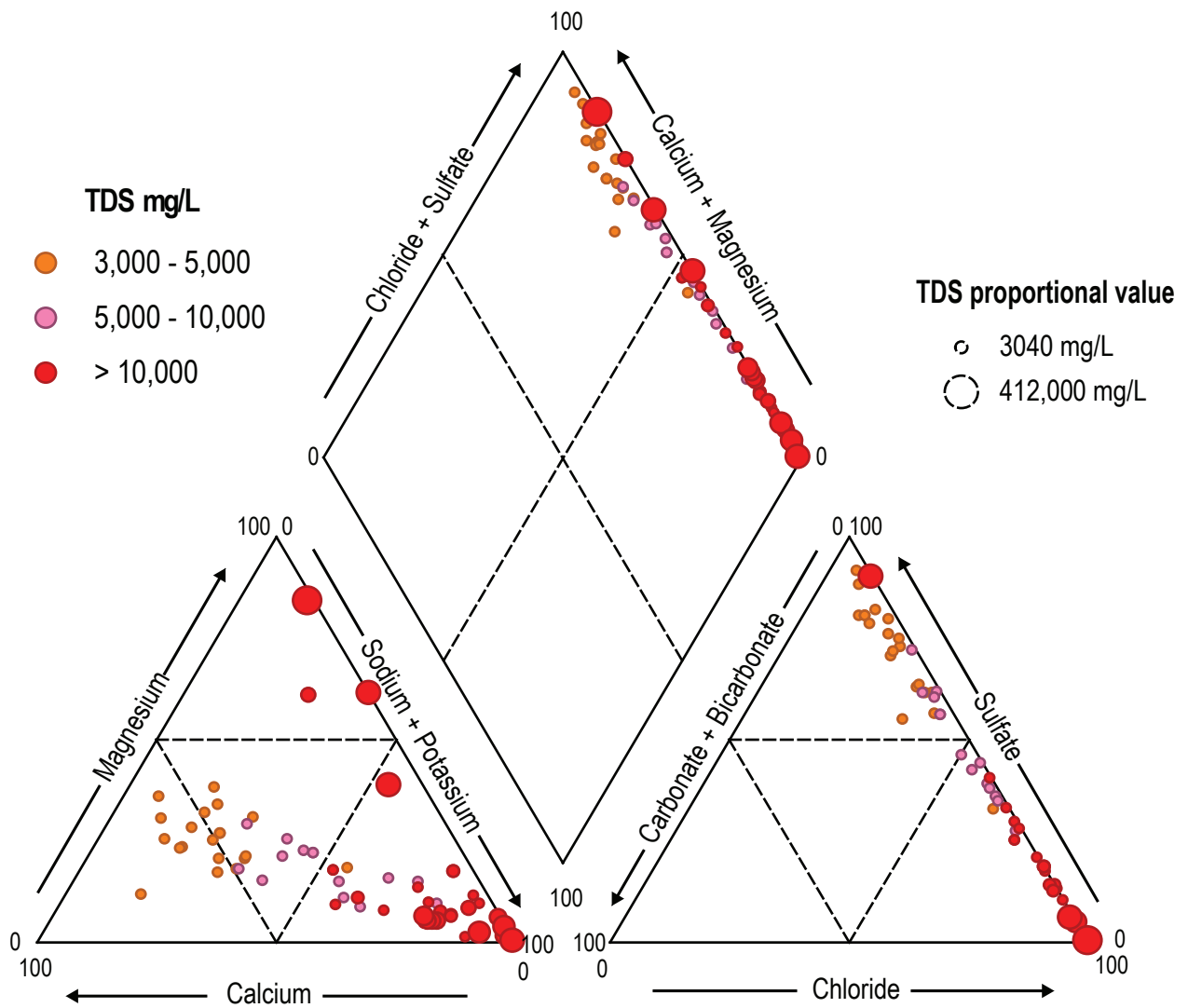
Figure 49. Piper diagram for water samples in DBAS with TDS above 3,000 mg/L. The sizes of data points are proportional to TDS concentrations.
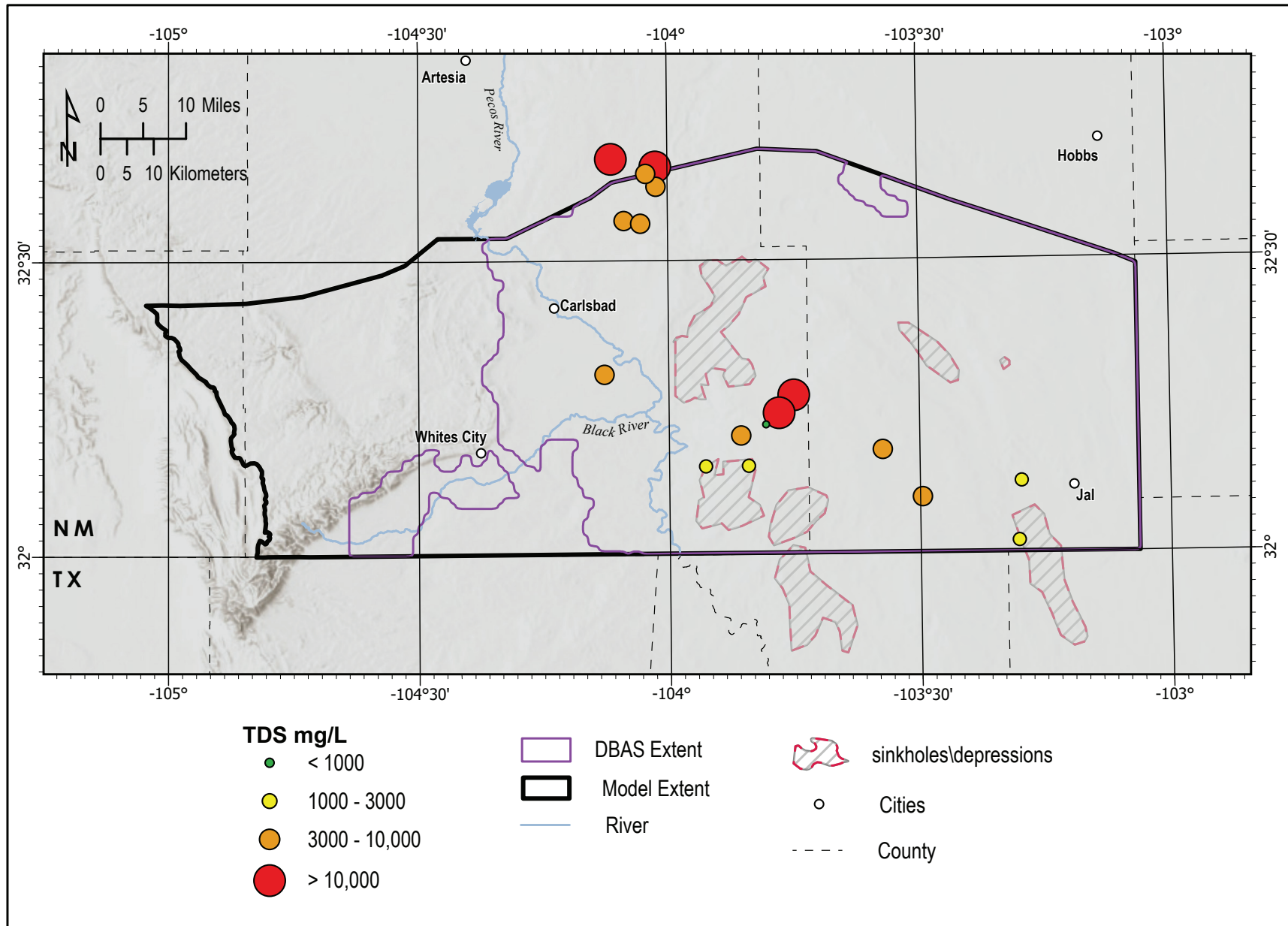
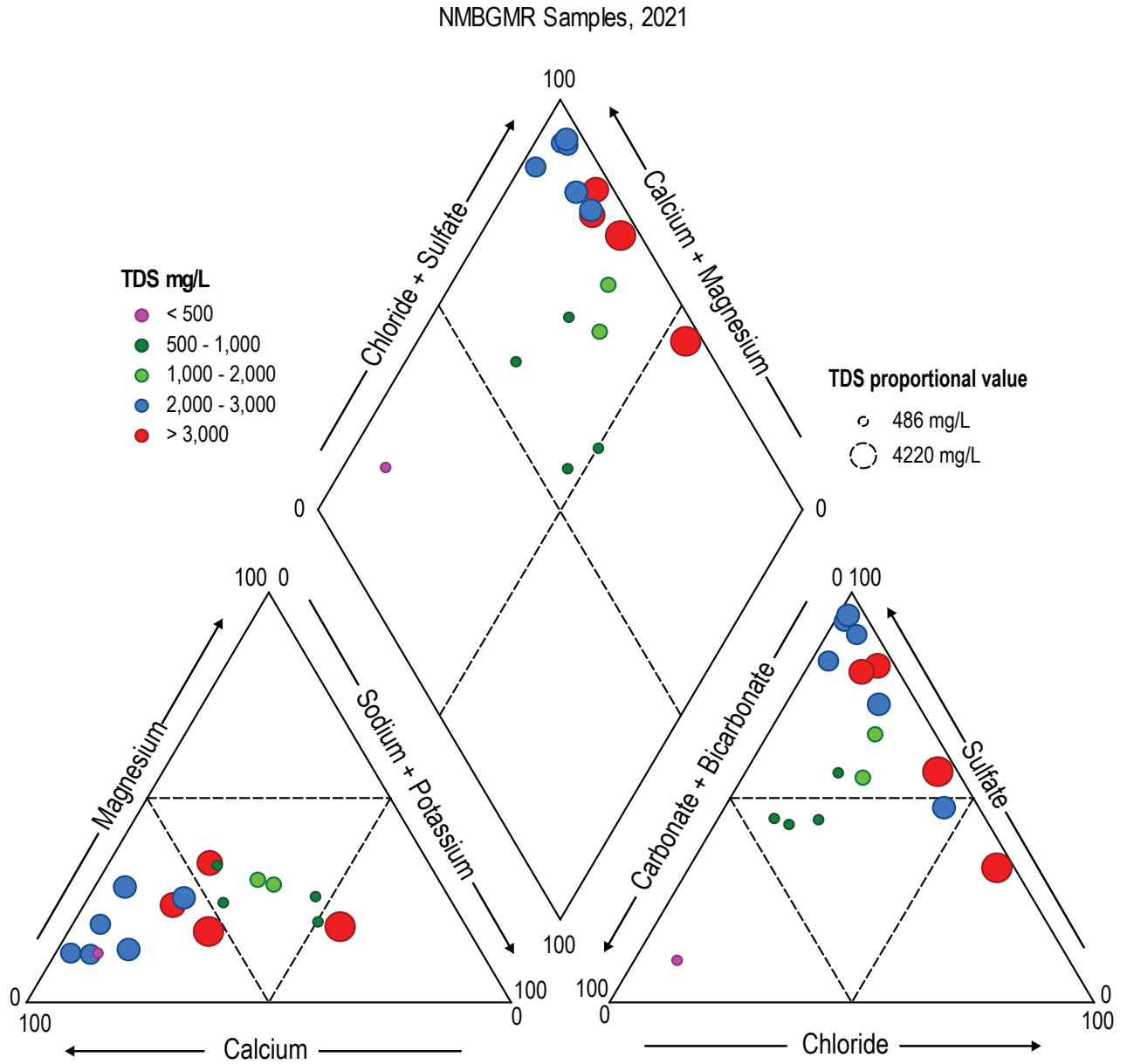**Figure 50.** Spatial variability of TDS concentrations for groundwater samples collected for this study in 2021.

Figure 51. Piper diagram of water chemistry data for groundwater samples collected by NMBGMR for this study in 2021.
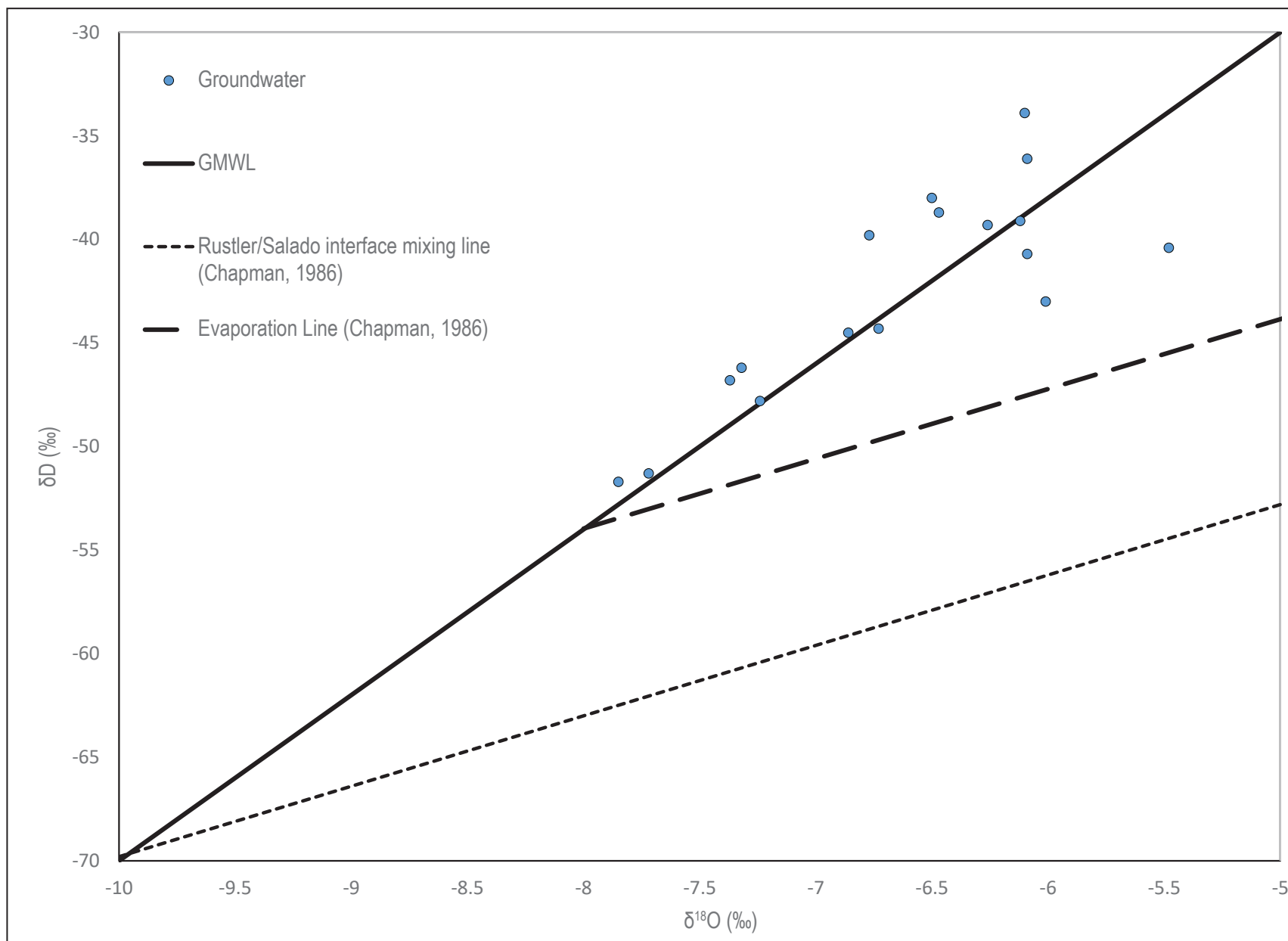
Figure 52. Stable isotopic composition for groundwater samples collected by NMBGMR in 2021.
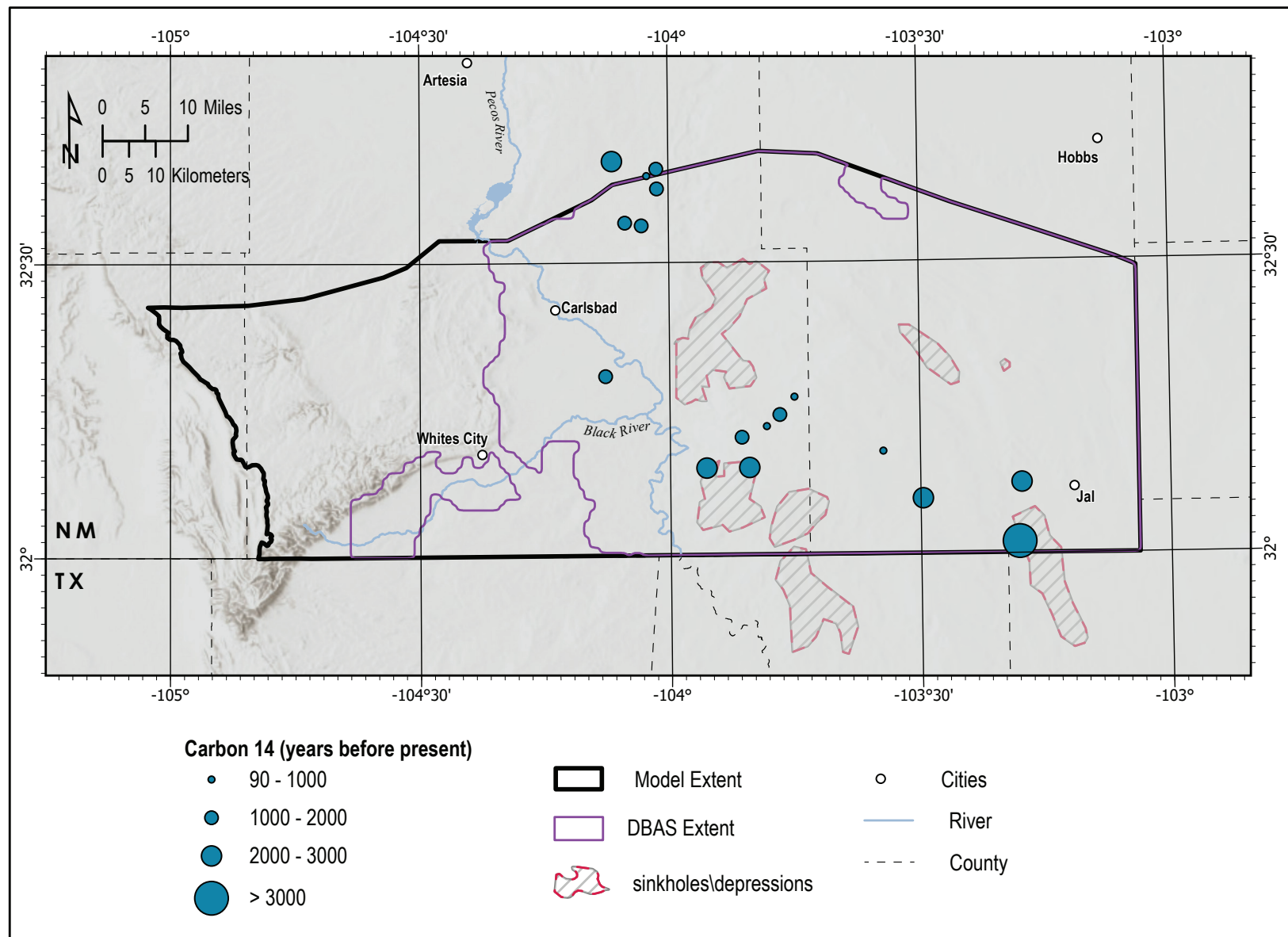
Figure 53. [14]C data plotted on map. The sizes of data points are proportional to uncorrected ^{14}C results for the age of the water (years before present). Labels for each point are tritium results for each sample (TU). Tritium concentrations close to 0 TU (including negative values) indicate that the groundwater is older than 50 or 60 years before present, while modern recharge (within 10 years or so) usually exhibits values between 4 and 8 TU. Intermediate values are due to mixing of old tritium-free water with modern recharge.
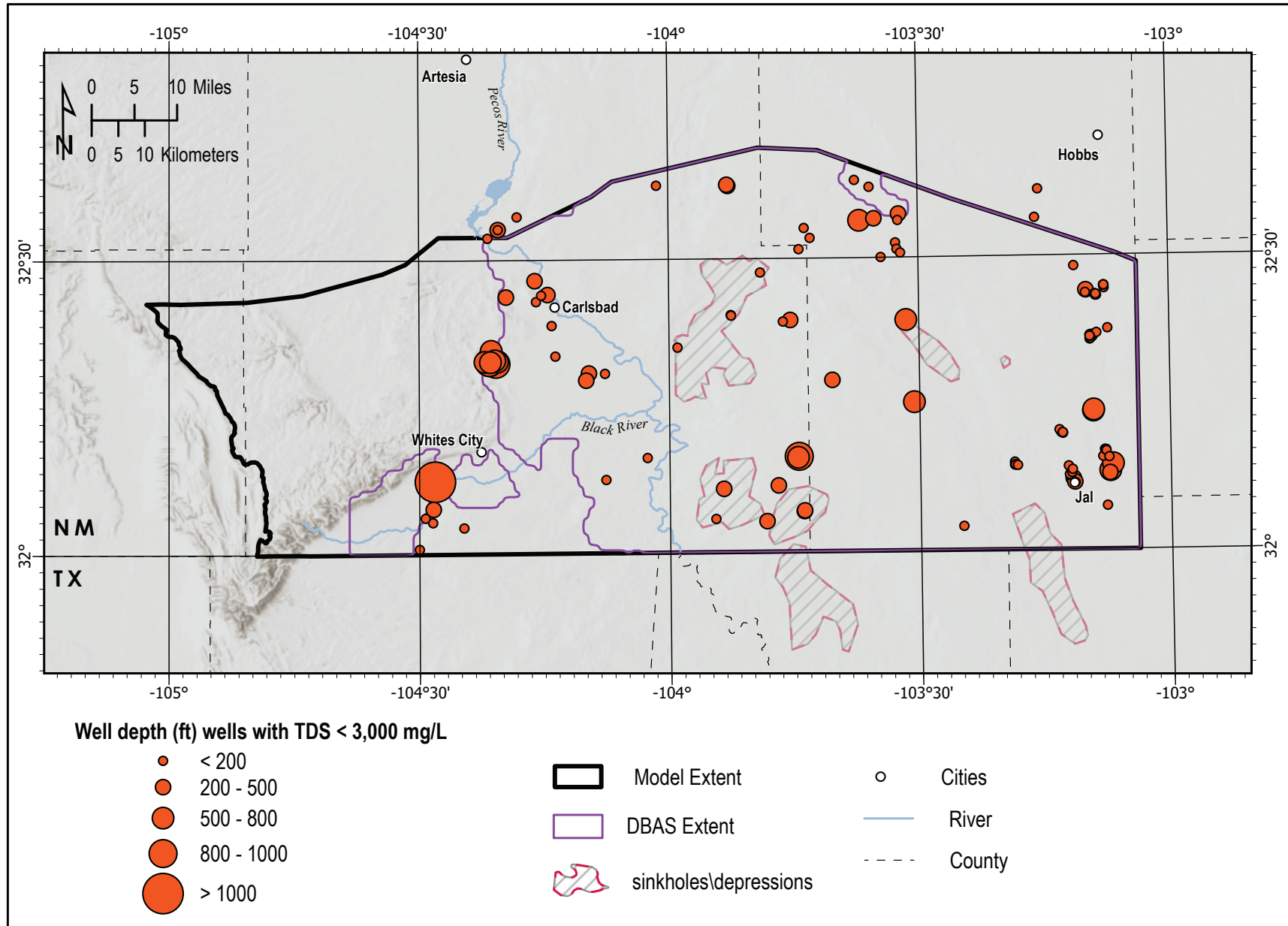
Figure 54. The wells shown in this map all have measured water quality below 3,000 mg/L total dissolved solids. In general, these wells are completed at depths below 500 ft; however, there are also deep wells with low TDS measurements, especially west of the Pecos River.
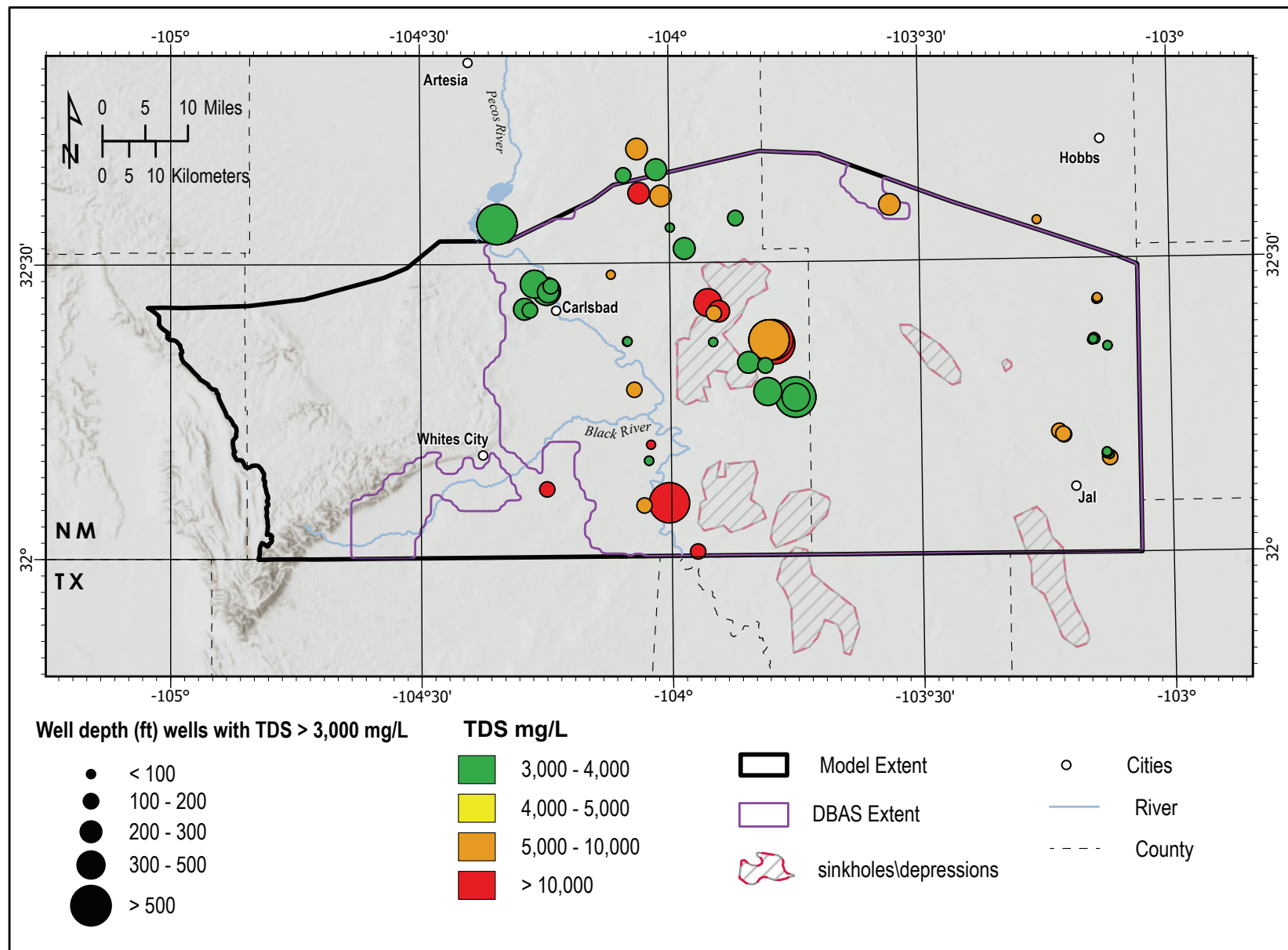
Figure 55. Locations for wells that produce water with TDS concentrations greater than 3,000 mg/L. The sizes of the points are proportional to the depths of the wells, ranging from 25 to 897 ft bgs. Colors represent ranges of TDS concentrations; green: 3,000–4,000 mg/L, yellow: 4,000–5,000 mg/L, orange: 5,000–10,000 mg/L, red: greater than 10,000 mg/L.
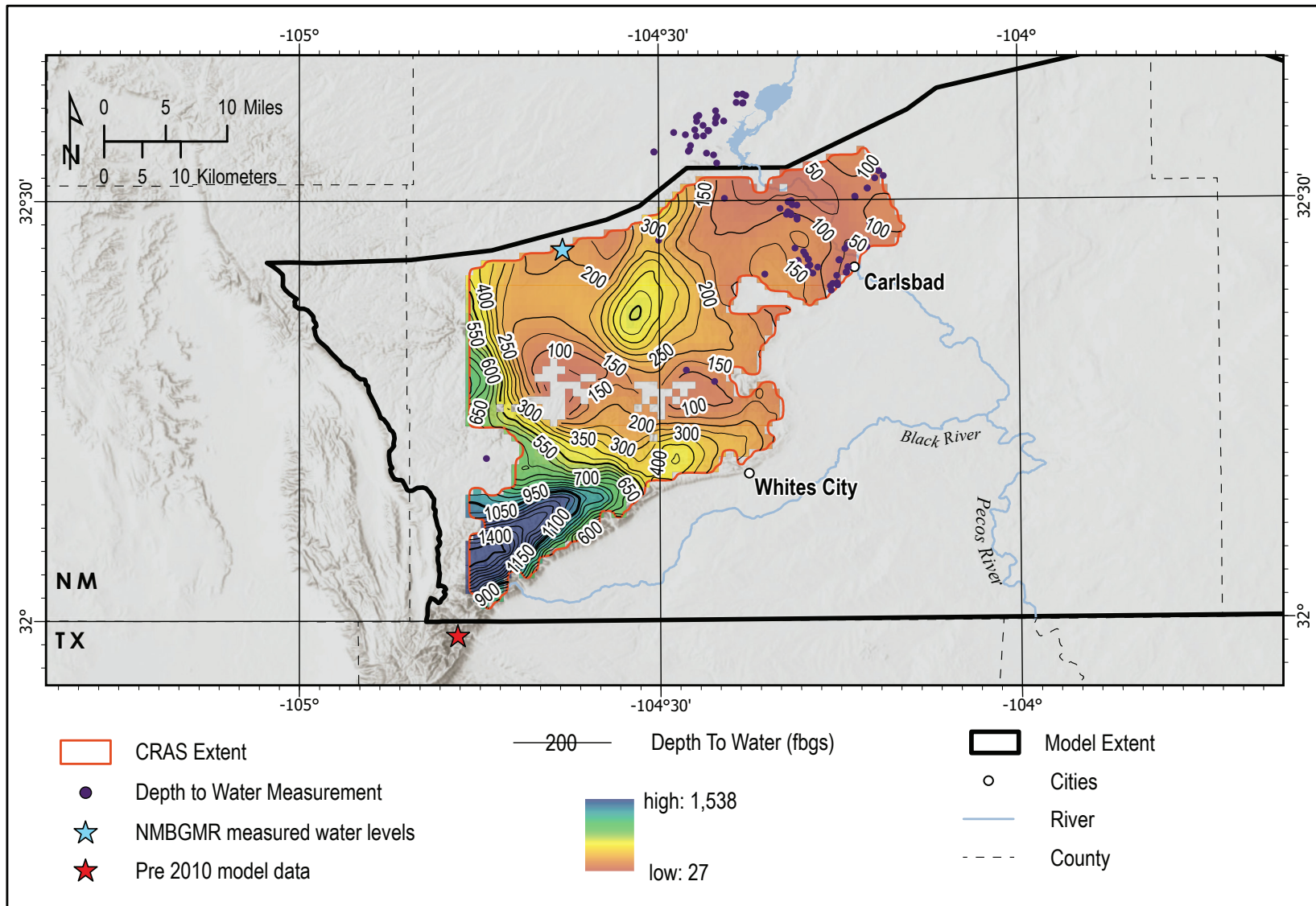
Figure 56. CRAS extent and locations of wells with depth-to-water data used to make the water level surface and contours. Measurements were not used if the well depth was unknown or if the measurement was from before 2010 (with one exception noted by a red star). The depth-to-water surface was calculated by subtracting the water level elevation surface values from the land surface elevation values of a 4.5-m digital elevation model; the resolution of the surface was 1 km. The extent of the system was discontinuous due to interpolated water level elevation values rising above the land surface where groundwater may discharge to the surface. The largest depths to water were calculated near Guadalupe Ridge, where a lack of measurements along with the topographic high of the Guadalupe Mountains likely combined to give an overestimation of the depth to water; this is likely also the case with the approximately 600-ft contour just west of 104°30' W.
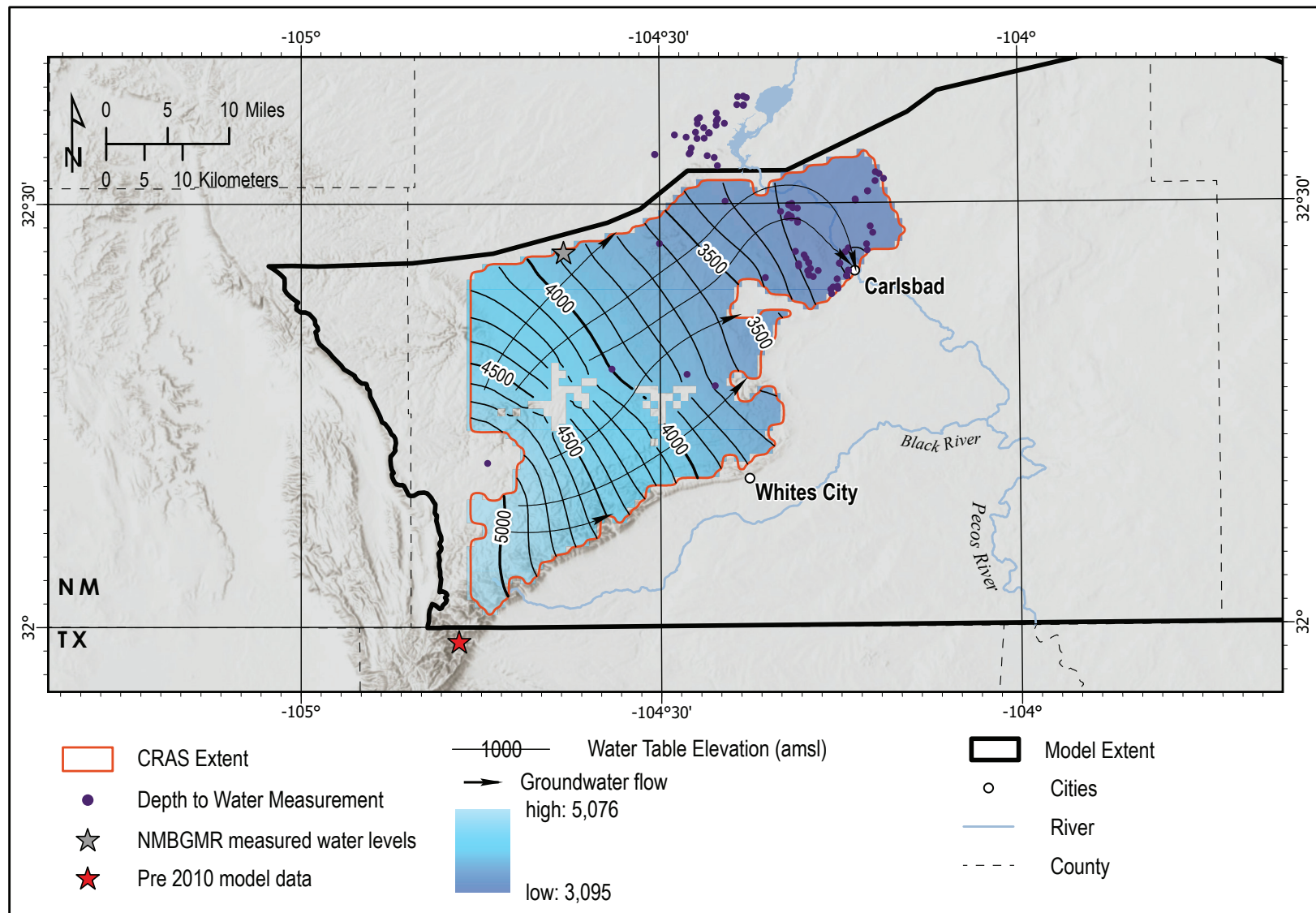
Figure 57. CRAS water table (ft amsl) interpolated surface, elevation contours, and groundwater flow lines. Measurements were not used if the well depth was unknown or if the measurement was from before 2010 (with one exception noted by a red star). The water level elevation surface was interpolated using the water level elevation values in the Esri Topo to Raster tool with default settings and a resolution of 1 km. The extent of the system was discontinuous due to interpolated water level elevation values rising above the land surface where groundwater discharges to the surface in the form of springs. Groundwater flow lines were created with the Esri Steepest Path function, then modified manually. Groundwater generally flows northeast from higher elevations in the Guadalupe Mountains toward the Pecos River. Some groundwater flows more east-southeast and discharges into the DBAS along the Guadalupe Mountain front, west-southwest of Whites City.
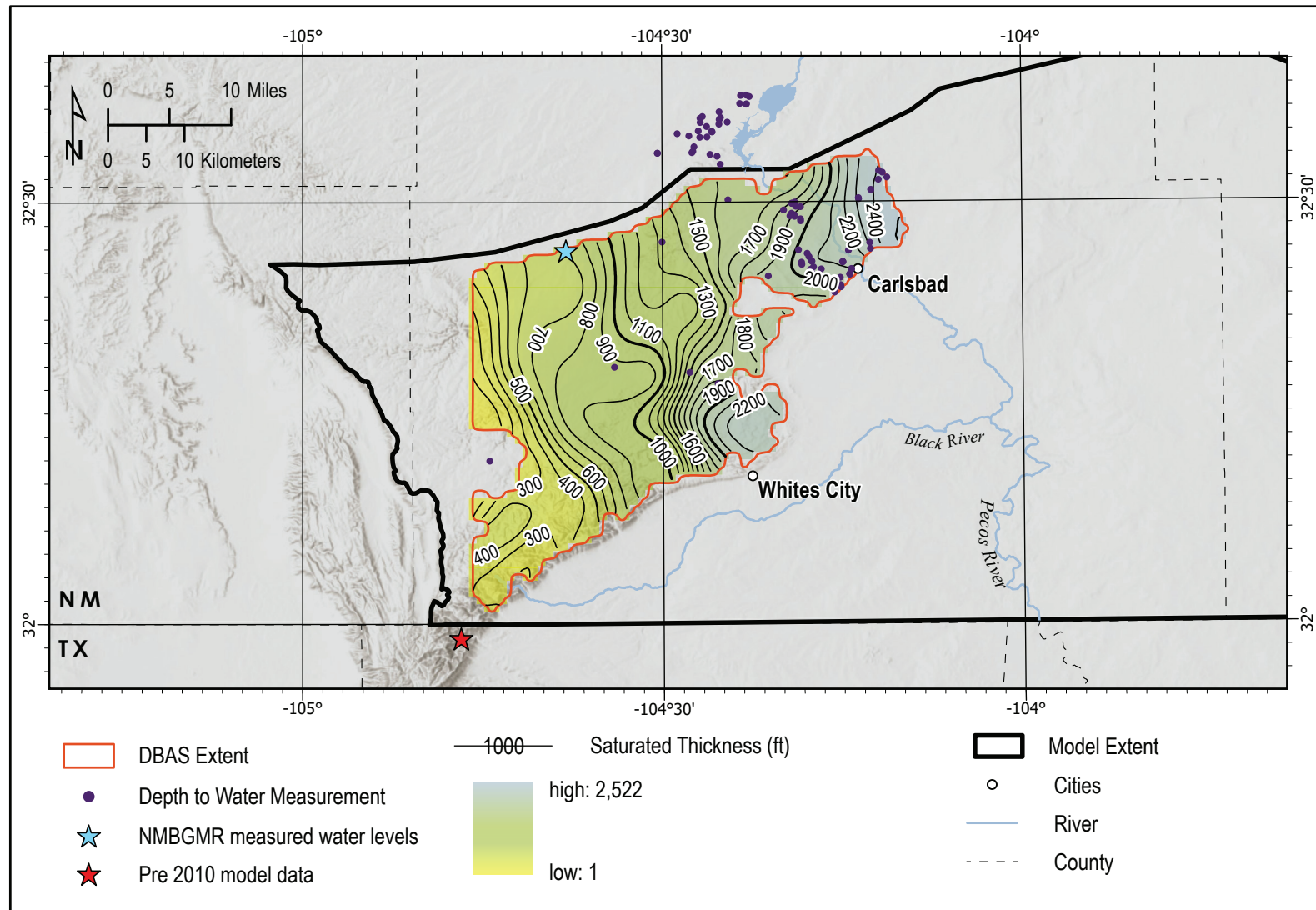
Figure 58. CRAS potential saturated thickness. The potential saturated thickness surface was created by subtracting the aquifer system base elevation values from the water level elevation values, which represent the top of the aquifer system. The largest potential saturated thickness values were driven by the base elevation of the Capitan Reef, where it quickly loses elevation heading to the east. The potential saturated thickness of the system overall is driven by the base elevation of the lower Ochoan due to its own high thickness, though it certainly carries water through interstitial spaces of impermeable layers and cavernous limestone and dolomite. Calculation of the potential saturated thickness of the system using water level elevations may also be misleading. Wells could be drawing water from multiple water-bearing units—either by design or through the degradation of the well casing—or the artesian pressure in a well could give the false impression of a large saturated thickness. Potential saturated thickness values should always be considered in the context of the local geology.
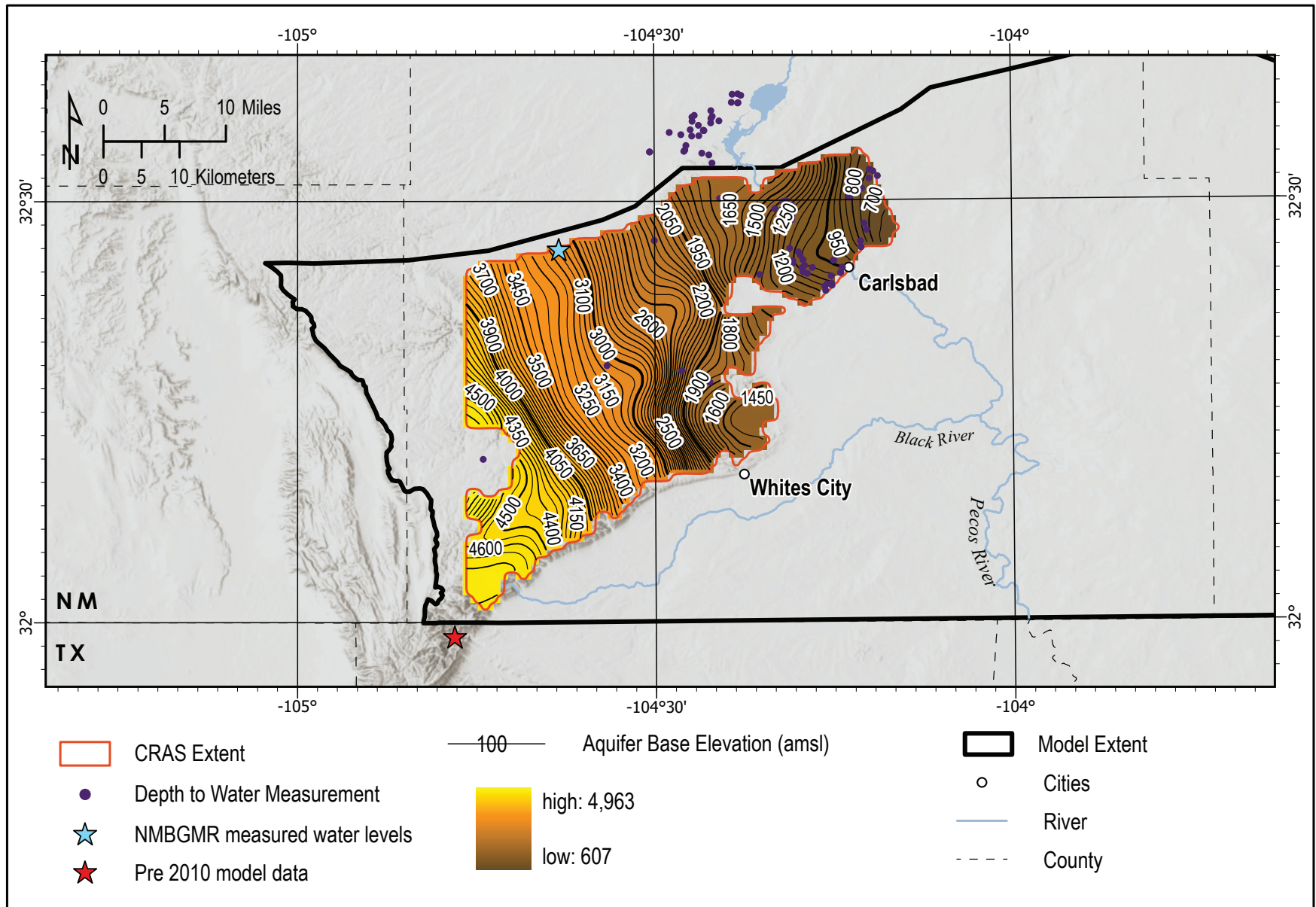
Figure 59. CRAS aquifer base elevation (elevation contours in ft). The base elevation surface of the aquifer system was created by combining the alluvium and upper Ochoan base elevation surfaces and smoothing the result with Esri Focal Statistics.
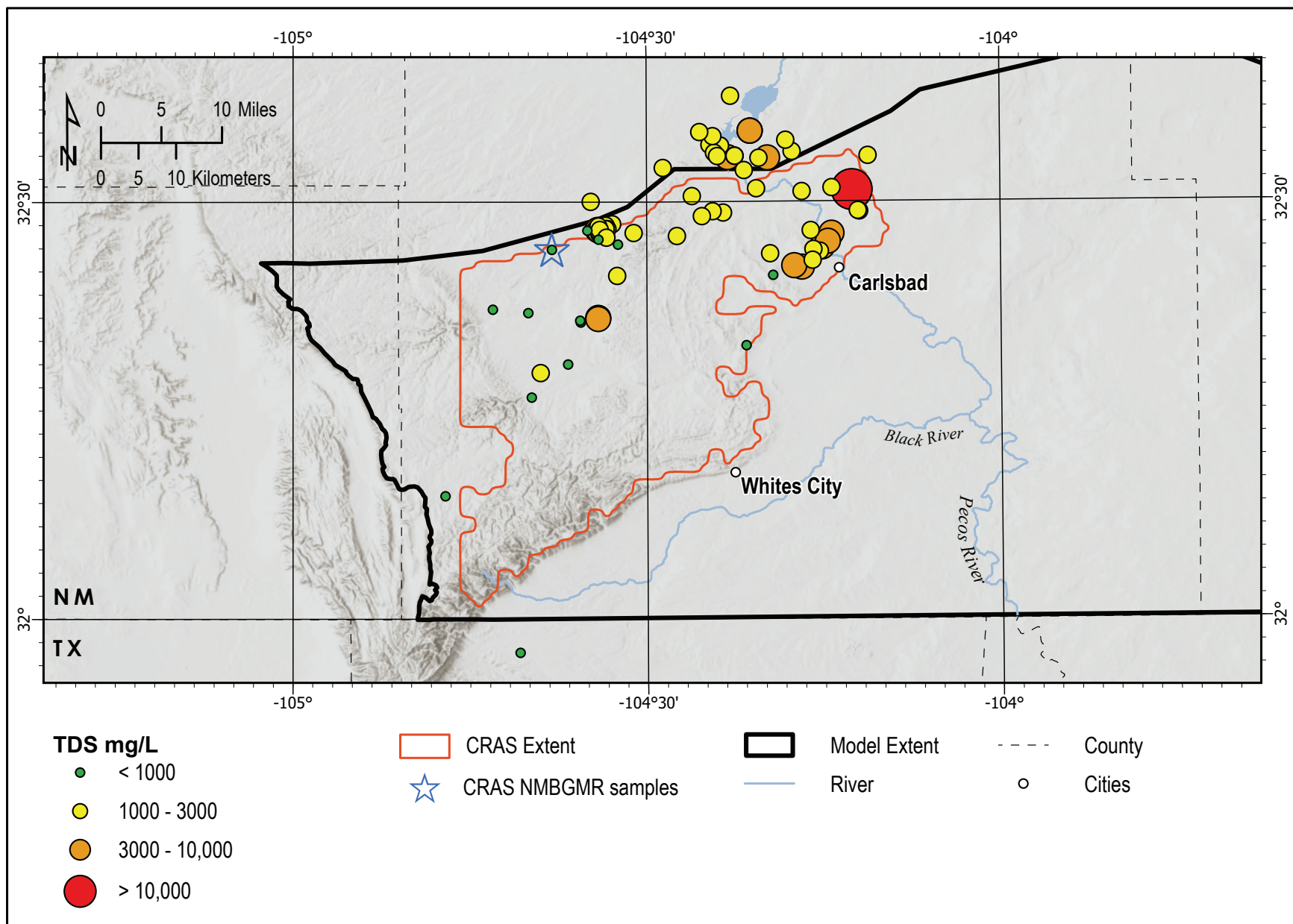
Figure 60. Locations of water quality wells found aerially within and completed/screened in the CRAS.
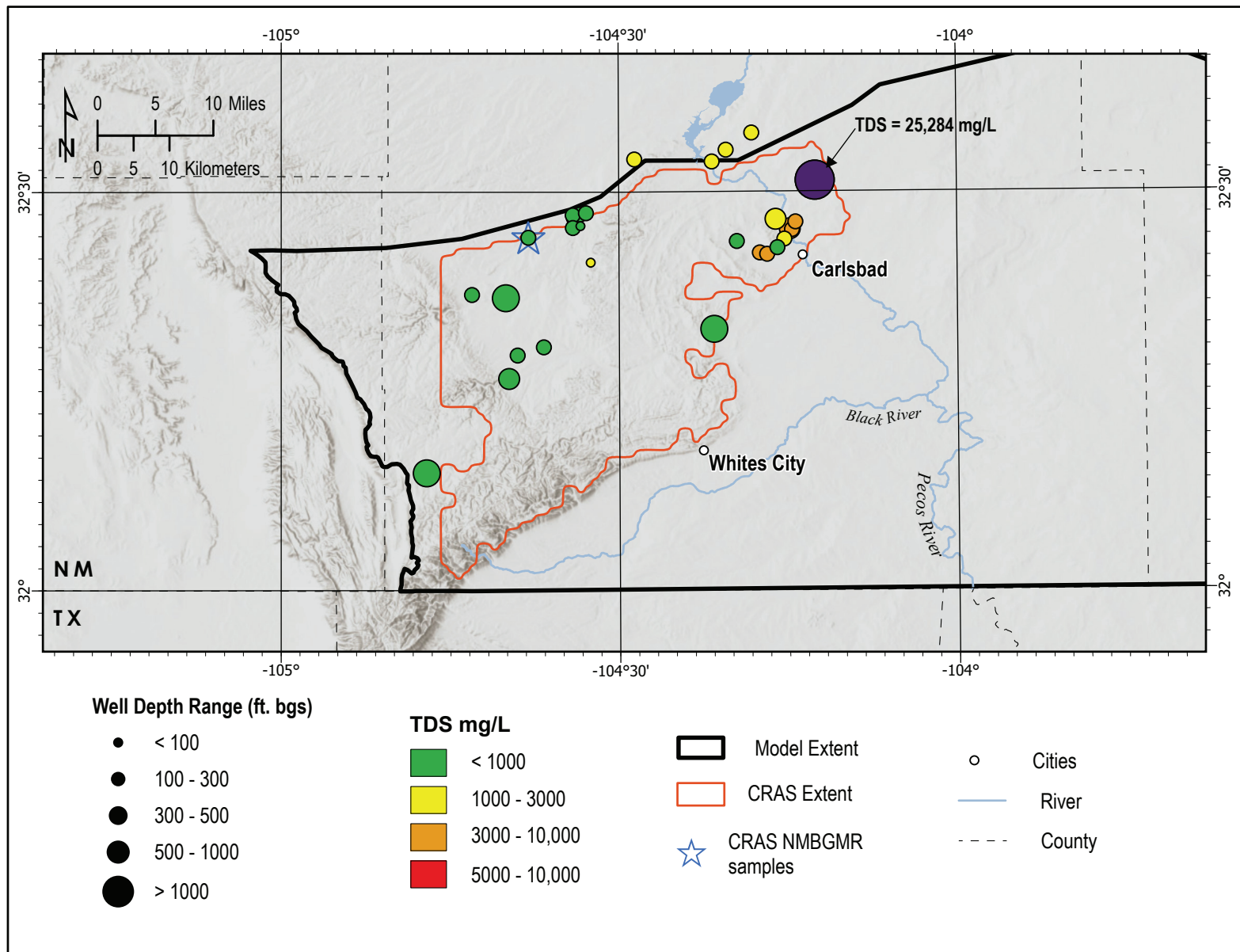
Figure 61. TDS concentrations in the CRAS. Points plotted on the map denote locations of wells in the CRAS. The size of the point is proportional to the total depth of the well, ranging from 22 to 2,500 ft bgs. Colors represent a range of TDS concentrations; green: less than 1,000 mg/L, yellow: 1,000–3,000 mg/L, orange: 3,000–5,000 mg/L, red: 5,000–10,000 mg/L, purple = 25,284 mg/L.
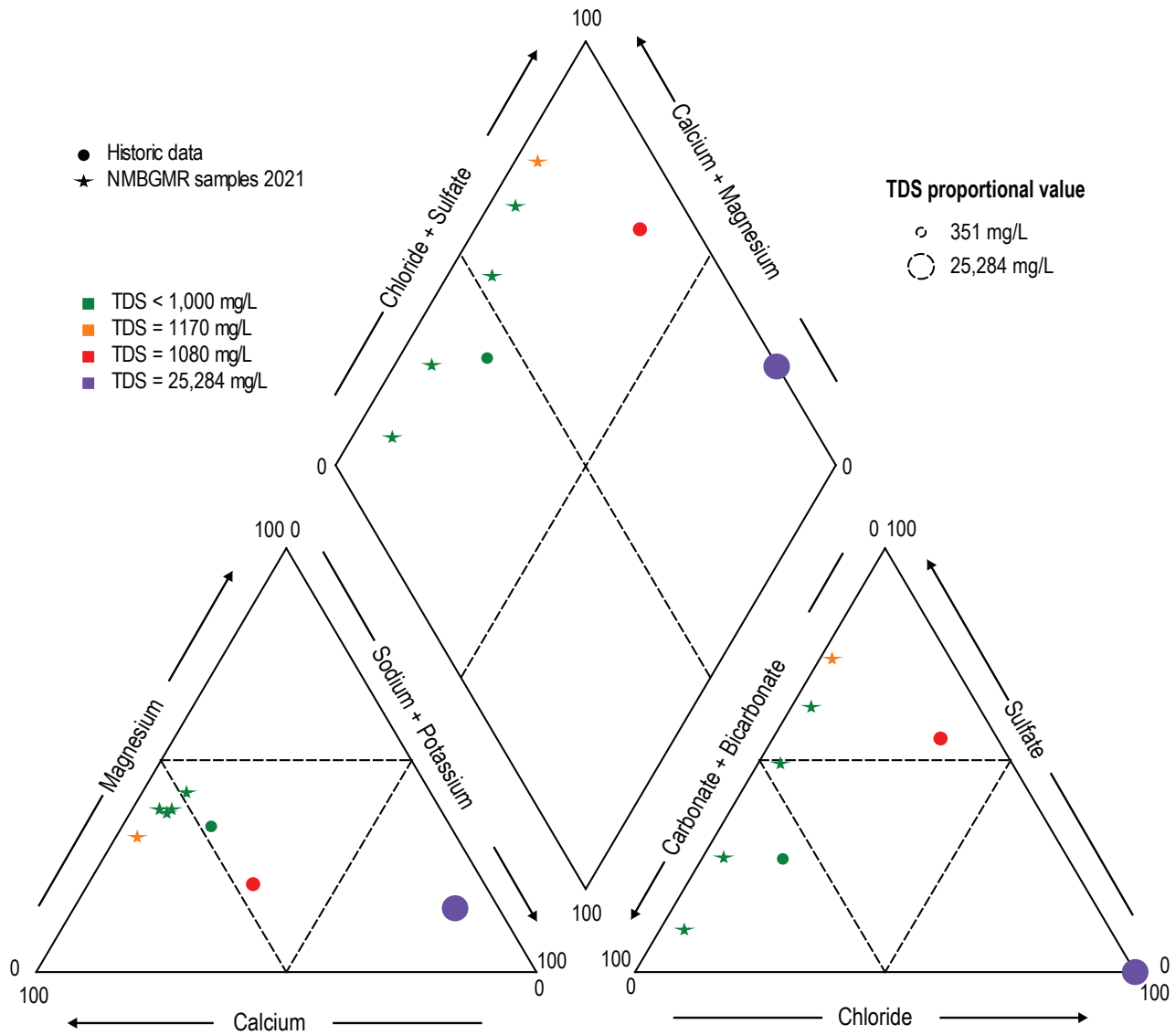
Figure 62. Piper diagram showing major cation and anion chemistry for groundwater samples in the CRAS, including samples collected by NMBGMR in 2021 (stars).
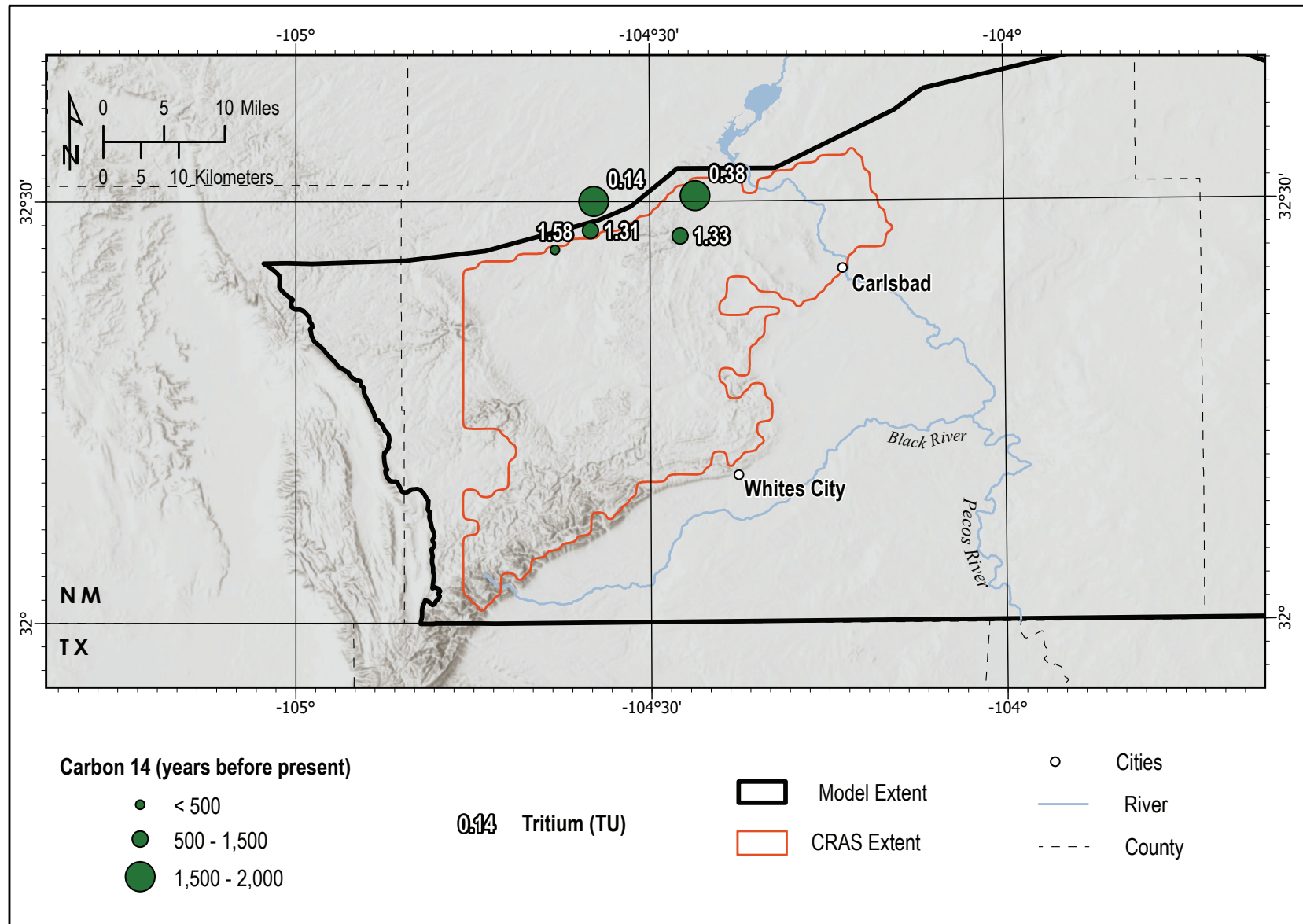
Figure 63. [14]C and tritium data for the CRAS. Points shown on map denote locations of wells. The sizes of data points are proportional to ^{14}C results for the age of the water (years before present). Labels for each point are tritium results for each sample (TU). Tritium concentrations close to 0 TU (including negative values) indicate that the groundwater is older than 50 or 60 years before present, while modern recharge (within 10 years or so) usually exhibits values between 4 and 8 TU. Intermediate values are due to mixing of old tritium-free water with modern recharge.
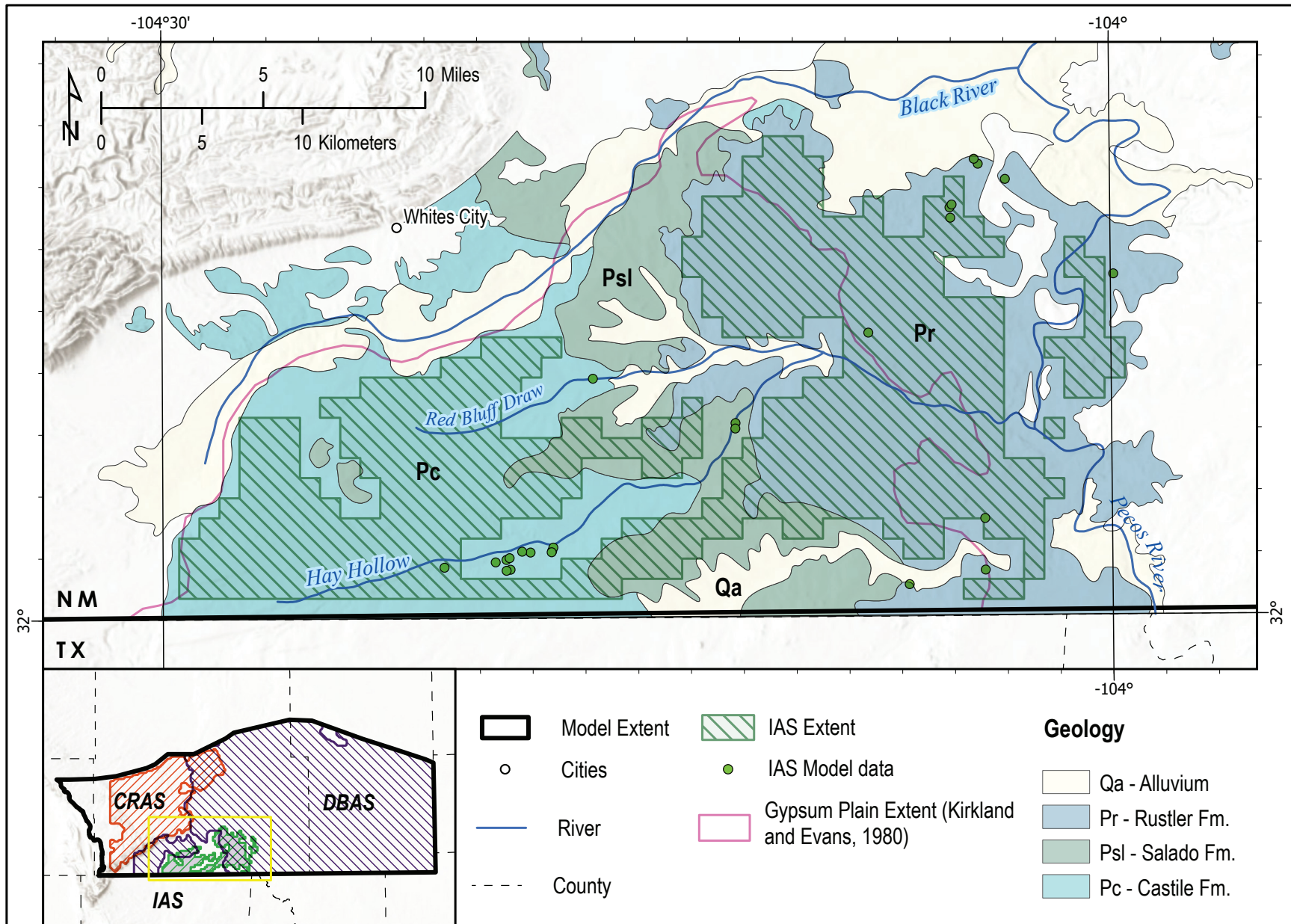
Figure 64. Water quality data and locations of water quality wells found aerially within and completed/screened in the intermittent alluvial aquifer.

SUMMARY

We developed a 3D, digital, GIS-based hydrogeologic framework of Delaware basin aquifers in southeastern New Mexico using ArcGIS and methods modified from Cikoski et al. (2020). The final product is a downloadable map package that contains (1) geologic model input data, (2) geologic structure maps, (3) groundwater level and water quality data, and (4) aquifer maps that represent roughly 4,000 mi^2 and nearly 6,000 vertical feet of subsurface geology and hydrology in southeastern New Mexico.

The digital elevation models (geologic-structure maps) depict the basal contacts of the following lithologic units (formations or groups, in ascending order): the Permian-age Capitan Formation (Standen et al., 2009), Artesia Group, Castile Formation, Rustler Formation, and Dewey Lake Formation; the Triassic Dockum Group; and undivided Cenozoic deposits, including the Ogallala Formation and Quaternary Pecos River valley alluvial and piedmont deposits. The final model includes over 10,000 geologic control points from sources outlined in Appendix A and Table 2.

Using the 3D geologic framework, we mapped three distinct aquifer systems: (1) the Delaware Basin Aquifer System (DBAS), (2) the Capitan Reef Aquifer System (CRAS), and (3) an intermittent alluvial aquifer. For the DBAS, we analyzed hydrochemical data for wells that are mostly producing water from the shallow phreatic aquifer, which includes (from oldest to youngest) the Rustler Formation, Dewey Lake Formation, upper and lower Dockum Group, Ogallala Formation, and Cenozoic alluvium. In general, water quality in this shallow system is fair to good, with TDS concentrations less than 3,500 mg/L. However, Na-Cl brines are observed to significantly impact water quality throughout this system in localized areas of the DBAS. More data are needed to refine the extent of these saltier zones within the DBAS.

The CRAS includes the Artesia Group and the Capitan Reef Limestone and contains relatively fresh water (TDS <700 mg/L) from the southern part of Carlsbad southwestward for over 20 mi (Bjorklund and Motts, 1959). These waters are Ca-HCO$_3$ water type due to the dissolution of limestone and dolomite. Underlying the western and northern parts of Carlsbad is water with TDS concentrations ranging from 700 to 1,700 mg/L. Going farther to the north toward Lake Avalon, water quality declines, with TDS concentrations above 1,700 mg/L. Water quality in this area also tends to decline with depth.

The Pecos River valley alluvial aquifer to the west of the Pecos River yields water of varying quality, with TDS concentrations ranging from 500 to over 4,000 mg/L. The best water in this aquifer occurs to the west of Carlsbad.

Potentiometric surface and saturated thickness maps should be used with caution in this region due to localized confining conditions that create artesian pressure. Depth-to-water data may be impacted by artesian pressure, causing water tables to rise above formation depths. While not accurate for drilling purposes, these depths and saturated thicknesses should be protected as potential freshwater-bearing zones.

REFERENCES

2003 Pecos Settlement Agreement, issued by the New Mexico Office of the State Engineer; New Mexico Interstate Stream Commission; U.S. Department of the Interior, Bureau of Reclamation; Carlsbad Irrigation District; and Pecos Valley Artesian Conservancy District.

Algeo, T.J., Wilson, J.L., and Lohmann, K.C., 1991, Eustatic and tectonic controls on cyclic sediment accumulation patterns in lower-middle Pennsylvanian strata of the Orogrande Basin, New Mexico, *in* Barker, J., Kues, B., Austin, G., and Lucas, S., eds., Geology of the Sierra Blanca, Sacramento and Capitan Ranges, New Mexico: New Mexico Geological Society Fall Field Conference Guidebook 42, p. 203–212. https://doi.org/10.56577/ffc-42.203

Anderson, R.Y., 1981, Deep-seated salt dissolution in the Delaware basin, Texas and New Mexico, *in* Wells, S.G., Lambert, W., and Callender, J.F., eds., Environmental Geology and Hydrology in New Mexico: New Mexico Geological Society Special Publication 10, p. 133–145.

Arbenz, J.K., 1989, Ouachita thrust belt and Arkoma basin, *in* Hatcher Jr., R.D., Thomas, W.A., and Viele, G.W., eds., The Appalachian-Ouachita Orogen in the United States: Geological Society of America, The Geology of North America, v. F-2, p. 621–634. https://doi.org/10.1130/DNAG-GNA-F2.621

Austin, G.S., 1978, Geology and mineral deposits of Ochoan rocks in Delaware basin and adjacent areas: New Mexico Bureau of Mines and Mineral Resources Circular 159, 88 p.

Bachman, G.O., 1980, Regional geology and Cenozoic history of Pecos region, southeastern New Mexico: U.S. Geological Survey Open-File Report 80-1099, 116 p. https://doi.org/10.3133/ofr801099

Bachman, G.O., 1987, Karst in evaporites in southeastern New Mexico: Sandia National Laboratories, SAND86-7078, 82 p.

Barnes, V.E., Hartmann, B.M., and Scranton, D.F., 1968, Geologic atlas of Texas, Van Horn-El Paso sheet: The University of Texas Bureau of Economic Geology, scale 1:250,000.

Barroll, P., Jordan, D., and Ruskauff, G., 2004, The Carlsbad area groundwater flow model: New Mexico Office of the State Engineer, 164 p.

Berry, R., 2011, Hydrological assessment and groundwater modeling report for the HB in-situ solution mine project EIS: Report submitted by AECOM to the Bureau of Land Management, Carlsbad, New Mexico, 151 p.

Bjorklund, L.J., 1957, Reconnaissance of ground-water conditions in the Crow Flats area Otero County, New Mexico: New Mexico Office of the State Engineer Technical Report 8, 31 p.

Bjorklund, L.J., and Motts, W.S., 1959, Geology and water resources of the Carlsbad area, Eddy County, New Mexico: U.S. Geological Survey Open-File Report 59-9, 576 p. https://doi.org/10.3133/ofr599

Bogener, S., 1993, Carlsbad Project: Bureau of Reclamation History Program, 29 p.

Bradley, R.G., and Kalaswad, S., 2003, Groundwater resources of the Dockum Aquifer in Texas: Texas Water Development Board, 73 p.

Budnik, R.T., 1986, Left-lateral intraplate deformation along the Ancestral Rocky Mountains—Implications for late Paleozoic plate motions: Tectonophysics, v. 132, no. 1–3, p. 195–214. https://doi.org/10.1016/0040-1951(86)90032-6

Bureau of Land Management (BLM), 2019, New Mexico water support document, 67 p.: https://www.blm.gov/sites/blm.gov/files/2019%20BLM%20NM%20Water%20Support%20Document_07122019_508.pdf

Chapman, J.B., 1986, Stable isotopes in southeastern New Mexico groundwater—Implications for dating recharge in the WIPP area: New Mexico Health and Environment Department report no. DOE/AL/10752-35, EEG-35, 76 p.

Cikoski, C., Fichera, M., Mamer, E., and Sturgis, L., 2020, A three-dimensional hydrogeologic model from the Pecos Slope to the Southern High Plains, Southeastern New Mexico: New Mexico Bureau of Geology and Mineral Resources Open-File Report 614, 136 p. https://doi.org/10.58799/OFR-614

Clark, I.D., and Fritz, P., 1997, Environmental Isotopes in Hydrogeology: New York, CRC Press, 342 p.

Cooper, J.B., and Glanzman, V.M., 1971, Geohydrology of Project Gnome Site, Eddy County, New Mexico: U.S. Geological Survey Professional Paper 712-A, 23 p. https://doi.org/10.3133/pp712A

Craig, H., 1961, Isotopic variations in meteoric waters: Science, v. 133, no. 3465, p. 1702–1703. https://doi.org/10.1126/science.133.3465.1702

Davidson, N.J.R., 2003, Groundwater and produced water quality of the Permian Basin, Southeast New Mexico [MS thesis]: Socorro, New Mexico Institute of Mining and Technology, 233 p.

Deeds, N.E., Harding, J.J., Jones, T.L., Singh, A., Hamlin, S., and Reedy, R.C., eds., 2015, Final conceptual model report for the High Plains aquifer system groundwater availability model: Texas Water Development Board, 590 p.

Dickerson, P.W., 2003, Intraplate mountain building in response to continent–continent collision—The Ancestral Rocky Mountains (North America) and inferences drawn from the Tien Shan (Central Asia): Tectonophysics, v. 365, no. 1–4, p. 129–142. https://doi.org/10.1016/S0040-1951(03)00019-2

Dickinson, W.R., and Lawton, T.F., 2003, Sequential intercontinental suturing as the ultimate control for Pennsylvanian Ancestral Rocky Mountains deformation: Geology, v. 31, no. 7, p. 609–612. https://doi.org/10.1130/0091-7613(2003)031%3C0609:SISATU%3E2.0.CO;2

Dutton, A.R., and Simpkins, W.W., 1986, Hydrogeochemistry and water resources of the Triassic lower Dockum Group in the Texas Panhandle and eastern New Mexico: University of Texas at Austin Bureau of Economic Geology Report of Investigations No. 161, 51 p. https://doi.org/10.23867/RI0161D

Eastoe, C.J., Watts, C.J., Ploughe, M., and Wright, W.E., 2012, Future use of tritium in mapping pre-bomb groundwater volumes: Groundwater, v. 50, no. 1, p. 87–93. https://doi.org/10.1111/j.1745-6584.2011.00806.x

Energy Information Administration, 2022, U.S. crude oil and natural gas proved reserves, year-end 2020: U.S. Department of Energy, 45 p. https://www.eia.gov/naturalgas/crudeoilreserves/archive/2020/pdf/usreserves.pdf

Engler, T.W., and Cather, M., 2014, Update to the reasonable foreseeable development (RFD) for the BLM Pecos District, SENM, final report, 51 p. https://eplanning.blm.gov/public_projects/lup/64444/80056/93025/Final_Report-SENM-DEC2014_updated_RFD.pdf

Ewing, T.E., 1993, Erosional margins and patterns of subsidence in the late Paleozoic west Texas basin and adjoining basins of west Texas and New Mexico, in Love, D.W., Hawley, J.W., Kues, B.W., Austin, G.S., and Lucas, S.G., eds., Carlsbad Region, New Mexico and West Texas: New Mexico Geological Society Fall Field Conference Guidebook 44, p. 155–66. https://doi.org/10.56577/FFC-44.155

Ewing, T.E., 2016, Texas through Time—Lone Star Geology, Landscapes, and Resources: The University of Texas Bureau of Economic Geology Udden Series No. 6, 431 p.

Ewing, J.E., et al., 2008, Groundwater availability model for the Dockum aquifer: Final report to the Texas Water Development Board, 420 p.

Ewing, J.E., Kelley, V.A., Jones, T.L., Yan, T., Singh, A., Powers, D.W., Holt, R.M., and Sharp, J.M., 2012, Final groundwater availability model report for the Rustler aquifer: Texas Water Development Board, 460 p.

Fallin, J.A.T., 1988, Hydrogeology of Lower Cretaceous strata under the southern High Plains of Texas and New Mexico: New Mexico Geology, v. 10, no. 1, p. 6–9. https://doi.org/10.58799/NMG-v10n1.6

Fallin, J.A.T., 1989, Hydrogeology of Lower Cretaceous strata under the southern High Plains of Texas and New Mexico: Texas Water Development Board Report 314, 39 p.

Galley, J.E., 1958, Oil and geology in the Permian basin of Texas and New Mexico, in Weeks, L.G., ed., Habitat of Oil: American Association of Petroleum Geologists Special Publication, p. 395–446.

Geohydrology Associates Inc., 1978, Collection of hydrologic data eastside Roswell range EIS area New Mexico: Report for Bureau of Land Management, Contract No. YA-512-CT7-217, 236 p.

Goetz, L.K., and Dickerson, P.W., 1985, A Paleozoic transform margin in Arizona, New Mexico, west Texas and northern Mexico, in Dickerson, P.W., and Muehlberger, W.R., eds., Structure and Tectonics of Trans-Pecos Texas: West Texas Geological Society, p. 173–184.

Hale, W.E., 1945, Ground-water conditions in the vicinity of Carlsbad, New Mexico: U.S. Geological Survey Open-File Report 45-106, 83 p. https://doi.org/10.3133/ofr45106

Havens, J.S., and Wilkins, D.W., 1979, Experimental salinity alleviation at Malaga Bend of the Pecos River, Eddy County, New Mexico: U.S. Geological Survey Water Resources Investigations Report 80-4, 65 p. https://doi.org/10.3133/wri804

Hayes, P.T., 1964, Geology of the Guadalupe Mountains, New Mexico: U.S. Geological Survey Professional Paper 446, 69 p., 3 plates. https://doi.org/10.3133/pp446

Hendrickson, G.E., and Jones, R.S., 1952, Geology and ground-water resources of Eddy County, New Mexico: New Mexico Institute of Mining and Technology/U.S. Geological Survey/State Engineer of New Mexico Ground-Water Report 3, 169 p. https://doi.org/10.58799/GW-3

Hill, C.A., 1996, Geology of the Delaware Basin, Guadalupe, Apache, and Glass Mountains, New Mexico and Texas: Permian Basin Section-SEPM Publication No. 96-39, 480 p.

Hills, J.M., 1984, Sedimentation, tectonism, and hydrocarbon generation in Delaware Basin, west Texas and southeastern New Mexico: AAPG bulletin, v. 68, no. 3, p. 250–267. https://doi.org/10.1306/AD460A08-16F7-11D7-8645000102C1865D

Hiss, W.L., 1973, Capitan aquifer observation— Well network, Carlsbad to Jal, New Mexico: New Mexico State Engineer Technical Report 38, 76 p.

Hiss, W.L., 1975a, Thickness of the Permian Guadalupian Capitan aquifer, southeast New Mexico and west Texas: New Mexico Bureau of Mines and Mineral Resources Resource Map 5, scale 1:500,000. https://doi.org/10.58799/RM-5

Hiss, W.L., 1975b, Stratigraphy and ground-water hydrology of the Capitan aquifer, southeastern New Mexico and western Texas [PhD dissertation]: Boulder, University of Colorado Department of Geological Sciences, 396 p.

Hiss, W.L., 1976, Structure of the Permian Ochoan Rustler Formation, southeast New Mexico and west Texas: New Mexico Bureau of Mines and Mineral Resources Resource Map 7, scale 1:5,000. https://doi.org/10.58799/RM-7

Hiss, W.L., 1980, Movement of ground water in Permian Guadalupian aquifer systems, southeastern New Mexico and western Texas, in Dickerson, P.W., Hoffer, J.M., and Callender, J.F., eds., Trans Pecos Region (West Texas): New Mexico Geological Society Fall Field Conference Guidebook 31, p. 289–294. https://doi.org/10.56577/FFC-31.289

Holt, R.M., and Powers, D.W., 1990, Geologic mapping of the air intake shaft at the Waste Isolation Pilot Plant: U.S. Department of Energy WIPP 90-051, 341 p. https://doi.org/10.2172/5492393

Hood, J.W., 1977, Hydrologic evaluation of the upper Duchesne River Valley, northern Uinta Basin area, Utah: Prepared by the U.S. Geological Survey in cooperation with the State of Utah Department of Natural Resources Technical Publication No. 57, 38 p.

Hood, J.W., and Kister, L.R., 1962, Saline-water resources of New Mexico: U.S. Geological Survey Water Supply Paper 1601, 70 p., 8 plates. https://doi.org/10.3133/wsp1601

Horak, R.L., 1985, Trans-Pecos tectonism and its effects on the Permian Basin, *in* Dickerson, P.W., and Muehlberger, W.R., eds., Structure and Tectonics of Trans-Pecos Texas: West Texas Geological Society, p. 81–87.

Jones, I.C., 2016, Groundwater availability model—Eastern arm of the Capitan Reef Complex aquifer of Texas: Texas Water Development Board, 494 p.

Kalin, R.M., 2000, Radiocarbon dating of groundwater systems, *in* Cook, P.G., and Herczeg, A.L., eds., Environmental Tracers in Subsurface Hydrology: New York, Springer, p. 111–144. https://doi.org/10.1007/978-1-4615-4557-6_4

Keller, G., Lidiak, E., Hinze, W., and Braile, L., 1983, The role of rifting in the tectonic development of the midcontinent, USA: Developments in Geotectonics, v. 19, p. 391–412. https://doi.org/10.1016/B978-0-444-42198-2.50028-6

Kelley, V.C., 1971, Geology of the Pecos country, southeastern New Mexico: New Mexico Bureau of Mines and Mineral Resources Memoir 24, 78 p. https://doi.org/10.58799/M-24

Kendall, A.C., and Harwood, G.M., 1989, Shallow-water gypsum in the Castile Formation—Significance and implications, *in* Harris, P.M., and Grover, G.A., eds., Subsurface and Outcrop Examination of the Capitan Shelf Margin, Northern Delaware Basin: SEPM Core Workshop no. 13, p. 451–457.

King, P.B., 1942, Permian of west Texas and southeastern New Mexico—PART 1: AAPG Bulletin, v. 26, no. 4, p. 535–649. https://doi.org/10.1306/3D933466-16B1-11D7-8645000102C1865D

Kirkland, D.W., and Anderson, R.Y., 1970, Microfolding in the Castile and Todilto evaporites, Texas and New Mexico: Geological Society of America Bulletin, v. 81, no. 11, p. 3259–3282. https://doi.org/10.1130/0016-7606(1970)81[3259:MITCAT]2.0.CO;2

Kluth, C.F., and Coney, P.J., 1981, Plate tectonics of the Ancestral Rocky Mountains: Geology, v. 9, no. 1, p. 10–15. https://doi.org/10.1130/0091-7613(1981)9%3C10:PTOTAR%3E2.0.CO;2

Kreie, K., and Findlay, R., 2017, 2016 groundwater monitoring and inspection report Gnome-Coach, New Mexico, site: U.S. Department of Energy, 40 p.

Kues, B.S., and Giles, K.A., 2004, The late Paleozoic Ancestral Rocky Mountains system in New Mexico, *in* Mack, G.H., and Giles, K.A., eds., The Geology of New Mexico—A Geologic History: New Mexico Geological Society Special Publication 11, p. 95–136. https://doi.org/10.56577/SP-11

Kunkler, J.L., 1980, Evaluation of the Malaga Bend salinity alleviation project Eddy County, New Mexico, U.S. Geological Survey Open-File Report 80-1111, 31 p. https://doi.org/10.3133/ofr801111

Lambert, S.J., and Harvey, D.M., 1987, Stable-isotope geochemistry of groundwaters in the Delaware Basin of southeastern New Mexico: Sandia National Laboratories report no. SAND-87-0138, 218 p.

Land, L., 2005, Evaluation of groundwater residence time in a karstic aquifer using environmental tracers—Roswell Artesian Basin, New Mexico, *in* Beck, B.F., ed., Sinkholes and the Engineering and Environmental Impacts of Karst, Proceedings of the 10th Multidisciplinary Conference, September 24–28, 2005, San Antonio, Texas, p. 432–440. https://doi.org/10.1061/40796(177)46

Land, L., 2016, Overview of fresh and brackish water quality in New Mexico: New Mexico Bureau of Geology and Mineral Resources Open-File Report 583, 55 p. https://doi.org/10.58799/OFR-583

Lehman, T.M., 1994, The saga of the Dockum Group and the case of the Texas/New Mexico boundary fault, *in* Ahlen, J., Peterson, J., Bowsher, A.L., and Zidek, J., eds., Geologic Activities in the 90s—Southwest Section of AAPG 1994, Ruidoso, New Mexico: New Mexico Bureau of Mines and Mineral Resources Bulletin 150, p. 37–51. https://doi.org/10.58799/B-150

Lehman, T.M., and Chatterjee, S., 2005, Depositional setting and vertebrate biostratigraphy of the Triassic Dockum Group of Texas: Journal of Earth System Science, v. 114, no. 3, p. 325–351. https://doi.org/10.1007/BF02702953

Li, Z.-X., et al., 2008, Assembly, configuration, and break-up history of Rodinia—A synthesis: Precambrian Research, v. 160, no. 1–2, p. 179–210. https://doi.org/10.1016/j.precamres.2007.04.021

Lowry, T.S., Schuhen, M.D., Roberts, B.L., Arnold, B.W., McKenna, S.A., and Kirby, C.L., 2015, BLM Lea County water study for the Dewey Lake and Santa Rosa Formations—Final Report: Sandia National Laboratories, 134 p.

Lowry, T.S., Schuhen, M.D., Lofton, O.W., Walker, L.T.N., Johnson, P.B., Powers, D.W., and Bowman, D.O., 2018, Water resource assessment in the New Mexico Permian Basin: Sandia National Laboratories, 86 p. https://doi.org/10.2172/1481567

Lucas, S.G., 2004, The Triassic and Jurassic systems in New Mexico, *in* Mack, G.H., and Giles, K.A., eds., The Geology of New Mexico—A Geologic History: New Mexico Geological Society Special Publication 11, p. 137–152. https://doi.org/10.56577/SP-11

Lucas, S.G., and Anderson, O.J., 1993, Stratigraphy of the Permian-Triassic boundary in southeastern New Mexico and west Texas, *in* Love, D.W., Hawley, J.W., Kues, B.S., Austin, G.S., and Lucas, S.G., eds., Carlsbad Region (New Mexico and west Texas): New Mexico Geological Society Fall Field Conference Guidebook 44, p. 219–230. https://doi.org/10.56577/FFC-44.219

Magnuson, M.L., Valdez, J.M., Lawler, C.R., Nelson, M., and Petronis, L., May 2019, New Mexico water use by categories 2015: New Mexico Office of the State Engineer Technical Report 55, 126 p.

Maley, V., and Huffington, R.M., 1953, Cenozoic fill and evaporate solution in the Delaware Basin, Texas and New Mexico: Geological Society of America Bulletin, v. 64, no. 5, p. 539–546. https://doi.org/10.1130/0016-7606(1953)64[539:CFAESI]2.0.CO;2

Mayer, J.R., 1995, The role of fractures in regional groundwater flow—Field evidence and model results from the basin-and-range of Texas and New Mexico [PhD thesis]: The University of Texas at Austin, 220 p. https://doi.org/10.15781/T2ZG6GC8F

McGowen, J.H., Granata, G.E., and Seni, S.J., 1977, Depositional systems, uranium occurrence and postulated groundwater history of the Triassic Dockum Group, Texas Panhandle-eastern New Mexico: The University of Texas at Austin Bureau of Economic Geology, 104 p.

Mercer, J.W., 1983, Geohydrology of the proposed Waste Isolation Plant, Los Medaños area, southeastern New Mexico: U.S. Geological Survey Water Resources Investigations Report 83-4016, 121 p. https://doi.org/10.3133/wri834016

Meyer, J.E., 2020, Brackish resources aquifer characterization system database data dictionary: Texas Water Development Board Open-File Report 12-02 (fifth edition), 260 p.

Meyer, J.E., Wise, M.R., and Kalaswad, S., 2012, Pecos Valley aquifer, west Texas—Structure and brackish groundwater: Texas Water Development Board Report 382, 86 p.

Motts, W.S., 1968, The control of ground-water occurrence by lithofacies in the Guadalupian Reef Complex near Carlsbad, New Mexico: Geological Society of America Bulletin, v. 79, no. 3, p. 283–298. https://doi.org/10.1130/0016-7606(1968)79[283:TCOGOB]2.0.CO;2

Muehlberger, W.R., 1965, Late Paleozoic movement along the Texas lineament: Transactions of the New York Academy of Sciences, v. 27, no. 4, series II, p. 385–392. https://doi.org/10.1111/j.2164-0947.1965.tb02976.x

Nance, H.S., 2009, Guadalupian (Artesia Group) and Ochoan shelf succession of the Permian basin—Effects of deposition, diagensis, and structure on reservoir development, *in* Ruppel, S.C., ed., Integrated Synthesis of the Permian Basin—Data and Models for Recovering Existing and Undiscovered Oil Resources from the Largest Oil-Bearing Basin in the U.S.: U.S. Department of Energy contract DE-FC2604NT15509 Final Report, p. 847–946. https://doi.org/10.2172/969666

National Water Quality Monitoring Council, 2021, Water quality portal: https://doi.org/10.5066/P9QRKUVJ

New Mexico Bureau of Geology and Mineral Resources, 2023, Data collected from wells participating in the Healy Collaborative Groundwater Monitoring Network: https://maps.nmt.edu/

New Mexico Environment, Minerals and Natural Resources Department Oil Conservation Division, n.d., Groundwater contamination abatement plans, spill reports, and discharge plan permits containing water level and water quality data (spill reports and discharge plans listed by OCD incident number): https://ocdimage.emnrd.nm.gov/imaging/AEOrderCriteria.aspx (accessed June–December 2020).

Newton, B.T., Rawling, G.C., Timmons, S., Land, L., Johnson, P.S., Kludt, T., and Timmons, J.M., 2012, Sacramento Mountains hydrogeology study—Final technical report: New Mexico Bureau of Geology and Mineral Resources Open-File Report 543, 82 p. https://doi.org/10.58799/OFR-512

Nicholson Jr., A., and Clebsch Jr., A., 1961, Geology and ground-water conditions in southern Lea County, New Mexico: New Mexico Institute of Mining and Technology Ground-Water Report 6, 123 p. https://doi.org/10.58799/GW-6

NMOSE, 2016a, Lea County Regional Water Plan: New Mexico Office of the State Engineer Interstate Stream Commission, 155 p.

NMOSE, 2016b, Lower Pecos Valley Regional Water Plan: New Mexico Office of the State Engineer Interstate Stream Commission, 264 p.

Pindell, J.L., 1985, Alleghenian reconstruction and subsequent evolution of the Gulf of Mexico, Bahamas, and Proto-Caribbean: Tectonics, v. 4, no. 1, p. 1–39. https://doi.org/10.1029/TC004i001p00001

Powers, D.W., and Holt, R.M., 1993, The upper Cenozoic Gatuña Formation of southeastern New Mexico, *in* Love, D.W., Hawley, J.W., Kues, B.S., Austin, G.S., and Lucas, S.G., eds., Carlsbad Region (New Mexico and West Texas): New Mexico Geological Society Fall Field Conference Guidebook 44, p. 271–282. https://doi.org/10.56577/FFC-44.271

Powers, D.W., and Holt, R.M., 2000, The salt that wasn't there—Mudflat facies equivalents to halite of the Permian Rustler Formation, southeastern New Mexico: Journal of Sedimentary Research, v. 70, no. 1, p. 29–36. https://doi.org/10.1306/2DC408FB-0E47-11D7-8643000102C1865D

Powers, D.W., Lambert, S.J., Shaffer, S., Hill, L.R, and Weart, W.D., 1978, Geological characterization report—Waste Isolation Pilot Plant (WIPP) site, southeastern New Mexico: Sandia National Laboratories SAND78-1596, 475 p. https://doi.org/10.2172/6441454

Powers, D.W., Holt, R.M., Beauheim, R., McKenna, S.A., Johnson, K., and Neal, J., 2003, Geological factors related to the transmissivity of the Culebra Dolomite Member, Permian Rustler Formation, Delaware Basin, southeastern New Mexico: Oklahoma Geological Survey Circular, v. 109, p. 211–218.

Reardon, A.J., Lofton, O.W., Johnson, P.B., and Lowry, T.S., 2021, Addendum to water resource assessment in the New Mexico Permian Basin: Sandia National Laboratories Report SAND2021-1869, 61 p. https://doi.org/10.2172/1769223

Reyes, F.R., 2014, Exploring the hydrogeologic controls on brackish water and its suitability for the use in hydraulic fracturing—The Dockum Aquifer, Midland Basin, Texas [MS thesis]: University of Texas at El Paso, 58 p. https://digitalcommons.utep.edu/open_etd/933

Richey, S.F., Wells, J.G., and Stephens, K.T., 1985, Geohydrology of the Delaware Basin and vicinity, Texas and New Mexico: U.S. Geological Survey Water-Resources Investigations Report 84-4077, 99 p. https://doi.org/10.3133/wri844077

Ross, C.A., 1986, Paleozoic evolution of southern margin of Permian basin: Geological Society of America Bulletin, v. 97, no. 5, p. 536–554. https://doi.org/10.1130/0016-7606(1986)97<536:PEOSMO>2.0.CO;2

Ross, C.A., and Ross, J.R., 1985, Paleozoic tectonics and sedimentation in West Texas, southern New Mexico, and southern Arizona, in Dickerson, P.W., and Muehlberger, W.R., eds., Structure and Tectonics of Trans-Pecos Texas: West Texas Geological Society, p. 85-81.

Sales, J.K., 1968, Crustal mechanics of Cordilleran foreland deformation—A regional and scale-model approach: AAPG Bulletin, v. 52, no. 10, p. 2016–2044.

Saller, A.H., Harris, P.M.M., Kirkland, B.L., and Mazzullo, S., 1999, Geologic framework of the Capitan depositional system—Previous studies, controversies, and contents of this special publication: Society for Sedimentary Geology Special Publication No. 65, p. 1–13. https://doi.org/10.2110/pec.99.65.0001

Schiel, K.A., 1988, The Dewey Lake Formation—End Stage Deposit of a Peripheral Foreland Basin [M.S. thesis]: The University of Texas at El Paso, 181 p.

Scholle, P., 2003, Geologic map of New Mexico: New Mexico Bureau of Geology and Mineral Resources, 1:500,000 scale, 2 sheets. https://doi.org/10.58799/116894

Seigel, M.D., Robinson, K.L., and Myers, J., 1991, Solute relationships in groundwater from the Culebra Dolomite and related rocks in the Waste Isolation Pilot Plant Area, southeastern New Mexico, in Seigel, M.D., Lambert, S.J., and Robinson, K.L., eds., Hydrogeochemical Studies of the Rustler Formation and Related Rocks in the Waste Isolation Pilot Plant Area, Southeastern New Mexico: Sandia National Laboratories Report SAND88-0196, p. 2-1–2-163.

Sigstedt, S.C., 2010, Environmental tracers in groundwater of the Salt basin, New Mexico, and implications for water resources [unpublished master's thesis]: Socorro, New Mexico Institute of Mining and Technology, 202 pp.

Solomon, D.K., and Sudicky, E.A., 1991, Tritium and helium 3 isotope ratios for direct estimation of spatial variations in groundwater recharge: Water Resources Research, v. 27, no. 9, p. 2309–2319. https://doi.org/10.1029/91WR01446

Soto-Kerans, G.M., Stockli, D.F., Janson, X., Lawton, T.F., and Covault, J.A., 2020, Orogen proximal sedimentation in the Permian foreland basin: Geosphere, v. 16, no. 2, p. 567–593. https://doi.org/10.1130/GES02108.1

Stafford, K.W., 2013, Evaporite karst and hydrogeology of the Castile Formation— Culberson County, Texas and Eddy County, New Mexico: Full Proceedings of the Thirteenth Multidisciplinary Conference on Sinkholes and the Engineering and Environmental Impacts of Karst, 10 p. http://doi.org/10.5038/9780979542275.1120

Stafford, K.W., Nance, R., Rosales-Lagarde, L., and Boston, P.J., 2008, Epigene and hypogene karst manifestations of the Castile Formation—Eddy County, New Mexico and Culberson County, Texas, USA: International Journal of Speleology, v. 37, no. 2, p. 83–98. http://dx.doi.org/10.5038/1827-806X.37.2.1

Standen, A., Finch, S., Williams, R., and Lee-Brand, B., 2009, Capitan Reef Complex structure and stratigraphy: Texas Water Development Board Contract Number 0804830794 Report, 53 p.

Texas Water Development Board, n.d., Brackish Resources Aquifer Characterization System (BRACS) Database: https://www.twdb.texas.gov/groundwater/bracs/database.asp (accessed June 2020–February 2021).

Texas Water Development Board, n.d., Groundwater Database (GWDB): https://www.twdb.texas.gov/groundwater/data/gwdbrpt.asp (accessed 2021).

U.S. Census Bureau, 2021, City and town population totals, 2010–2019: https://www.census.gov/quickfacts/fact/table/carlsbadcitynewmexico (accessed Dec. 21, 2022).

U.S. Geological Survey, n.d., National Water Information System: https://waterdata.usgs.gov/nwis/qw (accessed 2022).

U.S. Geological Survey, 2022, USGS water data for New Mexico: https://nwis.waterdata.usgs.gov/nm/nwis

Vine, J.D., 1960, Recent domal structures in southeastern New Mexico: American Association of Petroleum Geologists Bulletin, v. 44, no. 12, p. 1903–1911. https://doi.org/10.1306/0BDA6260-16BD-11D7-8645000102C1865D

Vine, J.D., 1963, Surface geology of the Nash Draw quadrangle, Eddy County, New Mexico: U.S. Geological Survey Bulletin 1141-B, 46 p. https://doi.org/10.3133/b1141B

Walper, J.L., 1982, Plate tectonic evolution of the Fort Worth Basin: Petroleum Geology of the Fort Worth Basin and Bend Arch Area, American Association of Petroleum Geologists/Dallas Geological Society database, p. 237–251.

Wood, J.W., 1968, Geology of Apache Mountains, trans-Pecos Texas: Texas Bureau of Economic Geology Map No. 35, scale 1:63,360, 32 p.

Yang, K.-M., and Dorobek, S.L., 1995, The Permian basin of west Texas and New Mexico—Flexural modeling and evidence for lithospheric heterogeneity across the Marathon Foreland, *in* Dorobek, S.L., and Ross, G.M., eds., Stratigraphic Evolution of Foreland Basins: SEPM Special Publication, v. 52, 14 p. https://doi.org/10.2110/pec.95.52.0037

Yuan, F., and Miyamoto, S., 2005, Dominant processes controlling water chemistry of the Pecos River in American Southwest: Geophysical Research Letters, v. 32, no. 17. https://doi.org/10.1029/2005GL023359

APPENDIX A: GEOLOGIC MODEL INPUT DATA

Model unit (model abbreviation)	Map data source	Original data source	Control feature	Data type	Comments	References
Cenozoic base (AB)	Bjorklund and Motts (1959)	Bjorklund and Motts (1959)	Top of carbonate and/or evaporite	Water well driller's logs	Digitized points from report	Bjorklund and Motts (1959)
	TWDB BRACs database	BEG, DBSA Capitan Reef study, Intera Inc. High Plains GAM, Intera Inc. Rustler Aquifer study, NM EMNRD, NMOSE WRRS, RRC, TCEQ, TDLR, TWDB	Dockum Group top pick	Geophysical logs, scout tickets, published cross sections, water well logs, water well reports	Accessed from TWDB BRACs database June 16, 2021	Standen et al. (2009), Deeds et al. (2015), Ewing et al. (2012), Meyer (2020)
Upper Dockum Gp. base (UDB)	NMBGMR	TWDB BRACs database	Lower Dockum Group top pick	Points generated along digital contours	Contours generated from TWDB BRACs data to add control points to dataset	Deeds et al. (2015)
	TWDB High Plains GAM GIS files	Intera Inc. High Plains GAM study	Lower Dockum Group top pick	Geophysical logs	GIS geodatabases downloaded from https://www.twdb.texas.gov/groundwater/models/download.asp	Deeds et al. (2015)
Santa Rosa Fm. top (SRT)	NMBGMR	NMBGMR	Santa Rosa Fm. top pick	Geophysical logs	Picks of the top of the Santa Rosa Fm., Dewey Lake Fm., and Rustler Fm. from geophysical well logs; compiled from NM OCD website	
Lower Dockum Gp. base (LDB)	NMBGMR	NMBGMR	Dewey Lake Fm. top pick	Geophysical logs	Picks of the top of the Santa Rosa Fm., Dewey Lake Fm., and Rustler Fm. from compiled geophysical well logs	
	NMBGMR	TWDB BRACs database	Dewey Lake Fm. top	Points generated along digital contours	Contours generated from TWDB BRACs data to add control points to dataset	Deeds et al. (2015)
	TWDB Rustler aquifer GAM GIS files	Intera Inc. Rustler aquifer study	Dewey Lake Fm. top pick	Geophysical logs	GIS geodatabases downloaded from https://www.twdb.texas.gov/groundwater/models/download.asp	Ewing et al. (2012)
Dewey Lake Fm. base (DLB)	NMBGMR	NMBGMR	Rustler Fm. top pick	Geophysical logs	Rustler Fm. top picks from geophysical logs (Appendix B) and from Broadhead and Ulmer-Scholle (unpublished data)	Broadhead and Ulmer-Scholle (unpublished data)
	NMBGMR	Hiss (1976)	Rustler Fm. top	Points generated along digital contours	Structure contour map was digitized in ArcMap, then points were generated along contour lines	Hiss (1976)

Model unit (model abbreviation)	Map data source	Original data source	Control feature	Data type	Comments	References
Rustler Fm. base (RB)	TWDB BRACs database	BEG, Intera Inc. High Plains GAM, Intera Inc. Rustler aquifer GAM	Salado Fm. top pick	Geophysical logs, water well logs, digital contours	Ewing et al. (2012) hand-contoured the top of the Salado Fm. due to the complex nature of Rustler Fm. structure. The hand contours were then digitized and made available for download.	Deeds et al. (2015), Ewing et al. (2012)
	NMBGMR	NMBGMR	Salado Fm. top pick	Geophysical logs		Broadhead and Ulmer-Scholle (unpublished data)
Lower Ochoan series base (LOB)	NM OCD	NM OCD	Delaware Mountain Gp. top pick (basin), Artesia Gp. top pick (shelf, Central Basin Platform)	Geophysical logs	Digitized formation top data reported by driller/operator; used in regions with low well control density	
	NMBGMR	NMBGMR	Tansill Fm. (Artesia Gp.) top pick, Delaware Mountain Gp. top pick	Geophysical logs		Broadhead and Ulmer-Scholle (unpublished data)
Artesia Gp. base (AGB)	NMBGMR	Kelley (1971)	San Andres top	Points generated along digitized contours		Kelley (1971)
	NMBGMR	NMBGMR	San Andres top pick	Geophysical logs		Broadhead and Ulmer-Scholle (unpublished data)
Capitan Fm. top, base, and thickness (CT, CB)	TWDB Capitan Reef Complex aquifer GAM GIS files	Standen et al. (2009)	See original source	See original source	GIS geodatabases downloaded from TWDB Capitan Reef Complex aquifer GAM: **https://www.twdb.texas.gov/ groundwater/models/download.asp**	Standen et al. (2009)

NMBGMR: New Mexico Bureau of Geology and Mineral Resources

NM OCD: New Mexico Oil Conservation Division

NMOSE WRRS: New Mexico Office of the State Engineer Water Rights Reporting System

NM EMNRD: New Mexico Energy, Minerals and Natural Resources Department

TWDB: Texas Water Development Board

BRACs: Texas Water Development Board Brackish Aquifer Characterization

BEG: University of Texas at Austin Bureau of Economic Geology

DBSA: Daniel B. Stephens and Associates

RRC: Railroad Commission of Texas

TCEQ: Texas Commission on Environmental Quality

TDLR: Texas Department of Licensing and Regulation

GAM: Groundwater availability model

APPENDIX B: GEOPHYSICAL LOG ANALYSIS

As part of a joint effort between the New Mexico Office of the State Engineer; the New Mexico Energy, Minerals and Natural Resources Department Oil Conservation Division; and the New Mexico Bureau of Geology and Mineral Resources to better understand the shallow subsurface geology and hydrology in southeastern New Mexico, analysis of cuttings from drilled wells and corresponding well logs began in 2019. Cutting analysis was determined to be too time-consuming and inaccurate early in the project, so the focus was changed to gamma-ray log analysis for the remaining duration.

The study area was selected based on the high demand for shallow groundwater by the oil and gas industry, spanning Townships 17S through 26S and Ranges 32E through 38E, including parts of both Lea and Eddy Counties in southeastern New Mexico. Each township/range section, I.E T17S R32E, is divided into 36 sections in a 6 × 6 block.

Gamma-ray logs from within the study area (one per section) were selected based on the appearance of a clear signal for the Rustler Formation. The Rustler's anhydrite composition clearly distinguishes it from the siliciclastic formations in adjacent layers, with a sharp drop in the gamma-ray signature. Within the selected study area, target formations generally occur within approximately 2,500 ft of the surface.

Gamma-ray logs were then loaded into ArcGIS in an array of six for ease of comparison with adjacent logs, and "georeferenced" with x equal to zero and y equal to the depth on the log, in order to ensure that all logs were displayed at the same scale.

Using formation signals outlined by Kathryn Schiel's 1988 thesis "The Dewey Lake Formation: End Stage Deposit of a Peripheral Foreland Basin," and corroborated by Dennis Powers and Ronald Richardson's various Waste Isolation Pilot Plant drillhole reports and Robert Holt and Dennis Powers' 1990 "Geologic mapping of the air intake shaft at the Waste Isolation Pilot Plant," the depths of the contacts between the Rustler and Dewey Lake, Dewey Lake and Santa Rosa, and Santa Rosa and Tecovas, as well as the upper limit of the Tecovas, were taken from the logs. From this, elevations and formation thicknesses were calculated. Side-by-side comparison was vital for determining formation depth across logs.

Latitude and longitude were used to plot the locations of wells, with each datum taken from the log as provided. The Kelly bushing was most frequently provided and was used when possible; however, drilling floor and ground surface elevations were sometimes used when Kelly bushing was not available. Depths for the formation contacts were determined from the log signal and by subtracting them from the datum, and the approximate elevations of formation contacts were calculated. The elevations for the upper and lower contacts for the target formations were then used to calculate their thickness.

Contact picks for each well log were reviewed for consistency between respective data, gamma-ray signatures, contact elevations, and formation thicknesses. Some wells and contact picks were eliminated from the final data due to inconsistencies. Data for Appendix B are available for download at https://geoinfo.nmt.edu/publications/openfile/details.cfml?Volume=623

APPENDIX C: WATER QUALITY DATA

Water quality data are available for download at
https://geoinfo.nmt.edu/publications/openfile/details.cfml?Volume=623

APPENDIX D: MAP PACKAGE

Map package files are available for download at
https://geoinfo.nmt.edu/publications/openfile/details.cfml?Volume=623

APPENDIX E: WATER LEVEL DATA

Water level data are available for download at
https://geoinfo.nmt.edu/publications/openfile/details.cfml?Volume=623